STRUCTURAL STUDIES ON NATURAL SWEETENERS BY NMR SPECTROSCOPY AND COMPUTATIONAL METHODS

by

Gizem Oruç

B.S., Chemistry, Boğaziçi University, 2009

Submitted to the Institute for Graduate Studies in
Science and Engineering in partial fulfillment of
the requirements for the degree of
Master of Science

Graduate Program in Chemistry

Boğaziçi University

2012

to my family

ACKNOWLEDGEMENTS

I owe my gratitude to my thesis supervisor, Prof. Tereza Varnalı, for taking me into the project, for her endless support, motivation; for constructive feedbacks, understanding and sincerity throughout my graduate studies. I am also greatly thankful to my thesis co-supervisor, Somer Bekiroğlu, for his guidance, for sharing his knowledge generously, for motivating me to learn more and improve my skills. I feel extremely fortunate to have been involved in this team and for the cordiality of my supervisors.

I am thankful to Damjan Makuč for running the experiments and for the guidance during the hardest assignments. I also thank to Birgül Sağlam for her help and support to the work, and to Aslı Yıldırım for providing the vital script when I urgently needed.

I am grateful to my thesis examiners for their contribution to the final manuscript of my thesis. I would like to single out Assist. Prof. Ahu Akın for her careful review. I am also indebted to Chemistry Department, in particular to all of my professors for their encouragement and for teaching me the scientific perspective and discipline.

Special thanks to Sebla for her support during my studies and for the very first chemistry discussions; to Mayyasa for the "Molekülbaukasten"; to Özlem Yücer for her confidence in me; to İlker for showing me the blind spots of "science"; to Daniela for her support and taking care of my plants; to Asude Küçük for being in my life. I am profoundly grateful to Caro for her endless affection and solidarity.

I would like to express my deepest thanks to my dear family for their love, trust, support, and for letting me be who I am.

This project is funded by Boğaziçi University Scientific Research Fund (Grant No: 5183) and TÜBITAK (Grant No: 109T606). I would like to acknowledge Slovenian NMR Center for providing the experiments.

ABSTRACT

STRUCTURAL STUDIES ON NATURAL SWEETENERS BY NMR SPECTROSCOPY AND COMPUTATIONAL METHODS

In the present day, sweet tasting molecules have attracted a lot of attention being subject of escalating sugar-related diseases. The molecular recognition of sweet tasting molecules are known to be highly dependent on their conformation, which is mostly determined by non-bonding interactions with surrounding water molecules and the sweet taste receptor. Yet, the interaction of chemoreception at the molecular level still remains undiscovered. This study aims to elucidate the hydrogen bonding properties of selected sweeteners by employing an unconventional NMR spectroscopy method. The computational studies are integrated with experiments, in order to focus on sub-molecular events that are assumed to be responsible for the sweet-taste recognition. Our results show distinct hydrogen bonding properties possessed by all the molecules examined. The terminal hydroxyl groups show preference to exchange protons with surrounding water molecules, while internal hydroxy protons tend to form hydrogen bonds. Experimentally observed diastereotopicity of sweet-tasting molecules shows the importance of geometry in the molecular recognition level.

ÖZET

DOĞAL TATLANDIRICI BİLEŞİKLERİN YAPI-TAT İLİŞKİSİ AÇISINDAN NMR VE HESAPSAL YÖNTEMLERLE İNCELENMESİ

Artmakta olan şeker ilintili hastalıkların öznesi olması nedeniyle tatlı hissi veren moleküller günümüzde fazlasıyla ilgi çekmektedir. Tatlı duyumu sağlayan moleküllerin algılanmasında bu moleküllerin konformasyonlarının özellikle önem taşıdığı bilinmektedir. Tatlı moleküllerin çevrelerinde bulunan su molekülleri ve tatlı reseptörü ile gerçekleştirdikleri moleküler etkileşimler bu konformasyonların belirlenmesinde önemli bir etkendir. Ancak moleküler düzeyde gerçekleşen bu fiyolojik etkileşimler halen keşfedilememiştir. Bu çalışma, alışılagelmiş yöntemlerden farklı bir NMR spektroskopi yöntemi kullanarak, seçilen doğal tatlandırıcıların hidrojen bağı yapabilme özelliklerini aydınlatmayı amaçlamaktadır. Tatlı hissine sebep olduğu düşünülen moleküler altı durumlara odaklanmak amacıyla hesapsal yöntemler deneysel çalışmaya entegre edilmiştir. çalışmanın sonuçları seçilen moleküllerin tamamının belirgin bir hidrojen bağı yapma özelliğine sahip olduğunu göstermiştir. Uç hidroksil grupları ortamdaki su molekülleriyle proton değiştirmeyi tercih ederken daha içte bulunan hidroksit protonları hidrojen bağı oluşturmaya yatkındır. Tatlı hissi veren moleküllerin deneysel olarak gözlemlenen diastereotopikliği geometrinin moleküler tanımadaki önemini göstermektedir.

TABLE OF CONTENTS

LIST OF FIGURES

LIST OF TABLES

LIST OF SYMBOLS

^{1}H	Proton
$^2J_{\mathrm{XX}}$	Geminal scalar coupling
$^3J_{\mathrm{XX}}$	Vicinal scalar coupling
AH	Hydrogen bond donor
B	Hydrogen bond acceptor
$\mathbf{B}_0$	External magnetic field
$\mathbf{E}$	Energy
Hz	Hertz, frequency unit (s^{-1})
I	Nuclear spin quantum number
K	Kelvin
k_{ex}	Exchange rate
ppb	parts per billion (10^{-9})
ppm	parts per million (10^{-6})
s	second
Å	Ångström (1x10^{-10} meters)
°C	Degree Celcius
$\Delta\delta$	Chemical shift difference
$\overline{\Delta\delta}_{\mathrm{C}}$	Mean $\lvert\delta_{experimental}–\delta_{computational}\rvert$ of $\delta(^{13}\mathrm{C})$s
$\overline{\Delta\delta}_{\mathrm{H}}$	Mean $\lvert\delta_{experimental}–\delta_{computational}\rvert$ of $\delta(^{1}\mathrm{H})$s
$\rho(r)$	Electron density
δ	NMR chemical shift
τ_m	Mixing time
ϕ	Dihedral torsion angel

LIST OF ACRONYMS/ABBREVIATIONS

1D, 2D, 3D	One-, two- and three-dimensional
ab initio	"from the beginning" in Latin
B3LYP	Becke 3-Parameter, Lee, Yang and Parr hybrid functional
DFT	Density functional theory
DQF-COSY	Double quantum filtered correlation spectroscopy
FID	Free induction decay
FT	Fourier transform
HF	Hartree-Fock
HMBC	Heteronuclear multiple bond correlation
HSQC	Heteronuclear single quantum coherence
MM	Molecular mechanics
MMFF	Merck molecular force field
n/a	not available
NMR	Nuclear magnetic resonance
NOE	Nuclear Overhauser effect
NOESY	Nuclear Overhauser and exchange spectroscopy
PES	Potential energy surface
POLY	Polynomial baseline correction
PS	Phase correction
ROESY	Rotating-frame Overhauser enhancement spectroscopy
SP	Adjustable sine window function
TOCSY	Total correlation spectroscopy
ZF	Zero filling

1. INTRODUCTION

1.1. Sweet Taste and Sweeteners

The sense of taste in humans is the key component in recognition of nutrition quality. There are five different taste modalities identified in human taste perception: Sweet, bitter, salty, sour and umami [1]. Among them, the sweet taste plays a vital role for the evolution of humans as well as other vertebrates, being an indication for carbohydrates that have high nutritive value [2]. In the present day, consumption of sweet-tasting nutrients is directly linked to diseases, such as obesity, diabetes, hyperlipemia and caries, which affect increasing number of people [3]. Such health-related issues led to the use of artificial sweeteners that are as sweet as natural ones but less harmful to health. On the other hand, consumption of widely accepted artificial sweeteners such as saccharine, aspartame, acesulfame K, sucralose and neotame is still a concern of health [4]. Synthesis of safer artificial sweeteners is an urge; however sweet taste stimulation is still not completely elucidated, which is the reason of serendipitous discovery of commonly used artificial sweeteners. The discovery of sweet taste receptor in 2001 [5–7] started a new era on the research of sweet taste stimulation. Nevertheless many peculiarities remain unresolved. Understanding the mechanism between sweeteners and sweet taste receptor at molecular level is essential to design new, safe and low calorie sweeteners.

Sweet-tasting molecules can significantly vary in size and chemical nature. In addition to the most well-known class of sweet compounds that is sugars; amino acids, peptides, olefinic alcohols, proteins and many other organic compounds can trigger the same stimulation. The sweet stimulation is also closely related to spatial geometry of sweeteners: for instance only amino acids in D-configuration taste sweet [8]. Such high specificity of sweet stimulating molecules as well as the low affinity of sweet taste receptor to its ligands (only at concentrations of maximum 0.1 molar) are considered to be the reasons of late discovery of the receptor [9, 10]

1.2. Early Sweetener Models

Until the discovery of sweet taste receptor, the attempts to explain the mechanism behind the sweetness stimulus were mainly based on indirect mapping of active site of the receptor. A number of molecular molds were derived based on structures and activities of sweet-tasting ligands, assuming that there is only a single binding site on the receptor. The earliest explanations focused on the existence of glucophores, i.e., specific atoms or groups responsible for the sweet taste on the sweet tasting molecules [11]. The work of Shallenberger and Acree (1967) was the first widely accepted model, which states that all sweeteners contain a hydrogen bond donor (AH) and a hydrogen bond acceptor (B), separated by a distance of 2.5 to 4 Å (Figure 1.1a). The AH–B unit, namely glucophore, forms a pair of hydrogen bonds with the complimentary B–HA unit on the receptor [12]. Later Kier (1972) enhanced this linear AH–B theory by addition of a third component, X, called "dispersion point" (Figure 1.1b). The third component leads to hydrophobic interactions between glucophore and the receptor, which is believed to modulate sweet potency of the ligands [13].

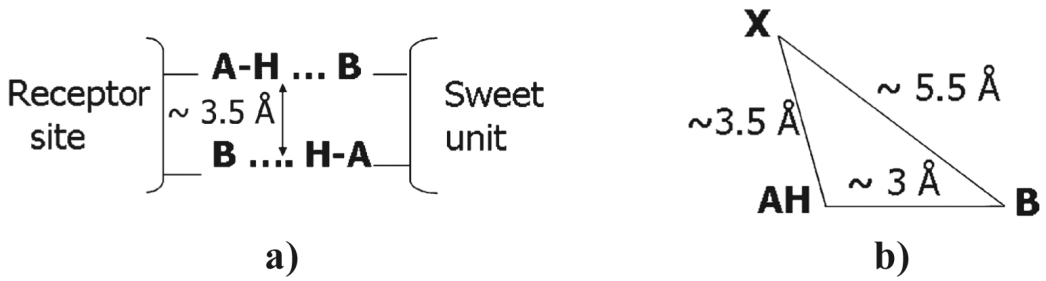

Figure 1.1. (a) Shallenberger and Acree model (b) Kier model [10].

Many other theories emerged subsequently for a better explanation of glucophore structure, each suggesting a common geometrical model for all sweet-tasting molecules [14, 15]. Among them, the work of Goodman et al. (1987), which is a combination of NMR spectroscopy with computational models, altered the orientation of AH–B and X units and included stereoisomeric features [16]. In 1996, Nofre and Tinti proposed a new model that comprises 6 recognition units in addition to AH and B sites. According to

this theory, hydrogen bonding interactions between the ligand and the receptor provoke significant conformational changes within the receptor and its binding sites [17]. In 2002 Goodman et al. further stressed the decisive role of hydrophobic group orientation on the potency of sweet taste [18]. None of the aforementioned models could entirely explain the structure-activity relationship of the sweet ligands or the possible structure of the receptor. Yet the common presence of AH–B glucophore in all of the models was subsequently proven to exist within the receptor [8].

1.3. Discovery of Sweet Taste Receptor and Outcomes

The discovery of sweet proteins [19] led to the belief that there might exist two different receptors, as the chemical nature of sweet proteins are very different from small sweeteners [20]. Soon after the discovery of sweet taste receptor in 2001, it has been shown that all the sweet molecules activate the same heterodimer T1R2_T1R3 receptor [21]. Several researches have been carried on to model complete crystal structure of the receptor. Subsequent results state that large and small molecules activate different binding sites on the sweet taste receptor [22]. Moreover the receptor is found out to have at least three binding sites, which explains the chemical variety of sweet tasting molecules [23]. According to one of the newest receptor homology models proposed by Morini, Bassoli and Temussi groups, carbohydrate sweeteners activate one single site [24, 25].

1.4. Role of Water

Water is the key component of many biological processes, being the primary solvent of physiological events [26]. It has uppermost importance regarding the taste chemoreception, since the taste perception requires the solvation of tasty molecules in water. At the level of molecular recognition, water molecules are known to be an active participant of carbohydrate-protein interactions [27]. Key polar interactions and perturbed water regions are two important notions proposed by Lemieux, which prove the determinant role of water on the specificity of binding. According to Lemieux, the

polar groups of both the ligand and the receptor are totally hydrated before complexation, thus water molecules have to be displaced for binding to occur. Furthermore, only key polar groups of the epitope and key hydroxyl groups of the sugar unit could provoke strong associations. The region where the binding occurs is known to be polyamphiphilic, i.e., has both polar and nonpolar regions [28]. The structure of water molecules are perturbed at such surfaces, thereby the return of these water molecules back to bulk is a entropically favored process [29]. Water mobility, which determines the packing attributes of sweet molecules, is another frequently used concept to explain sweetness potency [30]. The water mobility is assumed to decrease as the sugar concentration increases, since hydrogen bonding interactions of water molecules with sugar molecules as well as sugar molecules with themselves increase [31]. The vital role of water points to the importance of non-bonding interactions between ligand, water molecules and the receptor.

2. AIM OF THE STUDY

2.1. Importance of Hydroxy Protons in Conformational Analysis

Hydrogen bonding features of sweet tasting molecules as well as their interactions with water molecules have indisputable importance at the molecular level of sweet taste recognition, as claimed by the findings mentioned so far. Therefore, conformational analysis has to focus mainly on the characteristics of hydroxy protons of the sweet tasting molecules in aqueous solutions in this regard.

2.2. NMR Spectroscopy and Computational Methods

Nuclear Magnetic Spectroscopy (NMR) is the experimental research technique used throughout this study. NMR is a very powerful structural analysis tool and excessively used for the investigation of organic molecules in particular. The results of an NMR experiment stem from an ensemble of conformations present in the solution. For that reason, NMR is not sufficient for a conformational analysis that is focused on sub-molecular events. In order to obtain more detailed information on conformations, computational methods were employed together with NMR experiments. This study basically focuses on the comparison of experimental and calculated NMR resutlts, which might give a general trend on conformations of selected natural sweeteners. The findings would give more detailed knowledge about the conformations which bring about the sweet-taste recognition, and thence might be used to design new synthetic sweeteners.

2.3. Selected Sweeteners

Molecules selected to be analyzed in this work are natural, relatively small and widely used sweeteners including glycerol, erythritol, xylitol, mannitol, sorbitol as poly-alcohols (polyols); tagatose, fructose as monosaccharides and sucrose as a disaccharide

(Figure 2.1). Additionally ethylene glycol is taken into account. Even though it is known to be toxic, glycol has a sweet taste as well and as being the smallest polyol, it is considered as a building block of selected sweeteners.

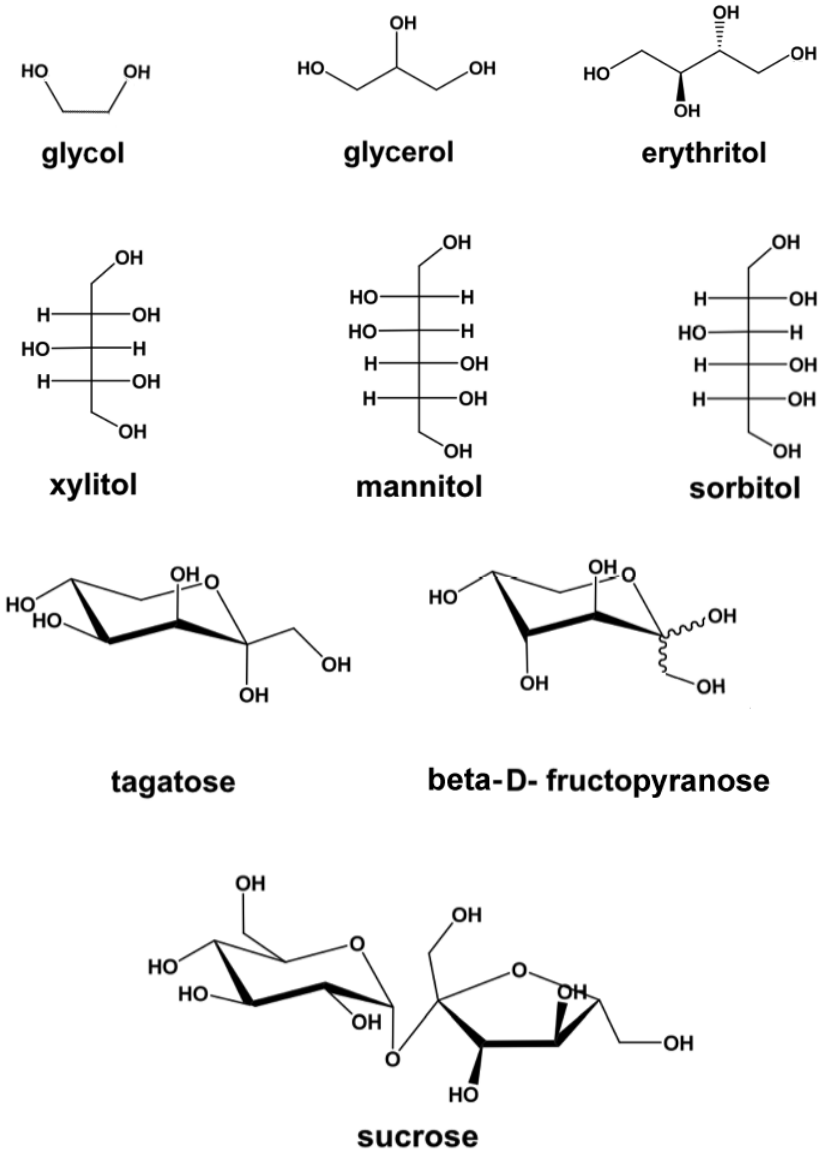

Figure 2.1. Selected natural sweeteners.

3. METHODOLOGY

3.1. Nuclear Magnetic Resonance Spectroscopy

3.1.1. Introduction

A nuclei with non-zero spin quantum number ($I \neq 0$) has a magnetic moment. When such a nuclei is placed in an external magnetic field $\mathbf{B}_0$, the spin vector would orient itself according to one of the possible $2I+1$ orientations. These allowed orientations have different energy levels (α and β as seen in Figure 3.1). The energy difference between states depends on the magnetic moment of the nuclei and applied magnetic field strength. Nuclear magnetic resonance is a phenomenon that occurs when a nuclei is excited to a spin state of higher energy by an applied electromagnetic radiation and subsequently emits with the resonance frequency. The resonance frequency is then measured as a signal called "Free induction decay" (FID) and processed to give an NMR spectrum, where nuclei in different magnetic environments give distinct responses.

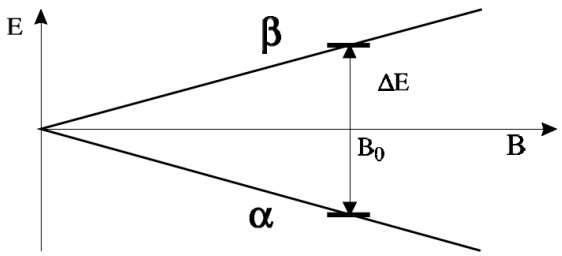

Figure 3.1. Effect of $\mathbf{B}_0$ on spin energy levels.

Sensitivity of nuclear magnetic moments to their surroundings makes NMR Spectroscopy a powerful method for the identification of structural and dynamical properties of molecules. It can be further improved by 2D NMR experiments that provide information about homonuclear/heteronuclear correlations resulting from either through-bond or through-space interactions.

Several NMR methods have been frequently used for structural determination of carbohydrates [32]. Numerous studies have shown that NMR spectroscopy can be used to observe and track characteristics of exchangeable hydroxy protons in various biologically important molecules [33–44]. For instance, the hydroxyl groups of Lewis b tetrasaccharide derivative that participate in key polar interactions have distinct NMR features [41]. The properties of exchangeable protons acquired by NMR studies include:

- Chemical shifts (δ)
- Spin-spin coupling (J-coupling) constants
- Temperature coefficients ($\mathrm{d}\delta/\mathrm{d}\,T$)
- Exchange rates (k_{ex})
- Chemical shift differences ($\Delta\delta$)

Relatively small temperature dependence, vicinal coupling constants and slow exchange rates are indications of hydrogen bond interactions [41, 42, 44, 45]. Therefore, NMR spectroscopy provides adequate outputs to investigate the key hydroxyl groups.

3.1.2. Chemical shifts

Magnetic field at the nuclei is directly proportional to the sum of local, neighbor and solvent contributions to the shielding of the nuclei by surrounding electrons. The extent of shielding is described by the very basic output of an NMR spectrum, that is, the chemical shift (δ). A nuclei with small chemical shift (upfield) is said to be shielded, whereas large chemical shift (downfield) of a nuclei is the evidence of deshielding. For instance, a hydroxy proton has a downfield shift, due to strong deshielding by the electron-withdrawing power of the adjacent oxygen atom. However, the NMR signals of hydroxy protons that take part in hydrogen bondings and interactions with solvent molecules cannot be observed by NMR experiments where deuterated solvents are used. The reason behind is the displacement of hydroxy protons with deuterium by a fast exchange reaction. In order to observe exchangeable protons, a recent NMR method was employed throughout this work, in which ordinary water is used as the solvent [34].

3.1.3. Spin-spin coupling constants

Scalar spin coupling constant, J, is another valuable information that yields from NMR experiments. Couplings result from the magnetic transfer between nuclei that are chemically bound, and is independent of the magnetic field strength. Vicinal ($^3J_{\mathrm{HH}}$) coupling constants are directly correlated to dihedral torsion angel between H–C(or O)–C–H, defined as ϕ (Figure 3.2). Dihedral angles can be estimated by Karplus Equation (3.1). Hydroxy protons that are in fast exchange appear as broad signals without any splitting, thus couplings cannot be observed. As the chemical exchange gets slower, the couplings might become visible. A modified Karplus equation estimates that the hydroxy protons have $^3J_{\mathrm{H–O–C–H}}$ values of 5.5 ± 0.5 Hz, if C–O bond rotates freely [46]. Hydroxy protons that participate in hydrogen bonding, hence do not rotate freely around C–H bond, are expected to have vicinal coupling constants that significantly deviate from that value.

$$^3J = A\cos^2\phi + B\cos\phi + C \tag{3.1}$$

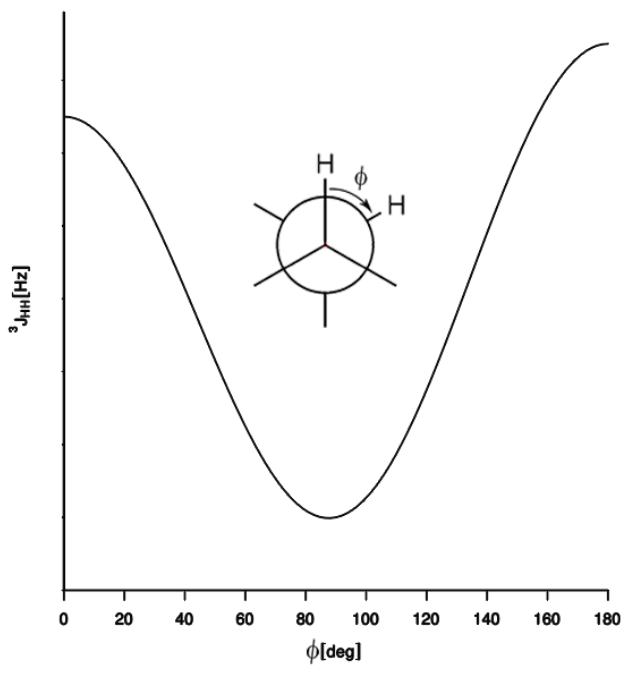

Figure 3.2. Relationship of $^3J_{\mathrm{HH}}$ with dihedral angle ϕ.

3.1.4. Temperature coefficients

Temperature coefficient ($\mathrm{d}\delta/\mathrm{d}\,T$), indicates the dependency of chemical shifts on temperature. It is calculated as the slope of the fitted line of plotted chemical shifts (ppb) versus temperature (K or °C) graph (Figure 3.3). Low temperature dependence is an indication of hydrogen bonding interaction due to less effective anisotropy on hydroxy protons that take part in hydrogen bonding [34]. A temperature coefficient value lower than 3 ppb deg^{-1} is accepted to be an indication of hydrogen bonding for saccharides in DMSO [36]. For trisaccharides in aqueous medium, temperature coefficients have been calculated to be as low as 4 ppb deg^{-1} [40].

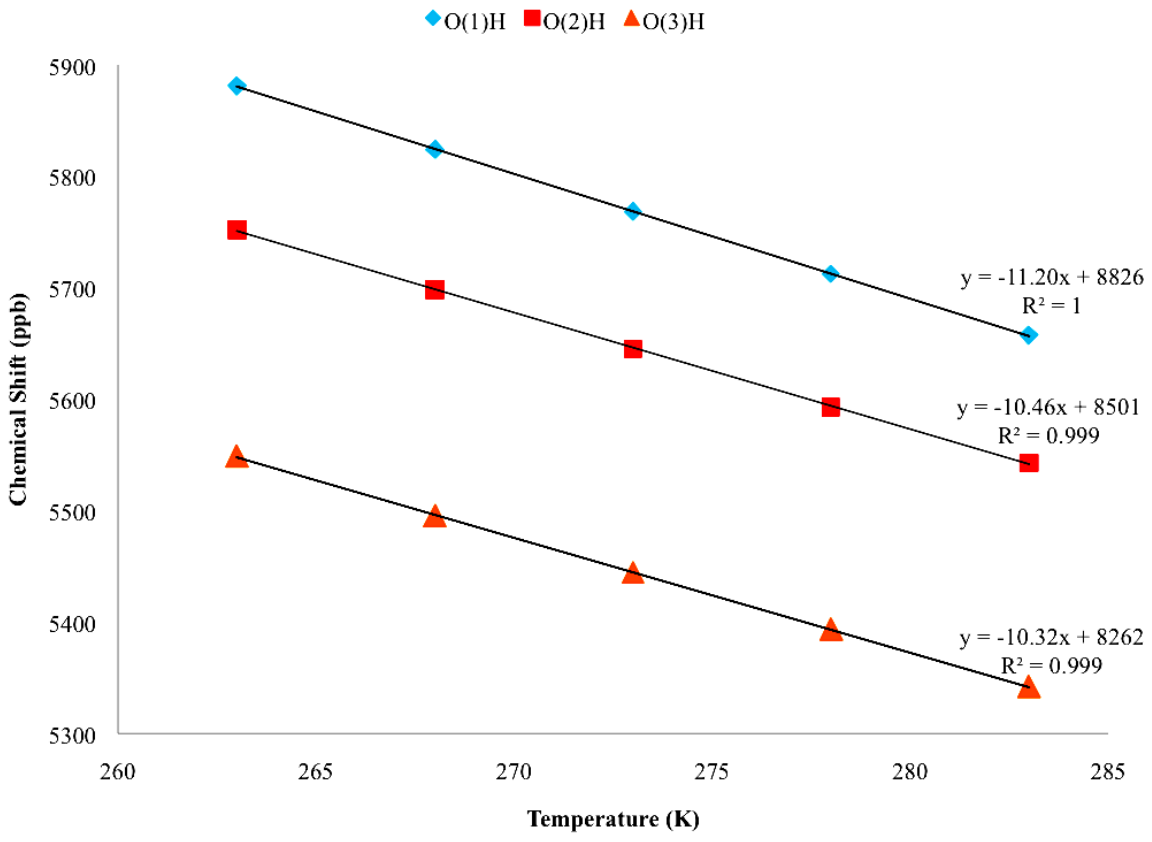

Figure 3.3. Chemical shift vs. temperature graph of xylitol hydroxy protons. $\mathrm{d}\delta/\mathrm{d}\,T$ is calculated as the slope of the fitted line.

3.1.5. Exchange rates

The hydroxy protons are subject to chemical exchange with the protons of solvent molecules, as seen in Equation 3.2 [47]. The rate of the exchange is defined as the number of protons transferred in unit time (s^{-1}).

$$AH + B \rightleftharpoons (AH \cdots B \rightleftharpoons A \cdots BH) \rightleftharpoons A + BH \tag{3.2}$$

Nuclear Overhauser effect (NOE) is a phenomenon that is described by the change in the intensity of an NMR signal when the resonance of another spatially close nuclei is saturated. NOE is basically due to magnetization transfer as in J-couplings, yet unlike J-couplings, NOEs take place through space (within $\leqslant$ 5 Å). Therefore, NOEs give crucial information about the topology of the molecule.

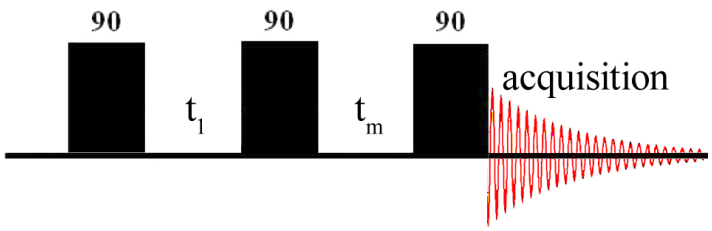

Figure 3.4. The NOESY pulse sequence.

The basic pulse sequence of the NOESY experiment is shown in Figure 3.4. The mixing time, τ_m, is the duration when magnetization transfer occurs. On the condition that a NOESY spectrum is obtained by a pulse with short τ_m, generated cross peaks are known to result from chemical exchange only [48]. At longer τ_m, NOEs are influenced by many additional factors. Even decrease of the peak intensities is observed as mixing time gets longer [49]. Therefore, the calculation of the exchange rate require the selection of short mixing times.

In order to calculate exchange rates of hydroxy protons, their diagonal NOE peak volumes as well as volumes of cross peaks with water have to be measured at several mixing times. The observation of NOEs of hydroxy protons can be accomplished by careful water suppressing pulses [50]. Exchange rate is calculated as the ratio of the initial build-up rates of exchange peaks over the volume of the diagonal peaks at zero mixing time [39–41, 43, 51, 52]. The diagonal peak volume at zero mixing time is extrapolated from the data points (Figure 3.5).

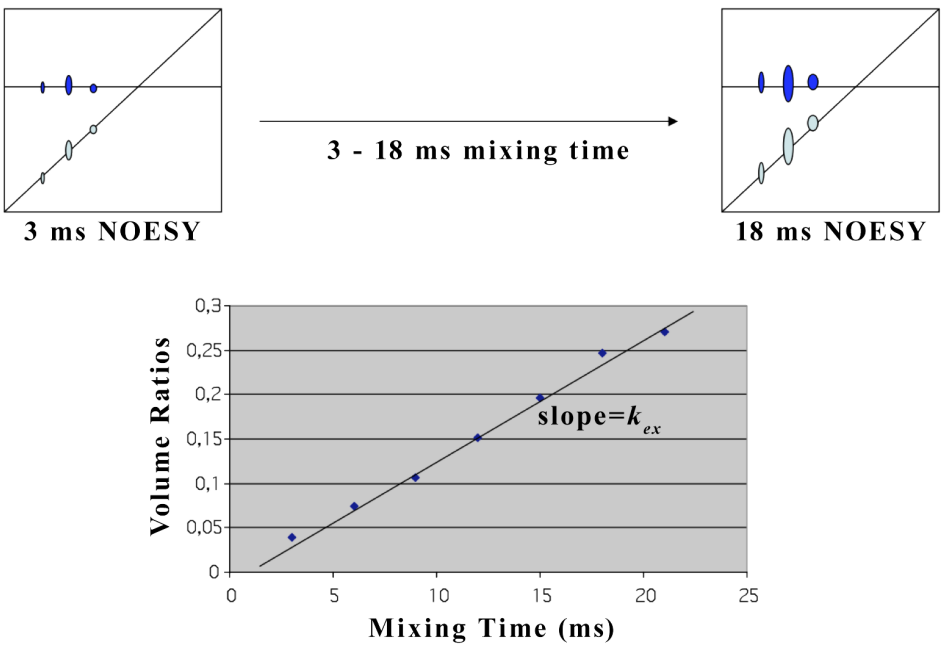

Figure 3.5. Calculation of k_{ex}.

The magnitude of the proton exchange is directly linked to steric factors affecting the spatial geometry of hydroxyl groups. As stated before, slow exchange rate of a hydroxy proton is an indication of hydrogen bonding, where the hydroxy proton prefers to involve in a hydrogen bond rather than exchanging with protons of water.

The rate of exchange is affected by many other elements as well, such as the temperature or ionic residues that would facilitate the exchange reaction. Thus the comparison of hydroxy proton exchange rates should be done within a single molecule.

3.1.6. Chemical shift differences

It has been previously reported that the chemical shift differences of hydroxy protons of an oligosaccharide from its corresponding monosaccharide can provide structural information. Large negative $\Delta\delta$ values can result from the proximity of the hydroxy proton to the ring oxygen, or to another hydroxyl group [39–41,43]. It has been further noted that relatively larger negative $\Delta\delta$ value of a hydroxy proton is a consequence of reduced accessibility of water. Downfield shifts, on the other hand, is attributed to hydrogen bonding interactions [44].

3.1.7. Experimental

3.1.7.1. Sample preparation. The observation of exchangeable hydroxy protons by NMR spectroscopy is accomplished by using H_2O as solvent, and lowering the exchange rate of hydroxy protons with water. Additionally, pH values of the samples should be between 6.5–6.9 [47]. Contaminated ionic species can catalyze the exchange reaction, hence increase k_{ex}. Therefore, ionic impurities have to be removed by elaborate cleansing of NMR test tubes. The cleaning procedure involves rinsing and soaking with (*i*) acetone (*ii*) methanol (*iii*) water respectively. Decreasing the temperature also minimizes the rate of exchange [33, 51, 53, 54]. In this work, the temperature was set down to –10°C (263 K). In order to avoid freezing of the aqueous sample solutions, acetone-d_6 was added with a volume ratio of 15%. Acetone-d_6 also provides the reference signal at δ=2.204 ppm for proton and δ=32.320 ppm for carbon chemical shift calibrations. The sample solutions were prepared in a molarity range of 14 mM to 21 mM.

3.1.7.2. Experiments. In addition to 1D spectra, NMR experiments of this study include both homonuclear and heteronuclear 2D experiments. Through bond correlations were obtained from DQF-COSY and TOCSY spectra for ^{1}H-^{1}H interactions and by HSQC spectra for ^{1}H-^{13}C interactions. ^{1}H-^{1}H through space correlations were acquired from either NOESY or ROESY spectrum. All 1D ^{1}H, ^{13}C and 2D DQF-COSY, NOESY, ROESY and TOCSY experiments were performed on a Varian VNMRS-600

MHz spectrometer. 2D HSQC experiments were performed on a Varian Unity Inova 300 MHz spectrometer.

Since water constitutes the major component of the sample solutions, the traditional NMR techniques were replaced with water suppressing techniques. A combination of WATERGATE (WATER suppression by GrAdient-Tailored Excitation) and DPFGSE (Double Pulsed Field Gradient Spin Echo) pulse sequences were optimized and employed throughout the study. DPFGSE pulse sequence is used for 1D proton and 2D NOESY, ROESY and TOCSY, WATERGATE pulse sequence is used for DQF-COSY experiments.

3.1.7.3. Processing of FIDs. For 1D experiments, the processing of acquired FIDs were done by employing MestReNova software. The processing of 2D NMR data was done by nmrPipe program; for assignments, peak listing and image capture Sparky software was employed. Data processing was done by applying a set of functions, including Fourier Transformation (FT), zero filling (ZF), window function (SP), phase correction (PS) and polynomial baseline correction (POLY). Processing procedure for 2D experiments was performed by executing a series of nmrPipe scripts for each experiment (Table 3.1).

3.1.7.4. Assignments. Assignments are done using several 1D and 2D spectra. In order to assign hydroxy protons, NOESY, ROESY and TOCSY spectra were exploited. Unless noted, the chemical shifts are read from 1D ^{1}H and ^{13}C APT spectra. In case of an ambiguity, chemical shifts are measured preferably from HSQC spectrum due to its high resolution.

In solution, fructose is known to exist mostly in the form of β-D-fructopyranose [55]. The equilibrium of tagatose solution has 71.3% of α-D-tagatopyranose [56]. The assignments and computational calculations of fructose and tagatose were done considering these isomeric forms.

Table 3.1. nmrPipe script used to process HSQC spectrum.

```
#!/bin/csh

var2pipe -in ./fid \
 -noaswap  \
  -xN 488 -yN 512  \
  -xT 244 -yT 256 \
  -xMODE Complex -yMODE Rance-Kay  \
  -xSW 2382.370 -ySW 6739.112  \
  -xOBS 297.800 -yOBS 74.886  \
  -xCAR 5.107 -yCAR 67.529  \
  -xLAB H1 -yLAB C13  \
  -ndim 2 -aq2D States \
  -out ./temp -verb -ov
nmrPipe -in ./temp \
| nmrPipe -fn POLY -time \
| nmrPipe -fn SP -off 0.5 -end 0.98 -pow 2 -c 0.5 \
| nmrPipe -fn ZF -size 4096 \
| nmrPipe -fn FT          \
| nmrPipe -fn PS -p0 100.0 -p1 -22.0 -di -verb  \
| nmrPipe -fn TP          \
| nmrPipe -fn SP -off 0.5 -end 0.98 -pow 2 -c 0.5 \
| nmrPipe -fn ZF -size 1024 \
| nmrPipe -fn FT   \
| nmrPipe -fn PS -p0 247.8  -p1 55.0   \
| nmrPipe -fn TP          \
| nmrPipe -fn POLY -auto -xn 50              \
| nmrPipe -fn POLY -auto -x1 50              \
  -out ./hsqc.ft2 -verb -ov
```

3.1.7.5. Coupling constants. Coupling constants were measured from 1D proton spectra by using multiplet analyzer tool of MestReNova software. The coupling constants that could not be measured due to spectral overlapping or broadened signals are indicated as "n/a" (not available) in the experimental tables. Spin simulation tool implemented in MestReNova is used to calculate coupling constants of erythritol, xylitol and sorbitol, since overlapping of signals prevents direct measurements of $J_{\text{H–H}}$.

A $^{3}J_{\text{HC-OH}}$ value that deviates from 5.5 ± 0.5 Hz is an evidence of a hydrogen bonding interaction, as explained in Subsection 3.1.3. The interval was revised in

order to improve the reliability of the results. The modified Karplus equation referred in Subsection 3.1.3 is as follows [46]:

$$^{3}J_{\text{H-C-O-H}} = 10.4\cos^2\phi - 1.5\cos\phi + 0.2 \tag{3.3}$$

Dihedral angle calculations were done according to Equation 3.3 for four different $^{3}J_{\text{HC-OH}}$ intervals: 5.5 ± 0.5, ± 1.0, ± 1.5, ± 2.0. The results are reported in Table 3.2. Since dihedral angle values do not change significantly for different $^{3}J_{\text{HC-OH}}$ intervals, vicinal coupling constants of the order of 5.5 ± 1.5 Hz are defined to indicate a free rotation.

Table 3.2. Dihedral angles calculated from modified Karplus equation.

$^{3}J_{\text{HC-OH}}$	Dihedral Angle ϕ				
5.5 ± 0.5 Hz	Lower	34.7	127.7	227.3	319.1
	Upper	40.9	132.7	232.3	325.3
	Mean	37.8	130.1	229.9	322.2
	Interval	6.2	5.0	5.0	6.2
5.5 ± 1.0 Hz	Lower	31.4	125.1	224.8	316.0
	Upper	44.0	135.1	234.9	328.6
	Mean	37.8	130.1	229.9	322.2
	Interval	12.6	10.0	10.1	12.6
5.5 ± 1.5 Hz	Lower	27.9	122.5	222.3	313.0
	Upper	47.0	137.7	237.5	332.1
	Mean	37.8	130.1	229.9	322.2
	Interval	19.1	15.2	15.2	19.1
5.5 ± 2.0 Hz	Lower	24.1	119.8	219.8	309.8
	Upper	50.2	140.2	240.2	335.9
	Mean	37.8	130.1	229.9	322.2
	Interval	26.1	20.4	20.4	26.1

3.1.7.6. Temperature coefficients. The chemical shifts of exchangeable hydroxy protons were extracted from 1D spectra recorded at temperatures varying from -10°C to +10°C in 5°C steps. Chemical shift versus temperature graph was plotted, and temperature coefficient was calculated as the slope of the fitted line through the data points.

3.1.7.7. Exchange rates. NOE volumes of diagonal and cross peaks were measured from NOESY spectra with mixing times of 3ms, 6ms, 9ms, 12ms, 15ms and 18ms at -10°C. The data processing was done with the same processing parameters within each sample. The method and parameters for peak volume integrations in Sparky software were optimized for glycerol. The optimized method was then utilized to measure peak volumes throughout the work.

3.1.7.8. Chemical shift differences. The chemical shift difference has been a useful parameter for the structural analysis of oligosaccharides. In this work, $\Delta\delta$ value is empirically defined as the difference of the hydroxy proton chemical shift from that of glycol molecule, which is the smallest polyol.

3.2. Computational Studies in Conformational Analysis

3.2.1. Introduction

Computational chemistry utilizes chemistry theories in order to decipher behaviors of molecules. It is a fundamental tool that has been used in various fields of chemistry, including pharmaceutical researches, explanation of reactions as well as conformational analysis. Computational chemistry approaches principally consist of *ab initio*, semi-empirical and empirical methods, each of which uses different levels of approximations for low computational cost with accurate results.

3.2.2. Molecular mechanics

Molecular mechanics (MM) approach is based on Newtonian mechanics in which neither wave functions nor electron density calculations are considered. Energy of a molecule is calculated by a set of parametrized algebraic equations called "force field". The constants of the equations are obtained either experimentally or from *ab initio* calculations. Therefore, MM calculations are rather simple, and require relatively low computational cost [57]. For that reason, MM calculations have been excessively used for conformational analysis. Although MM methods are known to give large errors while transition state barriers are the subject, ground state geometries can be calculated with high accuracy when the conformational alterations are hindered by steric factors in particular [58].

A force-field consists of various terms to describe molecular features, such as bond stretching, bond bending, torsions, electrostatic interactions and van der Waals interactions. Among them, those who designate single property of the shape of a molecule are called "valence terms", whereas the others that stand for interactions between molecules are called "cross terms". Different force-fields contain different terms and constants. The force-field used for this study is Merck Molecular Force Field (MMFF) [59], which is a widely used and relatively novel force-field. MMFF contains

bond-stretching (EB_{ij}), angle bending (EA_{ijk}), out-of-plane bending ($EOOP_{ijk;l}$), torsion interactions (ET_{ijkl}), van der Waals interactions ($EvdW_{ij}$) and electrostatic interactions (EQ_{ij}) as valence terms; and stretch-bend interactions (EBA_{ijk}) as a cross term in the energy expression (Equation 3.4). Atoms are designated as *i*, *j*, *k*, and so on. Almost all parameters employed in MMFF were derived from *ab initio* calculations [60].

$$\mathbf{E}_{\mathrm{MMFF}} = \sum \mathrm{EB}_{ij} + \sum \mathrm{EA}_{ijk} + \sum \mathrm{EBA}_{ijk} + \sum \mathrm{EOOP}_{ijk;l} + \sum \mathrm{ET}_{ijkl} + \sum \mathrm{EvdW}_{ij} + \sum \mathrm{EQ}_{ij} \tag{3.4}$$

3.2.3. Density functional theory

Density functional theory (DFT) is a fairly new computational method that utilizes the electron density $\rho(r)$ to determine molecular properties. Since $\rho(r)$ is a function of wavefunction, it is defined as a functional. The wavefunction principally has to deal with 3N spatial coordinates for an N-electron system. However, electron density is independent of the number of electrons, and it is a function of three spatial coordinates as variables. Thus it provides simplicity and affordable computational cost.

According to Hohenberg–Kohn Theorem proposed in 1964, the ground state energy is at minimum if the electron density is correctly measured for the ground state. It is also proposed that any molecular property can be calculated from electron density functional of the ground state [61]. The energy of the molecule is therefore a functional of the electron density, and can simply be written as

$$E = F\left[\rho(x, y, z)\right] \tag{3.5}$$

where F stands for *functional*. According to Kohn and Sham Method [62], which expressed the density for the first time, the total ground state energy is defined as

$$E_{DFT}\left[\rho\right] = T_e\left[\rho\right] + E_{ne}\left[\rho\right] + J\left[\rho\right] + E_{xc}\left[\rho\right] \tag{3.6}$$

where energy (E), kinetic energy of electrons (T_e), nuclear-electron attraction (E_{ne}), electron-electron repulsion (J) and electron-electron exchange correlation energy (E_{xc}) are all determined by the electron density functional.

The determination of the functionals requires a great number of approximations, which vary in different methods. A gross categorization of methods includes *local density approximation* (LDA), *gradient corrected* and *hybrid* methods. Among these three, hybrid functions utilize the combination of functionals of other methods integrated with Hartree–Fock calculations. In particular, B3LYP (Becke 3 term with Lee, Yang, Parr exchange) hybrid functional [63] is the most common method used in conformational studies of carbohydrates [64].

Density functional theory treats electron correlations more efficiently than semi-empirical quantum mechanical methods, which do not give accurate energies for carbohydrates [65]. *Ab initio* quantum mechanics such as Hartree–Fock (HF), is also causing systematical errors and incorrect energy evaluation for low-energy conformers due to the lack of Coulomb-type electron correlations [64, 66]. Furthermore, for hydrogen bond containing molecules, it has been shown that energies and geometries of most significant conformations in gas phase can be determined well accurately by B3LYP functional, including glycerol [67–69] and erythritol [70]. B3LYP method with 6–311+G** basis set level is found out to be highly sufficient for geometry and energy calculations of carbohydrates [64, 71].

3.2.4. Computational NMR studies

In the present time, the prediction of NMR properties by computational methods is a common practice. It has been used frequently to assign the spectra, to assist one-to-one assignment and reassign as a cross-check of experimental results. The choice of method in NMR calculations has been shown not to require large basis sets. B3LYP hybrid functional with a basis set that includes diffuse functions are found out to improve the accuracy of the results [72]. There are a number of methods used for NMR

calculations. Among them, GIAO (Gauge-Independent Atomic Orbital) is excessively used due to its applicability and higher accuracy on smaller basis sets, as well as rapid convergence on both ^{1}H and ^{13}C chemical shift calculations [72–74].

NMR calculations require a full geometry optimization of molecules beforehand. B3LYP level of theory with 6-31G(d) or a higher basis set is found out to be appropriate for the geometry optimization prior to NMR calculations [74]. NMR shielding constants do not need to be computed by using the same basis set of geometry optimization [75]. Obtaining the correct chemical shifts values requires the subtraction of the reference shifts (frequently TMS) from the calculated isotropic shielding constants. For those atoms that are experimentally not distinguishable, the calculated chemical shifts are averaged. The error interval of calculated chemical shifts can be up to 0.4 ppm for proton and 10 ppm for carbon chemical shifts [75].

3.2.5. Calculations

3.2.5.1. Conformer distribution and geometry optimization. A preliminary set of low energy conformations was obtained by Monte Carlo method included in Spartan'04 software package [76], following the energy minimization by MMFF methodology. Monte Carlo is a powerful statistical method since it enables the search of conformations randomly on the Potential Energy Surface. It is found out to be efficient particularly for small molecules like polyols [77], and applicable on oligosaccharides [78]. Maximum conformer number acquired from conformer distribution research was limited to 100. For better precision in energy, single point calculations were carried out by DFT method with B3LYP hybrid functional at the 6–31G* level of theory. The computational method of choice should principally consider nonbonded interactions, since geometries of polyols depend mostly on hydrogen bondings as stated before.

The conformers acquired from single point calculations at the B3LYP/6–31G* level were then sorted according to their energies in kcal/mol. Further elimination among 100 conformers was required. That is a reasonable approach because the more

populated the conformer, the more it contributes to NMR shifts. Our calculations show that a single hydrogen bond at B3LYP/6–31G* level results in lowering the energy by maximum ∼2.8 kcal/mol. Therefore, conformers with relative energies larger than 7 kcal/mol were filtered out. 7 kcal/mol interval corresponds to 2.5 hydrogen bonds. For all the molecules investigated, the number of conformers remaining comprises almost the half of the number of conformers acquired by Monte Carlo method, which shows our hypothesis was highly reliable. Therefore, the most populated conformers were assumed to be included within this energy interval.

For polyols, the geometry optimization was carried out for each conformer first at B3LYP/6–31G*, and consequently at B3LYP/6–311+G** basis set levels. An additional geometry optimization was carried out to improve the convergence criterion by lowering the gradient tolerance from the default value 4.5 x 10^{-4} to 1.4 x 10^{-5}. This calculation corresponds to the "tight" option.

Due to high computational costs, tight optimization for cyclic molecules was not performed. In order to clarify how much the calculated NMR shifts vary between small and large basis sets, NMR calculations were performed for two different sets of glycol conformers; one with B3LYP/6–311+G**, the other with tight B3LYP/6–311+G** geometries. The results do not exhibit any significant difference. Therefore, NMR calculations for tagatose, fructose and sucrose are done for conformers that are optimized at B3LYP/6–31G* level. Full geometry optimization was followed by frequency calculations. NMR calculations were then performed for conformers with zero imaginary frequencies.

Since NMR responses is an average of stable conformers, a nomenclature was derived according to dihedral angles in order to categorize the conformers: G(+ or -) for gauche, T for trans positions. This nomenclature is summarized in Table 3.3.

Table 3.3. Nomenclature of dihedral angles.

Label		Dihedral Angle ϕ	
Heavy Atom Class	Hydroxy Proton Class	Minimum	Maximum
G+	g+	15	135
T	t	±135	±180
G-	g-	-135	-15
ECL	ecl	-15	15

3.2.5.2. Chemical shift calculations. NMR calculations were run on Gaussian 09 package [79] with GIAO method at the B3LYP/6–311+G** level. In order to have a reference shift NMR chemical shifts of TMS were also calculated at B3LYP/6–311+G** level. For experimentally indistinguishable atoms, the calculated shifts were averaged and the comparison with the experimental values were done accordingly. $\overline{\Delta\delta}_{\mathrm{C}}$ and $\overline{\Delta\delta}_{\mathrm{H}}$ values of each conformer were calculated as the mean absolute chemical shift difference between experimental and computational shifts of carbon and proton atom respectively.

4. RESULTS AND DISCUSSION

4.1. NMR Spectroscopy

The NMR method of choice provides the observation of exchangeable hydroxy protons once the mandatory criterion of low chemical exchange is met. Therefore, the removal of ionic catalyzers as well as the pH adjustments are of great importance. Furthermore, water suppressing pulse sequence has a great significance in order not to suppress hydroxy proton signals which lie very close to the huge water signal.

NMR active nuclei give equivalent responses as they sense the same magnetic environment. Therefore, the symmetry in poly-alcohol structures revealed identical NMR features for equivalent atoms. Except for sorbitol, polyols have a reflection plane bisecting the carbon backbone. Sorbitol has no such symmetry element, for that reason each atom behaves individually on NMR. The cyclic molecules of interest belong to C_1 point group, therefore possess no symmetry.

4.1.1. Hydroxy protons

Hydroxyl group is the common functional group that exists in all carbohydrate molecules. Hydrogen bonding attributes and hydration properties of hydroxyl groups are significantly important in terms of protein-carbohydrate complexation [28]. As the rate of chemical exchange decreases, hydroxy protons that are not observable in NMR time-scale become visible. The additional information acquired from exchangeable protons results in increased number of NOEs, thus an improved structural analysis. Furthermore, hydrogen bonding interactions can be exploited by means of the parameters mentioned in Section 3.1.

Chemical shifts (δ) and vicinal coupling constants ($^3J_{\text{HC-OH}}$), temperature coefficients ($\mathrm{d}\delta/\mathrm{d}T$), exchange rates ($k_{\text{ex}}$) and chemical shift differences ($\Delta\delta$) of hydroxy

protons are the measurable properties of exchangeable protons and can be used as structural probes. For selected natural sweeteners, these properties are given in Tables 4.1–4.9. Temperature coefficient together with $^3J_{\text{HC-OH}}$ provide the data for the comparison of hydrogen bonding properties in different molecules, whereas k_{ex} values can be examined within a single sample. The reason is the undetectable ionic content that can catalyze exchange reaction within a specific sample. Employment of different processing parameters for different samples would cause artificial differences in calculations of k_{ex}, which is entirely dependent on correct determinations of NOE peak volumes.

4.1.1.1. Vicinal coupling constants. When a hydroxy proton exchanges significantly fast with water molecules, the proton peak becomes short and broad. Thus, fast exchange prevents measuring the vicinal coupling constants. Another factor that hinders the determination of $^3J_{\text{HC-OH}}$ is spectral overlapping. As mentioned in Section 3.1.7.5, $^3J_{\text{HC-OH}}$ that deviates from 5.5 ± 1.5 Hz indicates a hydrogen bonding. Among polyols, $^3J_{\text{HC-OH}}$ could be measured only for xylitol, mannitol and sorbitol. Hydroxy protons of xylitol exhibit values of $^3J_{\text{HC-OH}}$ out of this interval. In mannitol and sorbitol, O(3)H proton exhibits 3.9 and 7.2 Hz respectively. Sorbitol's O(2)H and O(4)H protons also show notable vicinal coupling constants with a value of 7.0 Hz. These values provide a basis to state that innermost hydroxy protons are more probably involved in hydrogen bonding interactions.

The protons of hydroxyl groups bonded to anomeric carbon give a sharp singlet in both tagatose and fructose. No hydroxy proton splittings were observed for these molecules except that of O(3)H proton. This hydroxyl group is located next to the anomeric carbon and hydroxy proton signals exhibit a remarkable splitting. This is the same property in both furanose and pyranose ring of sucrose, where adjacent hydroxyl group protons split by a value of 7.5 Hz. This can be interpreted as an intramolecular hydrogen bonding interaction between these protons with the ring oxygen.

4.1.1.2. Temperature coefficients. Among NMR properties investigated, temperature coefficient calculations could give the most accurate results due to the straightforward nature of the calculation as well as low experimental and analytical errors during the determination of $\mathrm{d}\delta/\mathrm{d}T$. The investigation of temperature dependence should be made by using absolute values $\mathrm{d}\delta/\mathrm{d}T$s, since it describes the dependence of chemical shifts on temperature. The negative sign of $\mathrm{d}\delta/\mathrm{d}T$s originate from the direction of the line plotted on $\mathrm{d}\delta/\mathrm{d}T$ vs. temperature graph.

Polyol temperature coefficients that could be measured have values varying from –9.8 to –12.0 ppb deg^{-1}. For cyclic molecules of this study which are tagatose, fructose and sucrose, $\mathrm{d}\delta/\mathrm{d}T$s are in the range of –9.2 to –14.1 ppb deg^{-1}. The results are veritably higher than the previous work done for saccharides in DMSO, which states that $\mathrm{d}\delta/\mathrm{d}T$s lower than |3| ppb deg^{-1} are indicators of hydrogen bonding interactions [36], yet are in accordance with the experiments done on aqueous solutions of trisaccharides as well as Lewis b tetrasaccharide, where temperature coefficients vary between –4.8 to –14.3 and –8.1 to –12.3 ppb deg^{-1} respectively [39, 41].

Hydroxy protons involved in hydrogen bonding interactions are expected to have lower temperature dependence. The comparison of $\mathrm{d}\delta/\mathrm{d}T$s within individual polyol molecules could not reveal any general trend since the differences are significantly small. The smallest value calculated is the O(4)H proton of sorbitol with –9.8 ppb deg^{-1}. This is in agreement with vicinal coupling constant analysis which stated that the innermost hydroxy protons are, to a greater extent, associated with hydrogen bonding interactions. The highest temperature dependence is seen for sorbitol's O(1)H and glycerol's O(2)H protons followed by hydroxy proton of glycol. Interpreting the rest of $\mathrm{d}\delta/\mathrm{d}T$s may lack of accuracy due to the magnitude of differences being only slight as mentioned earlier.

Among cyclic compounds, $\mathrm{d}\delta/\mathrm{d}T$ fructose could not be acquired due to severe spectral overlapping. Proton of O(2)H group that is connected to anomeric carbon has –9.2 ppb deg^{-1}, which exhibits rather low temperature dependence. The hydroxy

proton identically located in its isomer tagatose also shows relatively low $\mathrm{d}\delta/\mathrm{d}T$ with a value of –10.1 ppb deg^{-1}. Proton of O(3)H group in tagatose which is adjacent to the anomeric carbon has the highest temperature dependence among other hydroxy protons of the molecule. The same feature was observed in the furanose ring of sucrose: O(3′)H hydroxy proton has $\mathrm{d}\delta/\mathrm{d}T$ value of –14.1 ppb deg^{-1}. In contrast, O(2)H group which is neighboring the anomeric carbon on the pyranose ring of sucrose has the lowest $\mathrm{d}\delta/\mathrm{d}T$ (–9.4 ppb deg^{-1}). Other than being adjacent to the anomeric carbon, the configurational difference between O(2)H of sucrose and O(3)H of tagatose is their equatorial and axial positions respectively.

4.1.1.3. Exchange rates. Calculation of exchange rates consists of measuring the diagonal and cross peak NOE volumes as seen in Figure 4.1. Overlapping signals therefore, hampers k_{ex} calculations. Since k_{ex} is comparable within a single molecule, interpretations of hydrogen bonding behaviors cannot be done if NOE peak volume is not precisely measured. Particularly, exchange rates of hydroxy protons in sucrose and fructose could not be calculated due to overlapping of signals. This signifies that hydroxy protons within these molecules have similar magnetic environments resulting in similar chemical shifts.

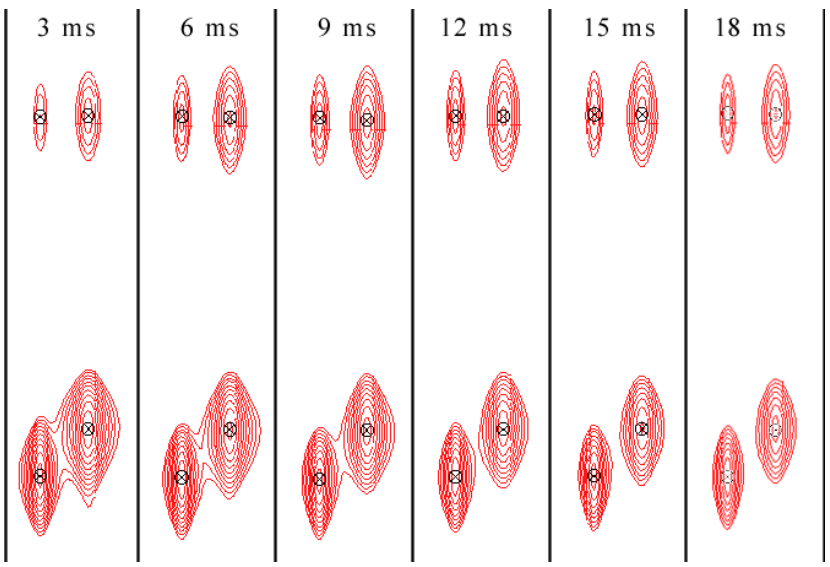

Figure 4.1. Hydroxy proton peaks in NOESY spectra of glycerol.

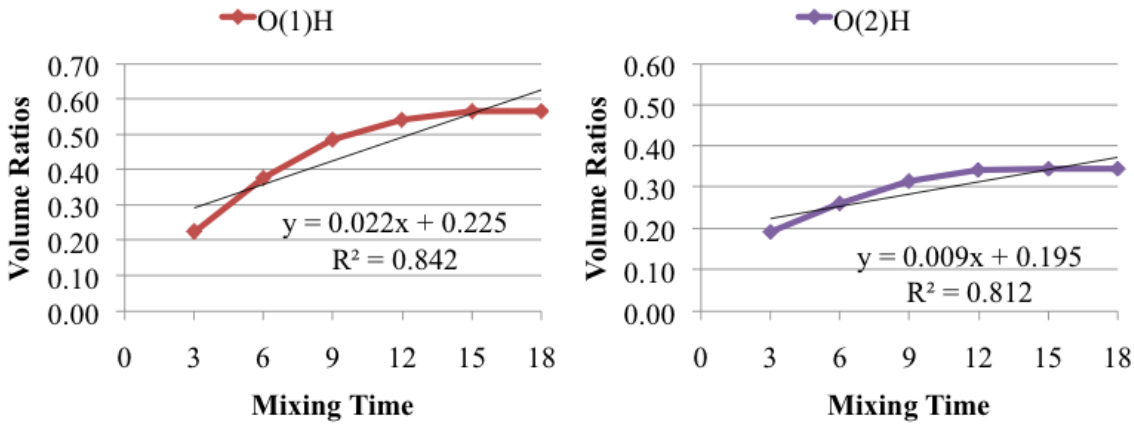

Figure 4.2. Dependence of volume ratios on the mixing time in NOESY spectra of glycerol. As the mixing time increases, the ratio of cross peak volume over diagonal peak volume decreases. k_{ex} is calculated as the slope of the line fitted through data points.

At the first glance, relatively fast exchange rate of hydroxy protons of hydroxymethyl groups is seen as the general trend on all studied molecules. This is undoubted consequence of terminal hydroxy protons being exposed to bulk water to a greater extent than inner hydroxy protons. Rapid exchange rates are also responsible for the disappearance of ${}^{3}J_{\mathrm{HC\text{-}OH}}$ that is an interaction through bonds.

Lower k_{ex} values of inner hydroxy protons examined indicate their greater tendency to be involved in hydrogen bonding interactions compared to terminal ones. There is only one type of inner hydroxy proton in glycerol and erythritol. In both molecules k_{ex} is the only property that can be compared in terms of hydrogen bonding since no vicinal coupling was observed and $\mathrm{d}\delta/\mathrm{d}T$ values are considerably similar.

The k_{ex} values O(2)H and O(3)H protons of xylitol do not differ notably. Their ${}^{3}J_{\mathrm{HC\text{-}OH}}$ values, as well as $\mathrm{d}\delta/\mathrm{d}T$ are also indistinguishable. Therefore, no conclusion can be drawn to rank hydrogen bonding tendencies of inner hydroxy protons of xylitol. Upon consideration of 6-carbon chains, mannitol and sorbitol, k_{ex} values of inner hydroxy protons differ to a greater extent. Exchange rate of the innermost hy-

droxy proton of mannitol, that is O(3)H, is notably smaller than of O(1)H proton. The ${}^3J_{\text{HC-OH}}$ value of O(3)H also indicates a restricted rotation, hence a hydrogen bonding. Comparison between O(2)H and O(3)H protons do not significantly differ regarding k_{ex} nor $\mathrm{d}\delta/\mathrm{d}T$ values. The identically located hydroxy protons of the other 6-carbon chain sorbitol are those attached to O(3)H and O(4)H groups. As stated earlier, sorbitol does not has a symmetry axis, hence atoms behave non equivalently. O(3)H proton of sorbitol was observed as having a relatively faster exchange rate than the other inner hydroxy protons. This very proton has no remarkable low temperature dependence either. However, the coupling constant value of 7.2 Hz reveals a hydrogen bonding possibility. O(4)H proton of sorbitol, which was identified as having relatively low temperature dependence (–9.8 ppb/K) and ${}^3J_{\text{HC-OH}}$ value of 7.0 Hz, has remarkably slow exchange rate. This hydroxy proton exhibits similar attributes to mannitol's O(3)H in terms of k_{ex} and $\mathrm{d}\delta/\mathrm{d}T$. In addition, ${}^3J_{\text{HC-OH}}$ values of both protons (3.9 Hz in mannitol, 7.0 Hz in sorbitol) are in the borders of the interval experimentally chosen as an indicator of hydrogen bonding, which is 5.5 ± 1.5 Hz. The innermost hydroxy protons in both molecules most likely take part in intramolecular hydrogen bondings.

Exchange rates of fructose did not yield any evidence concerning the hydrogen bonding attributes, since k_{ex} could be calculated only for one hydroxy proton. Sucrose is also missing k_{ex} values, for pyranose ring in particular. Similar to polyols, largest k_{ex} values were calculated for those protons that are bound to freely rotating hydroxy methyl groups in both tagatose and sucrose. The other relatively large k_{ex} values were calculated for O(4)H and O(5)H hydroxy protons of tagatose, which are in equatorial position and located distant to both anomeric carbon and ring oxygen. O(3)H proton has the lowest k_{ex}, yet its temperature dependence is more pronounced in contrast. Furthermore the ${}^3J_{\text{HC-OH}}$ value of this proton indicates a free rotation. These findings show that even though O(3)H proton exhibits a slow exchange with water, it does not get involved in hydrogen bonding apparently. This might be due to hindered contact with bulk water at its axial position. Such steric factors can also be observed for O(4′)H proton of sucrose, which is located in furanose ring. This hydroxy proton also displays distinctly low k_{ex} value but high temperature dependence and a ${}^3J_{\text{HC-OH}}$

value showing a free rotation. O(3′)H proton of sucrose has the lowest k_{ex} value and significant vicinal coupling constant, yet high temperature dependence. It is most likely included in a hydrogen bonding, nonetheless increasing the temperature alters its magnetic environment drastically.

4.1.1.4. Chemical shift differences in tagatose and fructose. The isomeric difference between tagatose and fructose is illustrated in Figure 4.3. Contrary to its isomer tagatose, hydroxy protons of fructose give overlapping signals. Therefore, examination of hydrogen bonding properties of hydroxy protons on fructose can be achieved by examination of $\Delta\delta$ values. Chemical shifts of O(5)H and C(6) groups of each molecule do not show any remarkable difference as expected. However O(2)H, O(3)H and O(4)H group hydroxy protons of tagatose have relatively large positive $\Delta\delta$ values as seen in Tables 4.7 and 4.8. Larger positive $\Delta\delta$ value is an indication of increase in hydrogen bonding cooperation with solvent molecules [54]. The comparison of geometrical structures also supports this finding; O(2)-O(3) as well as C(1)-O(4) proximity in fructose result in a geometry where contact to water molecules is somewhat reduced at both sides of the ring.

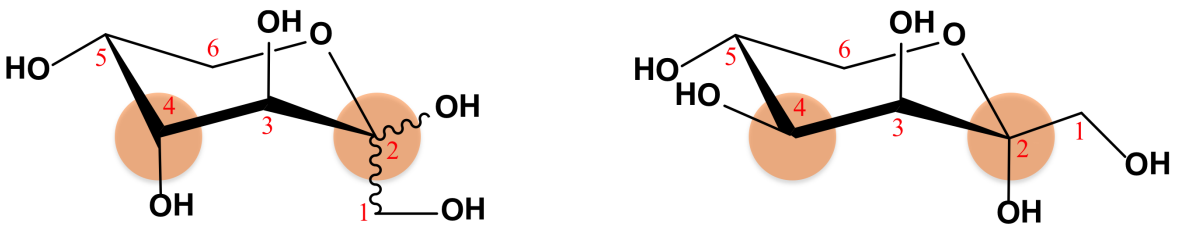

a) b)

Figure 4.3. Structural differences between (a)Fructose and (b)Tagatose.

Table 4.1. Glycol experimental results.

Group	δ (^{13}C) (ppm)	δ (^{1}H) (ppm)	$^{3}J_{\text{HC-OH}}$ (Hz)	$\mathrm{d}\delta/\mathrm{d}T$ (ppb deg^{-1})	k_{ex} (s^{-1})
C(1)H	65.161	3.673	n/a	-	-
O(1)H	-	5.871	n/a	-11.72	19.67[a]

[a] NOE cross peaks due to chemical exchange were observed only until τ=12 ms.

Table 4.2. Glycerol experimental results.

Group	δ (^{13}C) (ppm)	δ (^{1}H) (ppm)	$^{3}J_{\text{HC-OH}}$ (Hz)	$\mathrm{d}\delta/\mathrm{d}T$ (ppb deg^{-1})	k_{ex} (s^{-1})	$\Delta\delta$ (ppm)
C(1)H$_a$	65.319	3.656	n/a	-	-	-
C(1)H$_b$	65.319	3.561	n/a	-	-	-
C(2)H	75.013	3.782	n/a	-	-	-
O(1)H	-	5.884	n/a	-11.70	22.27	0.013
O(2)H	-	5.984	n/a	-11.96	9.90	0.113

Table 4.3. Eryhtritol experimental results.

Group	δ (^{13}C) (ppm)	δ (^{1}H) (ppm)	$^{3}J_{\text{HC-OH}}$ (Hz)	$\mathrm{d}\delta/\mathrm{d}T$ (ppb deg^{-1})	k_{ex}[a] (s^{-1})	$\Delta\delta$ (ppm)
C(1)H$_a$	65.254	3.801	n/a	-	-	-
C(1)H$_b$	65.254	3.636	n/a	-	-	-
C(2)H	75.392	3.658	n/a	-	-	-
O(1)H	-	5.802	n/a	-11.10	8.25	0.064
O(2)H	-	5.966	n/a	-11.00	0.90	0.098

[a] Outliers omitted and the graph plotted for values of 6, 12 and 15 ms only.

Table 4.4. Xylitol experimental results.

Group	δ (^{13}C) (ppm)	δ (^{1}H) (ppm)	$^{3}J_{\text{HC-OH}}$ (Hz)	$\mathrm{d}\delta/\mathrm{d}T$ (ppb deg^{-1})	k_{ex} (s^{-1})	$\Delta\delta$ (ppm)
C(1)H$_a$	65.449	3.732	n/a	-	-	-
C(1)H$_b$	65.449	3.656	n/a	-	-	-
C(2)H	74.847	3.815	4.3	-	-	-
C(3)H	73.645	3.652	5.5	-	-	-
O(1)H	-	5.881	n/a	–11.20	17.44	0.010
O(2)H	-	5.748	4.3	–10.46	9.44	0.123
O(3)H	-	5.555	5.5	–10.32	9.60	0.316

Table 4.5. Mannitol experimental results.

Group	δ (^{13}C) (ppm)	δ (^{1}H) (ppm)	$^{3}J_{\text{HC-OH}}$ (Hz)	$\mathrm{d}\delta/\mathrm{d}T$ (ppb deg^{-1})	k_{ex} (s^{-1})	$\Delta\delta$ (ppm)
C(1)H$_a$	66.216	3.892	n/a	-	-	-
C(1)H$_b$	66.216	3.679	n/a	-	-	-
C(2)H	73.437	3.764	5.8	-	-	-
C(3)H	71.846	3.809	3.9	-	-	-
O(1)H	-	5.798	n/a	-10.53	90.47	0.073
O(2)H	-	5.600	5.8	-11.02	14.12	0.271
O(3)H	-	5.874	3.9	-10.31	9.06	0.003

Table 4.6. Sorbitol experimental results.

Group	δ (^{13}C) (ppm)	δ (^{1}H) (ppm)	$^{3}J_{\text{HC-OH}}$ (Hz)	$\mathrm{d}\delta/\mathrm{d}T$ (ppb deg^{-1})	k_{ex} (s^{-1})	$\Delta\delta$ (ppm)
C(1)H$_a$	65.199	3.751	n/a	-	-	-
C(1)H$_b$	65.199	3.627	n/a	-	-	-
C(2)H	75.955	3.849	7.0[a]	-	-	-
C(3)H	72.484	3.862	7.2	-	-	-
C(4)H	73.737	3.643	7.0	-	-	-
C(5)H	73.663	3.776	6.0	-	-	-
C(6)H$_a$	65.739	3.845	n/a	-	-	-
C(6)H$_b$	65.739	3.651	n/a	-	-	-
O(1)H	-	5.872	n/a	-11.90	10.09	0.001
O(2)H	-	5.805	7.0[a]	n/a[b]	n/a[b]	0.066
O(3)H	-	5.501	7.2	-10.50	8.42	0.370
O(4)H	-	5.727	7.0	-9.80	3.92	0.144
O(5)H	-	5.924	6.0	-10.70	6.20	0.053
O(6)H	-	5.787	n/a	n/a[b]	n/a[b]	0.084

[a] Calculated by spin simulation.

[b] Chemical shifts and peak volumes cannot be measured due to overlapping.

Table 4.7. Tagatose experimental results.

Group	δ (^{13}C) (ppm)	δ (^{1}H) (ppm)	$^{3}J_{\text{HC-OH}}$ (Hz)	$\mathrm{d}\delta/\mathrm{d}T$ (ppb deg^{-1})	k_{ex} (s^{-1})	$\Delta\delta$ (ppm)
C(1)H$_a$	66.699	3.497	n/a	-	-	-
C(1)H$_b$	66.699	3.742	n/a	-	-	-
C(2)	101.178	-	-	-	-	-
C(3)H	72.511	3.903	5.9	-	-	-
C(4)H	73.863[b]	3.860[c]	n/a	-	-	-
C(5)H	69.297[b]	3.860[c]	n/a	-	-	-
C(6)H$_{ax}$	65.049	3.642[c]	-	-	-	-
C(6)H$_{eq}$	65.049	3.758	-	-	-	-
O(1)H	-	5.942	n/a	-11.06	17.85[a]	0.071
O(2)H	-	6.801	n/a	-10.12	8.69[a]	0.930
O(3)H	-	6.127	5.9	-12.16	6.35[a]	0.256
O(4)H	-	6.302	n/a	-11.04	10.30[a]	0.431
O(5)H	-	6.034	n/a	-10.80	13.71[a]	0.163

[a] NOESY spectra with 15 ms and 18 ms cannot be processed by the same parameters, hence calculation done until 12 ms.

[b] Ambiguity resolved by comparison with mannose, similar compound of which full assignment is accessible.

[c] Read from HSQC spectrum.

Table 4.8. Fructose experimental results.

Group	δ (^{13}C) (ppm)	δ (^{1}H) (ppm)	$^{3}J_{\text{HC-OH}}$ (Hz)	$\mathrm{d}\delta/\mathrm{d}T$ (ppb deg^{-1})	k_{ex} (s^{-1})	$\Delta\delta$ (ppm)
C(1)H$_a$	66.609	3.548	n/a	-	-	-
C(1)H$_b$	66.609	3.729	n/a	-	-	-
C(2)	101.021	-	-	-	-	-
C(3)H	70.196	3.816	6.7	-	-	-
C(4)H	72.598	3.904	n/a	-	-	-
C(5)H	72.153	3.999	n/a	-	-	-
C(6)H$_{ax}$	66.150	3.700	-	-	-	-
C(6)H$_{eq}$	66.150	4.036	-	-	-	-
O(1)H	-	5.935	n/a	n/a[a]	n/a[b]	0.064
O(2)H	-	6.475	n/a	-9.20	2.41	0.604
O(3)H	-	5.962	6.7	-11.46	n/a[b]	0.091
O(4)H	-	6.003	n/a	n/a[d]	n/a[c]	0.132
O(5)H	-	6.003	n/a	n/a[d]	n/a[c]	0.132

[a] Signal disappears at 273K.

[b,c] Peak volumes cannot be measured due to overlapping.

[d] Temperature coefficient calculated as -11.8, however signals are overlapped.

Table 4.9. Sucrose experimental results.

Group	δ (^{13}C)[a] (ppm)	δ (^{1}H) (ppm)	$^{3}J_{\text{HC-OH}}$ (Hz)	$\mathrm{d}\delta/\mathrm{d}T$ (ppb deg^{-1})	k_{ex} (s^{-1})	$\Delta\delta$ (ppm)
C(1)H	94.674	5.414	-	-	-	-
C(2)H	73.677	3.548	7.5	-	-	-
C(3)H	75.146	3.768	n/a	-	-	-
C(4)H	71.683	3.482	6.3	-	-	-
C(5)H	74.876	3.875	-	-	-	-
C(6)H	62.505	3.833	n/a	-	-	-
C(1′)H$_a$	63.550	3.678	n/a	-	-	-
C(1′)H$_b$	63.550	3.651	n/a	-	-	-
C(3′)H	78.529	4.237	7.5	-	-	-
C(4′)H	76.350	4.063	5.4	-	-	-
C(5′)H	83.990	3.894	-	-	-	-
C(6′)H	64.994	3.841	n/a	-	-	-
O(2)H	-	6.245	7.5	-9.38	5.72	0.374
O(3)H	-	6.376	n/a	-11.78[b]	n/a[c]	0.505
O(4)H	-	6.387	6.3	-10.92[b]	n/a[c]	0.516
O(6)H	-	5.903	n/a	-11.80	n/a[d]	0.032
O(1′)H	-	6.080	n/a	-10.96	12.27	0.209
O(3′)H	-	6.458	7.5	-14.08	3.29	0.587
O(4′)H	-	6.771	5.4	-10.60	3.78	0.900
O(6′)H	-	5.903	n/a	-11.80	n/a[d]	0.032

[a] Read from HSQC spectrum.

[b] Peaks disappear at 283K, calculation done by considering data points of 263K, 268K, 273K, 278K only.

[c,d] Peak volumes cannot be measured due to overlapping.

4.1.2. Observation of geminal coupling constants

4.1.2.1. Poly-alcohols. On account of the open-chain structure of polyols, they are expected to be highly flexible. Methylene hydrogens are chemically equivalent due to the rotation between hydroxymethyl group and adjacent carbon. Hydroxyl groups are sterically free to be involved in hydrogen bonding interactions with bulk water, which can further rotate torsions. This leads to an expectation that methylene protons would give identical NMR responses due to averaging of magnetic environments. Glycol, that is the smallest polyol with two –OH groups, no couplings were observed, displaying no restriction on geometry. However as the chain gets longer, methylene hydrogens starts to couple with each other due to the diastereotopicity.

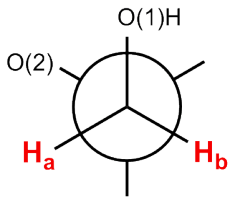

Figure 4.4. Schematic representation of geminal couplings of metylene protons.

A geminal coupling ($^2J_{\mathrm{H–H}}$) results from the magnetic environment difference of protons attached to the same carbon. The absence of geminal couplings in glycol shows that the methylene protons are magnetically equivalent. That is highly predictable due to low rotational barrier along C–C bond (Figure 4.5). Glycerol (Figure 4.6), which is also a fairly small molecule with only three carbon atoms, geminal coupling between methylene protons is observed as seen in Figure 4.7. This indicates that magnetic, hence chemical environment of these protons are not equivalent - displaying the diastereotopicity. The same feature is detected for other polyols examined as well (Tables 4.11–4.14).

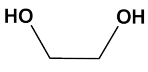

Figure 4.5. Glycol structure.

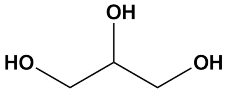

Figure 4.6. Glycerol structure.

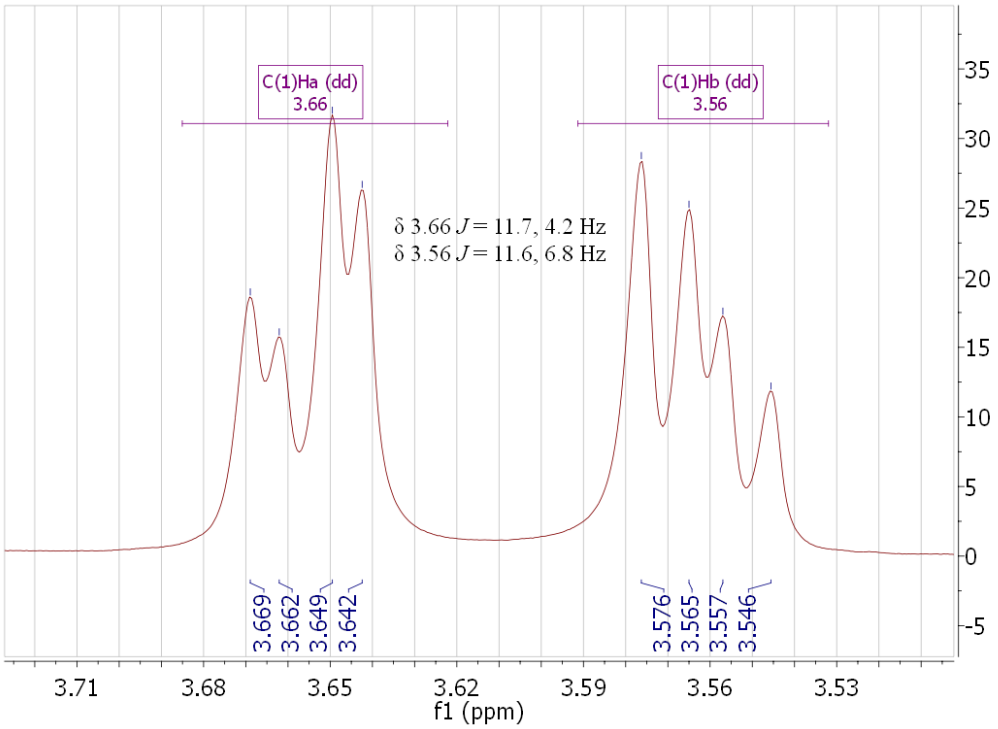

Figure 4.7. Geminal couplings of glycerol.

Table 4.10. Glycerol coupling constants.

Atom	$J_{\text{H–H}}$ (Hz)
C(1)$\mathbf{H}_a$-C(1)$\mathbf{H}_b$	-11.7
C(1)$\mathbf{H}_a$-C(2)$\mathbf{H}$	4.2
C(1)$\mathbf{H}_b$-C(2)$\mathbf{H}$	6.6

Table 4.11. Erythritol coupling constants.

Atom	$J_{\text{H–H}}$ (Hz)
C(1)$\mathbf{H}_a$-C(1)$\mathbf{H}_b$	-11.0
C(1)$\mathbf{H}_a$-C(2)$\mathbf{H}$	1.4[a]
C(1)$\mathbf{H}_b$-C(2)$\mathbf{H}$	4.3[a]

[a] Calculated by spin simulation.

Table 4.12. Xylitol coupling constants.

Atom	$J_{\text{H–H}}$ (Hz)
C(1)$\mathbf{H}_a$-C(1)$\mathbf{H}_b$	-11.3
C(1)$\mathbf{H}_a$-C(2)**H**	2.8
C(1)$\mathbf{H}_b$-C(2)**H**	7.0[a]
C(2)**H**-C(3)**H**	2.0[a]

[a] Calculated by spin simulation.

Table 4.13. Mannitol coupling constants.

Atom	$J_{\text{H–H}}$ (Hz)
C(1)$\mathbf{H}_a$-C(1)$\mathbf{H}_b$	-12.1
C(1)$\mathbf{H}_a$-C(2)**H**	1.3
C(1)$\mathbf{H}_b$-C(2)**H**	6.2
C(2)**H**-C(3)**H**	8.6

Table 4.14. Sorbitol coupling constants.

Atom	$J_{\text{H–H}}$ (Hz)
C(1)$\mathbf{H}_a$-C(1)$\mathbf{H}_b$	-12.0
C(1)$\mathbf{H}_a$-C(2)**H**	2.0
C(1)$\mathbf{H}_b$-C(2)**H**	3.0
C(2)**H**-C(3)**H**	5.8
C(3)**H**-C(4)**H**	3.2
C(4)**H**-C(5)**H**	3.0
C(5)**H**-C(6)$\mathbf{H}_a$	5.8
C(5)**H**-C(6)$\mathbf{H}_b$	7.3
C(6)$\mathbf{H}_a$-C(6)$\mathbf{H}_b$	-11.6

4.1.2.2. Cyclic natural sweeteners. Coupling constants of tagatose, fructose and sucrose are tabulated in Tables 4.15–4.17. The measurements on these cyclic molecules also reveal existence of geminal couplings. One being equatorial and the other axial, methylene protons in the ring of tagatose and fructose are chemically inequivalent, therefore couple with each other. The only "free-rotating" torsion outside the ring is C(1)–C(2) (Figure A.7a, A.8a). Yet geminal couplings are also observed for the hydroxymethyl groups attached to C(1), which indicates a restricted rotation along C(1)–C(2). This, however, is more likely to foresee due to the cyclic structure, as well as the geminal hydroxyl group –O(2)H, that is positioned axial on tagatose and equatorial on fructose. The geometrical restrictions lead to the diastereotopicity of the terminal methylene protons.

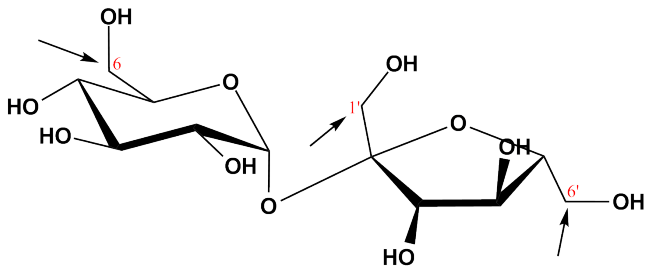

Figure 4.8. Methylene groups in sucrose structure.

Sucrose has three methylene groups; two on furanose and one on pyranose ring (Figure 4.8). HSQC spectrum illustrates C–H interactions on methylene groups as single cross peaks (Figure 4.9). Diastereotopic hydrogens give different cross peaks with the adjacent carbon atom, whereas homotopic protons behave as a single nuclei. Single cross peak therefore implies that magnetic behavior of methylene protons of sucrose do not exhibit any significant difference. This is an evidence of low rotational barrier along C(5)–C(6), C(1′)–C(2′) and C(5′)–C(6′) torsions. However on ^{1}H NMR spectrum, C(1′)H and C(6′)H signals are shaped in a manner showing diastereotopicity to some extent. For instance on ^{1}H NMR spectrum, consideration of C(6′)H (δ=3.841) and C(6)H (δ=3.833) peaks results in an integration ratio of 1:3 (Figure 4.10). It indicates that half of the C(6′)H peak lies under the strong singlet of C(6)H at δ=3.833. Thus it is clear that $^{2}J_{\mathrm{H–H}}$ exists, yet not possible to be measured due to spectral overlapping.

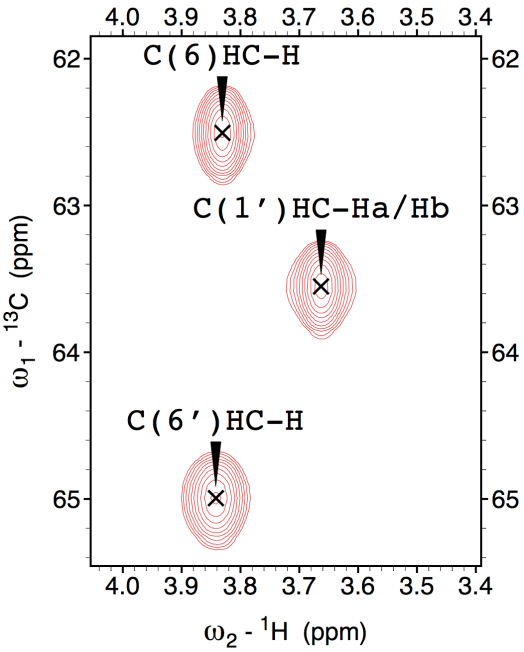

Figure 4.9. Methylene group crosspeaks of sucrose in HSQC spectrum.

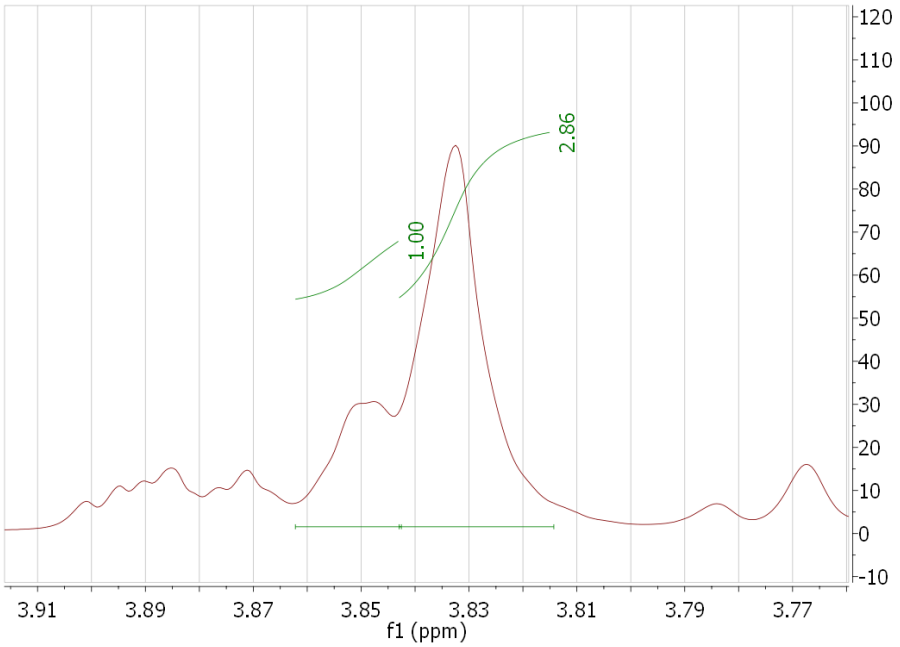

Figure 4.10. Integrations of C(6)H and C(6′)H signals on ^{1}H NMR spectrum of sucrose.

Examination of C(1′)H group, which is the other methylene group on furanose ring, also displays the presence of geminal couplings on ^{1}H NMR spectrum. Diastereotopic hydrogens of methylene groups form a AB spin system. When chemical shift difference between A and B is less than $^{2}J_{\mathrm{H-H}}$ (namely bearing a second order coupling), the integration of signals distorts in a way that coupling peaks close to each other become bigger than the outer coupling peaks. This distortion is called "roof effect". In Figure 4.11, the signal resulting from C(1′) protons leads to two doublet peaks under a strong roof effect. Therefore, it can be assumed that protons of C(1′)H group are diastereotopic and their chemical shifts are distinctly close to each other.

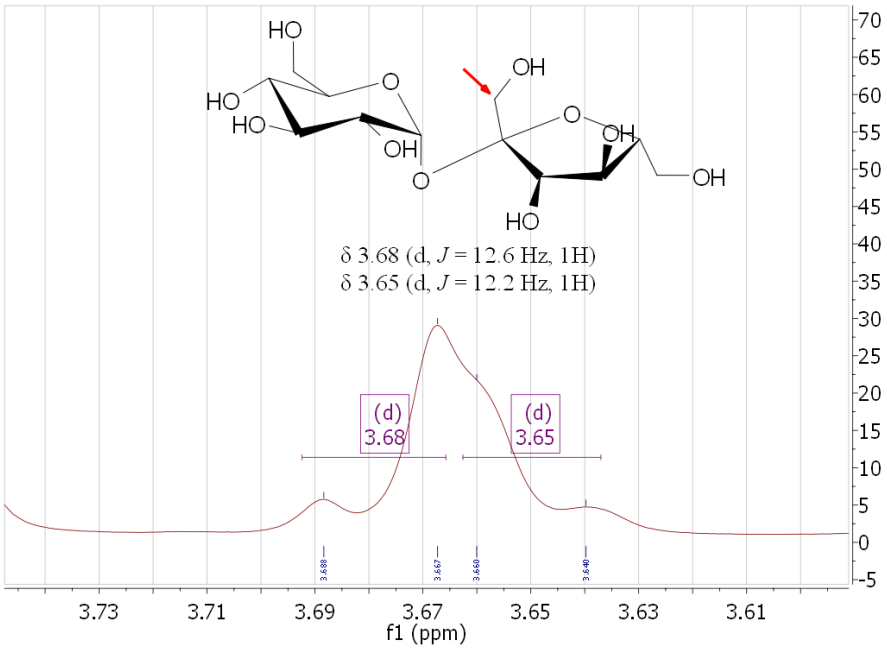

Figure 4.11. C(1′)H signals on ^{1}H NMR spectrum of sucrose.

The only methylene group on sucrose that does not exhibit any geminal coupling is the one situated in pyranose ring, C(6)H. It is observed as a sharp singlet at δ=3.833. These protons have the same magnetic environment contrary to its counterparts on furanose ring. The reason of diastereotopicity on furanose ring may arise from steric hindrances in five-membered ring.

Table 4.15. Tagatose coupling constants.

Atom	$J_{\text{H–H}}$ (Hz)
C(1)$\mathbf{H}_a$-C(1)$\mathbf{H}_b$	-12.5
C(3)**H**-C(4)**H**	3.8
C(4)**H**-C(5)**H**	n/a
C(5)**H**-C(6)$\mathbf{H}_{ax}$	n/a
C(5)**H**-C(6)$\mathbf{H}_{eq}$	n/a
C(6)$\mathbf{H}_{ax}$-C(6)$\mathbf{H}_{eq}$	-10.0

[a] Calculated by spin simulation.

Table 4.16. Fructose coupling constants.

Atom	$J_{\text{H–H}}$ (Hz)
C(1)$\mathbf{H}_a$-C(1)$\mathbf{H}_b$	-11.9
C(3)**H**-C(4)**H**	9.8
C(4)**H**-C(5)**H**	n/a
C(5)**H**-C(6)$\mathbf{H}_{ax}$	1.6
C(5)**H**-C(6)$\mathbf{H}_{eq}$	n/a
C(6)$\mathbf{H}_{ax}$-C(6)$\mathbf{H}_{eq}$	-13.3

Table 4.17. Sucrose coupling constants.

Atom	$J_{\mathrm{H–H}}$ (Hz)
C(1)**H**-C(2)**H**	3.8
C(2)**H**-C(3)**H**	10.0
C(3)**H**-C(4)**H**	10.0
C(4)**H**-C(5)**H**	4.2
C(5)**H**-C(6)**H**	n/a
C(1′)$\mathbf{H}_a$-C(1′)$\mathbf{H}_b$	-12.8
C(3′)**H**-C(4′)**H**	8.2
C(4′)**H**-C(5′)**H**	6.1
C(5′)**H**-C(6′)**H**	3.1

[a] Calculated by spin simulation.

4.2. Computational Results

Conformational analysis and NMR calculations integrated with experimental data can provide a satisfactory knowledge about real-life geometries of molecules. Conformational analysis of this work was basically done gathering single conformers located in different wells on the PES. For each different conformer, NMR calculations were performed. Experimental chemical shifts were then compared with calculated ones for each conformer.

Since this study focuses mostly on hydroxy protons, hydrogen bonding properties are immensely important. The computational methodology of molecular modeling deals with molecules *in vacuo*. Therefore, hydrogen bonding features with water cannot be analyzed. Since experimental NMR responses result from a set of most stable conformations in water, it is also applicable to search for conformers with chemical shifts that are close to experimental ones.

The range of ^{1}H shifts is considerably smaller than ^{13}C shifts. For instance, the maximum $\overline{\Delta\delta}_{\mathrm{C}}$ value of glycerol is 7.566, whereas it is 0.564 for ^{1}H. In order to widen the confidence interval, ^{13}C shift differences are compared primarily. In addition, ^{13}C shifts are less sensitive to non-bonding interactions. Hence it is obvious to have similar $\overline{\Delta\delta}_{\mathrm{C}}$ values for each heavy atom class. The data extracted from the results of calculations are presented in Table 4.18 and Tables 4.23–4.37, sorted in ascending order of $\overline{\Delta\delta}_{\mathrm{C}}$ values.

4.2.1. Comparison of computational and experimental results

Conformer distribution of glycol by Monte Carlo method led to 7 different conformations. This small number of conformers is due to glycol's having only one heavy atom torsion. In fact, a closer look would reveal only two different types of heavy atom classes; G(+ or -) and T. The difference within heavy atom group conformations is a consequence of different positions of hydroxy protons. As seen in Table 4.18, there is

no conformer that belongs to G+. It is clear that G+ is equivalent to G- when there is only one torsion. Not seeing any G+ conformer is basically an output of the software, where *symmetry* option is checked in order to simplify the calculations.

Table 4.18. Glycol computational results and $\overline{\Delta\delta}$ values.

Conformer	Rel. E (kcal/mol)	ϕ (degrees)			ϕ Class		$\overline{\Delta\delta}_{\mathrm{C}}$ (ppm)	$\overline{\Delta\delta}_{\mathrm{H}}$ (ppm)
		O1–C1–C2–O2	H1–O1–C1–C2	C1–C2–O2–H2	O–C–C–O	H–O–C–C		
04	2.72	180	180	180	T	tt	2.491	0.264
01	0.00	-62	166	53	G-	tg+	3.330	0.218
05	2.77	-180	-174	71	T	tg+	3.687	0.176
03	0.93	-60	82	82	G-	g+g+	4.289	0.126
06	2.76	180	-69	69	T	g-g+	4.784	0.246
02	0.51	-58	-75	45	G-	g-g+	4.849	0.058
08	3.10	-177	-65	-65	T	g-g-	5.007	0.129

Energetical ranking of glycol conformers indicates that hydrogen bonds lower the energy of the conformer. T class conformers, which do not have intramolecular hydrogen bondings, have relatively higher energy than of G- class, where energy is stabilized by a hydrogen bonding between H2$\cdots$O1. Table 4.18 shows that G- and T classes are almost equally occupied in aqueous medium. Among individual conformers, **04** has the closest $\overline{\Delta\delta}_{\mathrm{C}}$ to the experimental value. As discussed earlier, hydroxy protons of glycol are in fast exchange with water. Thus it can be assumed that chemical shifts of carbon atoms are not affected by hydroxy protons in the molecule. Conformer **04** has an inversion point between C–C bond (namely bears a C_i symmetry), where hydroxy protons are positioned totally opposite to each other, therefore, equivalent and

have the same magnetic contribution to carbon atoms. They *do* contribute to carbon shifts, yet by the same extent. This can be regarded as the reason of closest value to experimental results.

Glycerol structure can have maximum of two hydrogen bonds. In terms of hydrogen bondings, relative energies of conformations indicate a similar trend to those in glycol that possess two hydrogen bonds have lower energy. Energy order is followed by the conformers where two hydroxy protons of hydroxy methyl groups form a hydrogen bond with the oxygen atom in the middle. Sharing the hydrogen proton acceptor lessens the strength of interaction. Conformers with relatively high energies are those with only one hydrogen bond. The topological examination of conformers revealed the equivalence of certain heavy atom classes, as **G+T** is equivalent to TG-, **G+G+** to G-G-, **G-T** to TG+ and **G+G-** to G-G+. For the simplicity, labels in bold are used as the representative of the heavy atom class.

According to ranking of $\overline{\Delta\delta}_{\mathrm{C}}$ values, conformers of G+T class were found out to have the closest values to experimental results. This class involves only one hydrogen bond (Table 4.23). It is followed by G-G-, G-G+ and G-T classes subsequently. Both G-G- and G-G+ groups consist two hydrogen bonds, which are ranked second and third respectively. Fourthly ranked G-T class also involves one hydrogen bond. TT class conformers have the furthest $\overline{\Delta\delta}_{\mathrm{C}}$ values by a minimum value of 6.787 ppm. Even though TT class does not have the highest calculated energy, it has the fewest population in aqueous solution.

Conformers with the smallest $\overline{\Delta\delta}_{\mathrm{C}}$ within each group are extracted as the best class representatives (Table 4.19). The commonality between these conformers except conformer **20** is the involvement of O(2)H hydroxyl group in hydrogen bonding as either donor or acceptor. Conformer **20**, which has the highest $\overline{\Delta\delta}_{\mathrm{C}}$ among representatives, consists of a hydrogen bond between H1$\cdots$O3 and no involvement of O(2)H hydroxyl group in terms of non-bonding interactions by any means.

Among the conformers of G+T class, **05** has the closest $\overline{\Delta\delta}_C$ value (0.467 ppm) to experimental result. The conformer belonging to the same group but with the largest difference to experimental is **35** ($\overline{\Delta\delta}_C$=3.575 ppm). The difference between **05** and **35** is due to their different hydrogen bonding patterns. On conformer **05**, the hydrogen bond is established between H2$\cdots$O1. In other words, members of AH–B pair are located in adjacent positions. Whereas on **35**, O(3)H proton is in proximity to O(1), namely is interacting from one edge to the other. The absence of O(2)H group in hydrogen bonding interaction should also be stressed, as in the case of TT class with large $\overline{\Delta\delta}_C$ values. The same property that notably alters $\overline{\Delta\delta}_C$s is also observed in G+G- class. Conformer **12** which has the closest carbon chemical shifts to experimental results has two hydrogen bonds, H2$\cdots$O1 and H3$\cdots$O2. While belonging to the same group but with the largest $\overline{\Delta\delta}_C$ value, conformer **36** includes H2$\cdots$O3 and H3$\cdots$O1 interactions. It indicates that edge-to-edge hydrogen bondings, where O(2)H group is excluded from hydrogen bonding, dramatically decrease the accuracy of calculated shifts.

Table 4.19. Best class representative conformers of glycerol.

Conformer	Rel. E	ϕ Class		$\overline{\Delta\delta}_C$	$\overline{\Delta\delta}_H$
	(kcal/mol)	O–C–C–O	H–O–C–C	(ppm)	(ppm)
05	2.51	G+T	tg+t	0.467	0.069
01	0.00	G-G-	ttg+	2.216	0.098
12	0.66	G-G+	ttg-	3.322	0.361
40	2.42	G-T	ttt	3.854	0.498
20	3.01	TT	g-tt	6.787	0.296

Erythritol, having four –OH groups, can form three hydrogen bonds. The low energy conformers are therefore those that form three hydrogen bonds intramolecularly. However, the most energetically favored conformer of erythritol is **34**, which has two hydrogen bondings. Conformer **34** is sterically favored due to trans geometry of carbon backbone.

As in the case of previous molecules, different group labels might represent the same topology. For instance, when carbon backbone is in trans position, the hydroxyl dihedral class G+TT is the mirror image of TTG+. Therefore, even though there are six different conformer classes for trans positioned carbon backbone, there are four unique labels. In total, erythritol conformers constitute 11 unique classes. For each class, the conformations that have the smallest difference of carbon chemical shifts to real values are shown in Table 4.20.

Table 4.20. Best class representative conformers of erythritol.

Conformer	Rel. E	ϕ Class			$\overline{\Delta\delta}_{\mathrm{C}}$	$\overline{\Delta\delta}_{\mathrm{H}}$
	(kcal/mol)	C–C–C–C	O–C–C–O	H–O–C–C	(ppm)	(ppm)
38	1.88	T	G-TG+	tg-g-t	0.928	0.344
17	3.46	G-	TG-G-	tg+g+g-	1.540	0.232
12	1.45	G+	G+G+G-	tttg+	1.922	0.222
01	0.92	G+	G+G+G+	tttg-	2.246	0.224
51	3.62	G+	TG+T	tg-g+g-	2.597	0.241
25	2.49	T	G+TG+	g+tg-t	2.724	0.282
22	3.41	G+	G-G+T	g-g-tt	3.008	0.333
24	3.77	G-	G+G-T	ttg-g+	3.374	0.291
06	1.75	G+	G-G+G-	g-g-tg+	4.169	0.206
74	2.65	T	TTG+	g+tg-t	4.943	0.214
54	5.30	T	TTT	tg+tt	6.794	0.319

The number of intramolecular hydrogen bonds in erythritol conformers does not significantly affect $\overline{\Delta\delta}_{\mathrm{C}}$ ranking, as in the case of glycerol. It is also observed that when hydroxyl class bears more than one trans position, the $\overline{\Delta\delta}_{\mathrm{C}}$s are getting larger. That is a result of intramolecular hydrogen bonds formed between hydroxyl groups that are four-bonds away to each other. It is identical to the situation in glycerol, in which edge-to-edge hydrogen bonds deviates from experimental shifts. The smallest $\overline{\Delta\delta}_{\mathrm{C}}$ value was observed for conformer **38**, which has a pair of intramolecular hydrogen

bonds between H2$\cdots$O1 and H3$\cdots$O4. The hydroxyl oxygens O(1) and O(4) behave as hydrogen bond acceptor, and neighboring inner –OH groups behave as donor. It is a homologous pattern seen for glycerol, where involvement of inner hydroxyl oxygen in hydrogen bonding causes carbon chemical shifts to get closer to experimental values.

As the chain gets longer, the presumed class accumulations cannot be observed. Five-carbon chain xylitol have 31 classes identified among 42 conformers examined (Table 4.26). Steric factors are found out to be more determinant than hydrogen bonding interactions regarding the energy calculations. $\overline{\Delta\delta}_{\mathrm{C}}$ values slightly differ than each other, concluding that rotational energy barriers are significantly similar to each other. Therefore, a large number of different conformations of xylitol coexist in aqueous solution.

Conformer **20** of xylitol has the smallest $\overline{\Delta\delta}_{\mathrm{C}}$ value among other conformers (Table 4.26). In terms of non-bonding interactions, the similarity of **20** to those of smaller molecules is the involvement of terminal –OH group in hydrogen bonding as an acceptor. In conformer **20**, terminal hydroxyl oxygen O(1) is both proton acceptor and donor. The other terminal oxygen O(5) is solely a proton acceptor. The individual $\Delta\delta_{\text{exp-comp}}$ value of carbon adjacent to O(1) is 1.510 ppm, it is 0.848 for the carbon adjacent to O(5). It can be remarked that when terminal hydroxyl oxygen is proton acceptor, the carbon calculated shifts become closer to experimental values.

Analysis between conformers that belong to the same class indicates the importance of intramolecular hydrogen bondings. For instance, **17** ($\overline{\Delta\delta}_{\mathrm{C}}$=2.260), which has the second closest value to experimental results, consists of one more intramolecular hydrogen bond than the same-class conformer **28** ($\overline{\Delta\delta}_{\mathrm{C}}$=3.991). Those conformers which are classified as TT regarding the carbon backbone have the largest $\overline{\Delta\delta}_{\mathrm{C}}$. TT carbon backbone conformers possess hydrogen bonds formed between four-bond distant hydroxyl groups.

The lowest energy conformers of mannitol possess hydrogen bonding networks in a cyclic form. The energy gap between the most stable conformer **71** to the next lowest energy conformer **09** is due to the more compact geometry of the former. Interestingly, the lowest energy conformer **71** also yields the smallest $\overline{\Delta\delta}_{\mathrm{C}}$ value (1.388 ppm). Conformer **43** which lies in the same geometry class with conformer **71** has almost the same hydrogen bond array, except a shared H1$\cdots$O2$\cdots$H3 interaction. The innermost hydroxyl groups are involved in hydrogen bonding interaction, in accordance with experimental results. In conformer **71**, the terminal hydroxy oxygens are both proton donor and acceptor. In conformer **09** however, O(1) is only proton acceptor in contrast to O(6). As in the case of xylitol, calculated chemical shift of C(1) is more closer to experimental values than C(6), by an accuracy of $\sim$0.5 ppm.

Sorbitol has the same length of carbon chain as mannitol but different chirality. In contrast to mannitol, calculated chemical shifts of the lowest energy conformer **38** remarkably differ from the experimental values. Hydrogen bonding arrays of conformations are mostly positioned in either clockwise or counterclockwise. Conformer **46** has the closest chemical shifts to experimental values. In addition to the compact geometry of **46**, it has a completed hydrogen bonding network between hydroxyl groups from one edge to the other. Conformers with the largest $\overline{\Delta\delta}_{\mathrm{C}}$ values consists of hydrogen bonds between hydroxyl groups of four-bond distance as seen in other molecules.

In order to see the effect of intramolecular hydrogen bonding network, three conformers of sorbitol that belong to the same class are illustrated in Figure 4.12. Conformer **21** has a counterclockwise array of hydrogen bonds. Whereas in conformer **10**, this network is somewhat disturbed. The $\overline{\Delta\delta}_{\mathrm{C}}$ value of conformer **21** is closer to the experimental results by 0.8 ppm, compared to conformer **10**. In conformer **30** of the same class, the circular array is significantly diminished. The disturbance of hydrogen bond network results in large $\overline{\Delta\delta}_{\mathrm{C}}$ values.

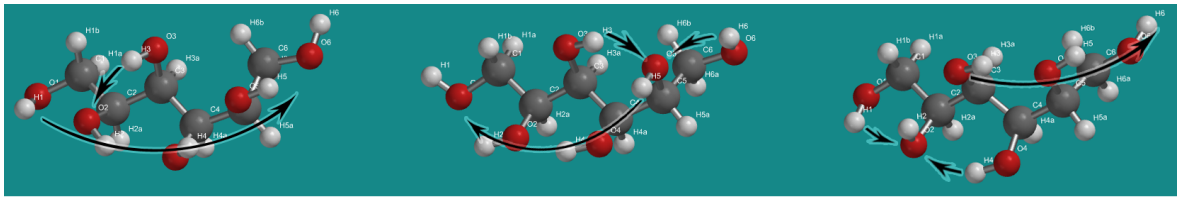

Conformer **21** $\overline{\Delta\delta}_C$ = 4.327 ppm

Conformer **10** $\overline{\Delta\delta}_C$ = 5.154 ppm

Conformer **30** $\overline{\Delta\delta}_C$ = 5.707 ppm

Figure 4.12. Hydrogen bonding arrays observed in TTG-G-G-G+G-G+ class conformers of sorbitol.

Energy calculations of tagatose conformers showed that one chair conformation is favored over the other. Both have two hydroxyl groups in axial position. The chair conformation with higher energy differs basically by the axial position of hydroxymethyl group. The conformer categorization revealed only four different classes (Table 4.21). Yet $\overline{\Delta\delta}_C$ values are remarkably similar. It is an evidence of almost balanced populations of classes in water solutions.

Table 4.21. Best class representative conformers of tagatose.

Conformer	Rel. E	ϕ Class			$\overline{\Delta\delta}_C$	$\overline{\Delta\delta}_H$
	(kcal/mol)	C–C–C–C	O–C–C–O	H–O–C–C	(ppm)	(ppm)
19	3.97	TG-G+	G-G-TG-G-	tg-g+g+g-	2.935	0.341
38	1.33	TG-G+	G-G+TG-G-	g+ttg-t	3.898	0.212
04	3.53	G+G+G-	G+G+G+G+T	g+tttg+	4.014	0.297
24	2.94	TG-G+	G-TTG-G-	g-g+tg-t	4.151	0.285

Among the conformers of tagatose, the smallest $\overline{\Delta\delta}_C$ value is possessed by conformer **19**. Conformer **11** takes part in the same class but the carbon chemical shifts significantly deviate from observed experimental values. Both conformers have a hydrogen bond network between O(3)H, O(4)H and O(5)H hydroxyl groups of the ring. There are three intramolecular hydrogen bondings in **19**, whereas **11** has two more; one of them between O(2) and the ring oxygen (Figure 4.13). The hydrogen bond

network in the ring is extended all the way to the free rotating hydroxy methyl group oxygen in **11**, which decreased $\overline{\Delta\delta}_C$ values in the previous molecules examined. The difference between $\overline{\Delta\delta}_C$ values of **11** and **19** may be attributed to tendency of oxygen atom in the free rotating hydroxyl group to be the hydrogen bond acceptor rather than the donor. Those conformers with the smallest $\overline{\Delta\delta}_C$ within their individual classes also show the same trend. Moreover it was observed for terminal carbon atoms of polyols that their individual chemical shift difference between computed and measured values decrease if the adjacent oxygen atom behaves as a proton acceptor.

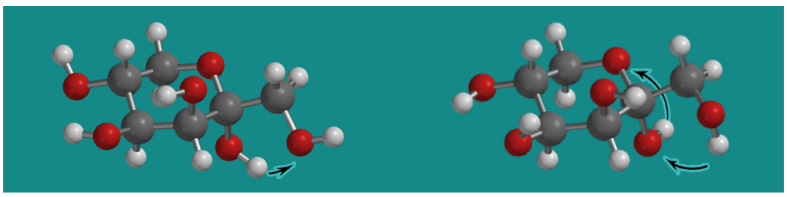

Figure 4.13. Hydrogen bonding properties of O(1)H and O(2)H groups in conformers **19** and **11** of tagatose.

Fructose conformers examined adopt a single chair conformation, since the other possible chair conformation was eliminated within 7 kcal/mol interval applied on DFT single point energies. The eliminated chair conformation has bulky hydroxy methyl group in axial position, therefore sterically unfavored. Since there is only one chair conformation examined, the classification is done according to the position of rotating hydroxy methyl group (Figure 4.14). As in the case of tagatose, the $\overline{\Delta\delta}_C$s slightly differ than each other indicating that populations of all three classes are very similar. Yet T class conformers are found to give results closer to experimental observations. That is followed by G+ and consequently G- class conformers.

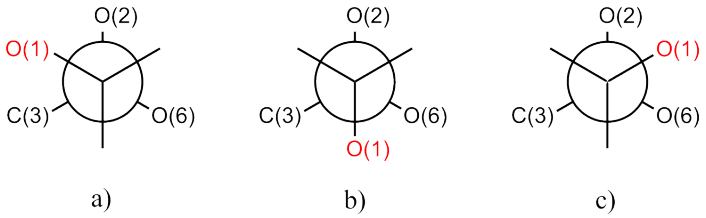

Figure 4.14. Newman projections of fructose classes: (a) G+ (b) T (c) G-

Among the representative conformers of fructose, $\overline{\Delta\delta}_C$ values do not differ significantly (Table 4.22). The $\overline{\Delta\delta}_C$ difference between best conformers of T and G- class is 0.244 ppm. Conformer **25** has three hydrogen bonds; H5$\cdots$O4, H4$\cdots$O3, H3$\cdots$O1 and an additional hydrogen bonding interaction of the ring oxygen with O(1)H and O(2)H protons. The hydroxy methyl group behaves both as donor and acceptor. Conformer **11** has the same hydrogen bonding array on the ring, but instead of H3$\cdots$O1, it bears H3$\cdots$O2 and H2$\cdots$O1 interactions. In the case of conformer **11**, O(1) behaves solely as proton acceptor.

Table 4.22. Best class representative conformers of fructose.

Conformer	Rel. E	ϕ Class		$\overline{\Delta\delta}_C$	$\overline{\Delta\delta}_H$
	(kcal/mol)	O1–C1–C2–O2	H–O–C–C	(ppm)	(ppm)
25	4.47	T	g+tttt	2.912	0.289
12	2.78	G-	ttg-tt	3.156	0.225
11	4.00	G+	tttt	4.516	0.211

Sucrose is a disaccharide composed of glucose and fructose. Due to its complex structure, conformational analysis on sucrose resulted in 15 classes among 22 conformers examined. The maximum difference in $\overline{\Delta\delta}_C$ values among all conformers is 3.045 ppm, which is a notably small value to make precise interpretations. A great number of conformers -whether they belong to the same class or not- adopt either a clockwise or counterclockwise hydrogen bonding array on the rings. The conformer **31** has the smallest $\overline{\Delta\delta}_C$ value. It has a clockwise hydrogen bonding array comprised of all

hydroxyl groups within the pyranose ring. O(1′)H proton of furanose ring is also in proximity to O(2), which defines an extended network. The other two terminal hydroxy protons of C(6)H and C(6′)H are interacting with the oxygen located within the pyranose ring. Such shared hydrogen bonding interaction with the ring oxygen was found out to decrease the $\overline{\Delta\delta}_{\mathrm{C}}$ value similar to the findings of conformer **25** of fructose.

Table 4.23. Computational results, ϕ classes and $\overline{\Delta\delta}$ values of glycerol conformers.

Conformer	Rel. E (kcal/mol)	ϕ (degrees)					ϕ Class		$\overline{\Delta\delta}_{\mathrm{C}}$ (ppm)	$\overline{\Delta\delta}_{\mathrm{H}}$ (ppm)
		O1–C1–C2–O2	O2–C2–C3–O3	H1–O1–C1–C2	H2–O2–C2–C3	H3–O3–C3–C2	O–C–C–O	H–O–C–C		
05	2.51	56	173	-172	82	177	G+T	tg+t	0.467	0.069
10	2.55	177	-58	167	42	-86	TG-	tg+g-	0.896	0.144
15	2.97	-178	-64	-88	51	165	TG-	g-g+t	1.374	0.181
18	2.74	-180	-55	76	42	-88	TG-	g+g+g-	1.490	0.564
13	2.90	-170	-58	-161	-178	56	TG-	ttg+	1.526	0.011
11	2.80	54	173	-175	82	-78	G+T	tg+g-	1.549	0.489
14	2.63	64	-180	-58	-56	84	G+T	g-g-g+	1.703	0.045
01	0.00	-55	-59	164	166	54	G-G-	ttg+	2.216	0.098
06	0.00	59	55	-54	-43	-164	G+G+	g-g-t	2.223	0.096
31	4.06	-174	-54	76	-76	48	TG-	g+g-g+	2.527	0.349
37	0.55	59	51	-54	-36	78	G+G+	g-g-g+	2.980	0.264
19	0.55	-51	-59	-78	159	54	G-G-	g-tg+	2.999	0.264
30	3.65	-173	-57	69	175	56	TG-	g+tg+	3.013	0.381
23	1.13	56	56	-167	82	-48	G+G+	tg+g-	3.070	0.161
12	0.66	-59	59	169	176	-51	G-G+	ttg-	3.322	0.361
28	5.05	70	59	85	-47	-163	G+G+	g+g-t	3.525	0.012
35	5.03	86	-170	-161	-57	75	G+T	tg-g+	3.575	0.190
40	2.42	-58	176	174	169	-175	G-T	ttt	3.854	0.498
38	1.63	-58	59	65	-129	-58	G-G+	g+g-g-	3.919	0.000
39	1.55	56	60	-50	-151	-56	G+G+	g-tg-	4.060	0.015
34	1.05	-59	55	52	-44	78	G-G+	g+g-g+	4.281	0.040

Table 4.23. Computational results, ϕ classes and $\overline{\Delta\delta}$ values of glycerol conformers. (cont.)

Conformer	Rel. E (kcal/mol)	ϕ (degrees)					ϕ Class		$\overline{\Delta\delta}_C$ (ppm)	$\overline{\Delta\delta}_H$ (ppm)
		O1–C1–C2–O2	O2–C2–C3–O3	H1–O1–C1–C2	H2–O2–C2–C3	H3–O3–C3–C2	O–C–C–O	H–O–C–C		
07	2.90	-61	176	54	-82	177	G-T	g+g-t	4.412	0.213
09	2.90	-176	61	-177	-156	-54	TG+	ttg-	4.462	0.214
24	3.45	-173	60	-78	-160	-52	TG+	g-tg-	4.487	0.129
04	2.44	-55	174	-80	163	-177	G-T	g-tt	4.743	0.068
32	4.50	-172	56	-77	72	-43	TG+	g-g+g-	4.922	0.047
03	2.41	-59	174	170	169	-74	G-T	ttg-	4.937	0.073
21	3.74	-176	58	174	67	-45	TG+	tg+g-	5.170	0.131
17	3.15	-63	178	56	-75	-68	G-T	g+g-g-	5.532	0.161
16	4.87	-70	-62	160	51	166	G-G-	tg+t	5.559	0.049
02	2.04	-59	59	44	63	-44	G-G+	g+g+g-	5.586	0.005
08	2.80	-173	56	78	-40	80	TG+	g+g-g+	5.768	0.323
36	0.58	74	-50	-170	37	-61	G+G-	tg+g-	5.897	0.378
22	3.65	-176	59	72	69	-46	TG+	g+g+g-	6.015	0.284
20	3.01	-168	-176	-53	-171	176	TT	g-tt	6.787	0.296
25	3.81	-167	-177	-52	-73	174	TT	g-g-t	6.846	0.243
26	3.21	-172	-179	-55	-178	-81	TT	g-tg-	7.294	0.026
33	3.71	-179	170	80	57	52	TT	g+g+g+	7.486	0.181
29	3.78	-166	-180	-50	70	180	TT	g-g+t	7.566	0.182

Table 4.24. Computational results of erythritol conformers.

Conformer	Rel. E (kcal/mol)	ϕ (degrees)							
		C1–C2–C3–C4	O1–C1–C2–O2	O2–C2–C3–O3	O3–C3–C4–O4	H1–O1–C1–C2	H2–O2–C2–C3	H3–O3–C3–C4	H4–O4–C4–C3
38	1.88	180	-53	180	53	176	-85	-39	-176
39	2.36	-168	-53	-167	61	174	-86	-42	84

Table 4.24. Computational results of erythritol conformers. (cont.)

Conformer	Rel. E (kcal/mol)	ϕ (degrees)							
		C1–C2–C3–C4	O1–C1–C2–O2	O2–C2–C3–O3	O3–C3–C4–O4	H1–O1–C1–C2	H2–O2–C2–C3	H3–O3–C3–C4	H4–O4–C4–C3
17	3.46	-56	-177	-56	-52	-168	48	38	-78
16	0.51	-60	-46	-56	-170	-77	-100	-85	160
28	3.52	56	51	56	179	80	-161	-173	74
12	1.45	58	54	58	-62	-167	-167	180	52
26	0.57	59	171	55	47	-77	-42	-30	78
51	3.62	50	160	52	173	179	-40	74	-79
01	0.92	56	54	56	53	-172	-167	-172	-53
02	2.00	59	50	59	-63	80	-160	179	52
22	3.41	61	-50	64	177	-59	-104	162	172
75	5.81	-55	179	-52	-51	-75	-76	-88	42
23	2.28	58	55	57	-62	-47	-43	55	168
11	0.32	60	167	59	53	74	-177	-175	-54
25	2.49	-178	53	178	53	80	-161	-39	-176
03	3.02	-57	-51	-53	-54	165	-89	-85	46
45	1.35	59	50	59	55	83	-162	-174	-55
24	3.77	-57	60	-57	-165	-166	-178	-84	78
42	4.40	57	52	54	-63	-44	-36	-60	48
55	4.18	175	58	174	54	-44	-62	-41	-173
19	1.87	-167	57	-169	62	-172	-167	-44	82
08	2.85	58	60	56	-63	-56	85	-177	54
67	1.52	-81	55	-83	50	-167	-172	-35	63
06	1.75	60	-50	63	-64	-58	-104	160	54
44	3.70	175	57	175	54	-173	-171	76	-48
27	3.94	58	56	59	51	-47	-50	86	-49
34	0.00	180	56	180	-56	-171	-167	45	171
15	1.74	-80	52	-83	50	80	-166	-35	63
74	2.65	177	170	173	53	55	173	-39	-171
29	3.41	-52	179	-53	75	-73	-57	-88	-169

Table 4.24. Computational results of erythritol conformers. (cont.)

Conformer	Rel. E (kcal/mol)	ϕ (degrees)							
		C1–C2–C3–C4	O1–C1–C2–O2	O2–C2–C3–O3	O3–C3–C4–O4	H1–O1–C1–C2	H2–O2–C2–C3	H3–O3–C3–C4	H4–O4–C4–C3
04	1.93	-178	53	-178	-56	82	-161	45	171
80	3.58	176	169	175	52	52	-77	-37	-175
52	4.92	56	-62	57	-64	-43	81	-179	55
81	4.98	-176	61	179	-55	-56	88	-71	43
18	2.65	180	53	180	-53	83	-162	40	-83
37	3.54	176	57	178	-57	-44	-59	45	169
63	2.32	-166	-180	-166	72	-91	75	-175	-61
68	4.16	173	57	169	-179	-51	48	-68	180
82	3.89	172	166	171	58	55	162	77	-52
57	4.13	-174	53	-177	-58	82	-161	-64	44
30	3.02	58	-85	54	64	-89	-41	-78	-162
48	2.52	-172	52	-172	-166	83	-162	63	-55
54	5.30	180	173	180	-173	177	35	-158	-177
73	2.66	179	175	179	-174	-79	36	-163	-178

Table 4.25. ϕ classes and $\overline{\Delta\delta}$ values of erythritol conformers.

Conformer	ϕ Class			$\overline{\Delta\delta}_C$ (ppm)	$\overline{\Delta\delta}_H$ (ppm)
	C–C–C–C	O–C–C–O	H–O–C–C		
38	T	G-TG+	tg-g-t	0.436	0.344
39	T	G-TG+	tg-g-g+	1.743	0.316
17	G-	TG-G-	tg+g+g-	1.755	0.232
16	G-	G-G-T	g-g-g-t	2.029	0.063
28	G+	G+G+T	g+ttg+	2.294	0.154
12	G+	G+G+G-	tttg+	2.320	0.222
26	G+	TG+G+	g-g-g-g+	2.510	0.129

Table 4.25. ϕ classes and $\overline{\Delta\delta}$ values of erythritol conformers. (cont.)

Conformer	ϕ Class			$\overline{\Delta\delta}_C$ (ppm)	$\overline{\Delta\delta}_H$ (ppm)
	C–C–C–C	O–C–C–O	H–O–C–C		
51	G+	TG+T	tg-g+g-	2.550	0.241
01	G+	G+G+G+	tttg-	2.644	0.224
02	G+	G+G+G-	g+ttg+	2.898	0.251
22	G+	G-G+T	g-g-tt	2.961	0.333
75	G-	TG-G-	g-g-g-g+	2.979	0.204
23	G+	G+G+G-	g-g-g+t	2.990	0.255
11	G+	TG+G+	g+ttg-	3.037	0.191
25	T	G+TG+	g+tg-t	3.122	0.282
03	G-	G-G-G-	tg-g-g+	3.123	0.161
45	G+	G+G+G+	g+ttg-	3.556	0.159
24	G-	G+G-T	ttg-g+	3.772	0.291
42	G+	G+G+G-	g-g-g-g+	3.826	0.301
55	T	G+TG+	g-g-g-t	3.845	0.342
19	T	G+TG+	ttg-g+	3.956	0.307
08	G+	G+G+G-	g-g+tg+	4.306	0.170
67	G-	G+G-G+	ttg-g+	4.307	0.309
06	G+	G-G+G-	g-g-tg+	4.440	0.206
44	T	G+TG+	ttg+g-	4.444	0.291
27	G+	G+G+G+	g-g-g+g-	4.446	0.112
34	T	G+TG-	ttg+t	4.632	0.196
15	G-	G+G-G+	g+tg-g+	4.834	0.289
74	T	TTG+	g+tg-t	4.896	0.214
29	G-	TG-G+	g-g-g-t	5.201	0.267
04	T	G+TG-	g+tg+t	5.203	0.176
80	T	TTG+	g+g-g-t	5.408	0.282
52	G+	G-G+G-	g-g+tg+	5.500	0.202
81	T	G+TG-	g-g+g-g+	5.639	0.191
18	T	G+TG-	g+tg+g-	5.769	0.173
37	T	G+TG-	g-g-g+t	5.889	0.175
63	T	TTG+	g-g+tg-	5.899	0.167

Table 4.25. ϕ classes and $\overline{\Delta\delta}$ values of erythritol conformers. (cont.)

Conformer	ϕ Class			$\overline{\Delta\delta_C}$ (ppm)	$\overline{\Delta\delta_H}$ (ppm)
	C–C–C–C	O–C–C–O	H–O–C–C		
68	T	G+TT	g-g+g-t	6.504	0.117
82	T	TTG+	g+tg+g-	6.521	0.167
57	T	G+TG-	g+tg-g+	6.567	0.210
30	G+	G-G+G+	g-g-g-t	6.712	0.323
48	T	G+TT	g+tg+g-	7.175	0.070
54	T	TTT	tg+tt	7.192	0.319
73	T	TTT	g-g+tt	7.704	0.223

Table 4.26. Computational results of xylitol conformers.

Conformer	Rel. E (kcal/mol)	ϕ (degrees)										
		C1–C2–C3–C4	C2–C3–C4–C5	O1–C1–C2–O2	O2–C2–C3–O3	O3–C3–C4–O4	O4–C4–C5–O5	H1–O1–C1–C2	H2–O2–C2–C3	H3–O3–C3–C4	H4–O4–C4–C5	H5–O5–C5–C4
20	3.14	178	54	53	177	53	50	88	86	-43	-37	81
17	3.69	-60	-173	49	-63	-171	-55	58	104	-163	41	171
38	4.32	52	61	-178	54	60	169	178	-53	-49	-54	72
01	2.88	55	58	-62	57	57	53	52	-57	-46	-41	-171
69	3.01	47	149	170	52	148	-71	163	-48	-65	162	59
13	3.18	55	61	54	56	59	52	-60	-49	-45	-42	-171
55	3.80	-55	-166	-163	-54	-169	59	-170	-161	-180	-158	-50
14	3.55	-62	-52	-166	-57	-55	61	-73	47	42	-58	-166
46	4.38	51	58	-61	53	55	55	168	-179	91	84	-47
84	4.27	51	148	173	54	153	-68	-80	-55	-71	47	167
96	3.83	53	151	175	56	152	-70	-74	-55	-68	-76	60
37	3.22	59	173	52	55	168	57	-158	89	83	-162	-50
32	3.47	48	166	175	51	162	53	-80	-161	88	-44	-172
61	3.78	-170	-49	-49	-166	-51	-174	-84	158	38	-73	80

Table 4.26. Computational results of xylitol conformers. (cont.)

Conformer	Rel. E (kcal/mol)	ϕ (degrees)										
		C1–C2–C3–C4	C2–C3–C4–C5	O1–C1–C2–O2	O2–C2–C3–O3	O3–C3–C4–O4	O4–C4–C5–O5	H1–O1–C1–C2	H2–O2–C2–C3	H3–O3–C3–C4	H4–O4–C4–C5	H5–O5–C5–C4
11	3.17	55	156	-59	57	155	-67	167	176	86	44	-79
28	3.50	-54	-177	74	-53	-180	-54	-168	41	72	39	-88
22	3.51	-60	94	-54	-57	92	-50	168	168	179	34	-65
06	3.25	172	58	-56	173	60	-48	173	166	-65	19	-60
29	3.58	-179	55	-165	-177	54	53	-55	180	-47	-43	-168
58	4.07	57	148	-61	60	149	-67	50	-59	-65	-81	57
05	0.00	61	160	56	61	161	-74	-56	-50	-69	-163	63
49	2.43	-53	-165	-162	-53	-167	-178	-177	39	-52	-161	174
52	4.48	54	163	173	53	163	53	-81	-47	-158	-46	-173
04	4.50	53	63	55	55	63	-45	-62	-58	-63	17	-66
48	3.75	-55	-180	-51	-53	179	166	-79	161	172	-56	53
25	4.20	-55	-174	-58	-52	-176	53	54	-90	168	-40	83
94	7.39	-47	78	66	-41	70	-60	-65	26	43	98	68
30	5.70	59	61	-61	63	56	-61	170	-177	62	96	71
83	3.84	-180	-176	57	-176	-178	55	-52	-39	69	-45	-170
44	6.63	55	58	54	54	53	-64	-164	90	70	96	72
53	3.53	174	167	-55	174	167	54	174	169	-75	178	-46
97	6.26	72	-60	172	71	-56	-174	-79	-90	32	78	-159
79	3.05	171	54	-58	175	54	-72	171	167	54	86	170
90	5.23	-68	-51	65	-67	-56	-51	-174	62	99	-174	59
15	4.29	-58	-63	87	-55	-67	58	88	41	78	-51	-171
71	4.44	-57	-178	47	-58	-180	166	62	108	-171	-58	53
50	3.76	171	173	-56	174	168	57	170	169	56	175	-49
99	4.23	55	174	48	58	167	168	-50	-142	79	-162	60
87	5.08	-78	-174	49	-78	-175	176	61	90	-42	69	179
75	4.34	-56	-176	72	-55	-179	169	-175	45	76	51	52
74	2.31	177	177	-53	178	176	174	-85	163	-37	164	-78
03	2.96	-179	174	-174	-178	172	163	-179	-34	157	-63	54

Table 4.27. ϕ classes and $\overline{\Delta\delta}$ values of xylitol conformers.

Conformer	ϕ Class			$\overline{\Delta\delta}_{\mathrm{C}}$ (ppm)	$\overline{\Delta\delta}_{\mathrm{H}}$ (ppm)
	C–C–C–C	O–C–C–O	H–O–C–C		
20	TG+	G+TG+G+	g+g+g-g-g+	1.175	0.313
17	G-T	G+G-TG-	g+g+tg+t	2.260	0.378
38	G+G+	TG+G+T	tg-g-g-g+	2.297	0.495
01	G+G+	G-G+G+G+	g+g-g-g-t	2.844	0.221
69	G+T	TG+TG-	tg-g-tg+	3.147	0.322
13	G+G+	G+G+G+G+	g-g-g-g-t	3.151	0.320
55	G-T	TG-TG+	ttttg-	3.278	0.284
14	G-G-	TG-G-G+	g-g+g+g-t	3.314	0.281
46	G+G+	G-G+G+G+	ttg+g+g-	3.331	0.225
84	G+T	TG+TG-	g-g-g-g+t	3.343	0.345
96	G+T	TG+TG-	g-g-g-g-g+	3.366	0.300
37	G+T	G+G+TG+	tg+g+tg-	3.578	0.303
32	G+T	TG+TG+	g-tg+g-t	3.617	0.255
61	TG-	G-TG-T	g-tg+g-g+	3.621	0.231
11	G+T	G-G+TG-	ttg+g+g-	3.981	0.275
28	G-T	G+G-TG-	tg+g+g+g-	3.991	0.388
22	G-G+	G-G-G+G-	tttg+g-	4.060	0.260
06	TG+	G-TG+G-	ttg-g+g-	4.099	0.280
29	TG+	TTG+G+	g-tg-g-t	4.171	0.346
58	G+T	G-G+TG-	g+g-g-g-g+	4.308	0.168
05	G+T	G+G+TG-	g-g-g-tg+	4.394	0.220
49	G-T	TG-TT	tg+g-tt	4.434	0.318
52	G+T	TG+TG+	g-g-tg-t	4.493	0.290
04	G+G+	G+G+G+G-	g-g-g-g+g-	4.528	0.346
48	G-T	G-G-TT	g-ttg-g+	4.632	0.245
25	G-T	G-G-TG+	g+g-tg-g+	4.672	0.329
94	G-G+	G+G-G+G-	g-g+g+g+g+	4.703	0.395
30	G+G+	G-G+G+G-	ttg+g+g+	4.981	0.401
83	TT	G+TTG+	g-g-g+g-t	5.112	0.216
44	G+G+	G+G+G+G-	tg+g+g+g+	5.199	0.248

Table 4.27. ϕ classes and $\overline{\Delta\delta}$ values of xylitol conformers. (cont.)

Conformer	ϕ Class			$\overline{\Delta\delta}_{\mathrm{C}}$ (ppm)	$\overline{\Delta\delta}_{\mathrm{H}}$ (ppm)
	C–C–C–C	O–C–C–O	H–O–C–C		
53	TT	G-TTG+	ttg-tg-	5.272	0.261
97	G+G-	TG+G-T	g-g-g+g+t	5.697	0.378
79	TG+	G-TG+G-	ttg+g+t	5.791	0.365
90	G-G-	G+G-G-G-	tg+g+tg+	5.804	0.382
15	G-G-	G+G-G-G+	g+g+g+g-t	5.825	0.335
71	G-T	G+G-TT	g+g+tg-g+	5.854	0.241
50	TT	G-TTG+	ttg+tg-	6.254	0.220
99	G+T	G+G+TT	g-tg+tg+	6.321	0.156
87	G-T	G+G-TT	g+g+g-g+t	6.924	0.270
75	G-T	G+G-TT	tg+g+g+g+	7.370	0.278
74	TT	G-TTT	g-tg-tg-	7.550	0.264
03	TT	TTTT	tg-tg-g+	8.614	0.304

Table 4.28. Computational results of mannitol conformers.

Conformer	Rel. E (kcal/mol)	ϕ (degrees)													
		C1–C2–C3–C4	C2–C3–C4–C5	C3–C4–C5–C6	O1–C1–C2–O2	O2–C2–C3–O3	O3–C3–C4–O4	O4–C4–C5–O5	O5–C5–C6–O6	H1–O1–C1–C2	H2–O2–C2–C3	H3–O3–C3–C4	H4–O4–C4–C5	H5–O5–C5–C6	H6–O6–C6–C5
71	0.00	-32	-170	-32	-37	-34	80	-34	-37	-61	-104	-101	29	25	-61
39	4.51	-30	-171	-52	-38	-31	77	-52	-178	-61	-104	-107	35	69	-169
17	6.26	41	165	59	-57	40	55	56	50	-73	-103	-170	-44	-39	-169
70	4.62	61	160	179	172	57	44	179	53	-159	-40	-32	-162	-40	80
58	6.71	-55	168	41	-175	-58	49	40	-75	-173	59	23	174	107	52
53	5.92	67	175	-53	164	59	57	-57	-179	-171	-43	35	-178	-178	-175
43	5.07	-63	-173	-32	-62	-61	75	-32	-38	65	-46	-86	25	26	-59
98	7.47	44	159	63	-73	46	46	57	169	166	-42	73	138	82	-164
18	6.35	173	66	58	-52	177	-53	60	-47	178	-89	42	-67	18	-59
54	5.81	-58	166	40	-50	-60	47	39	-73	62	57	23	-179	111	52
99	6.25	-64	104	-176	-55	-62	-21	-171	54	56	51	30	-121	78	-44
36	5.44	177	166	-64	56	177	48	-66	63	-172	-169	58	98	-150	-56
04	5.42	-80	159	57	54	-82	45	58	55	-169	-171	-38	-167	83	-47
68	5.40	60	174	-62	51	57	63	-60	-55	-172	-165	-176	46	87	66
23	5.72	58	160	-80	56	59	45	-82	52	-48	-47	66	87	-41	81
94	5.67	163	66	177	52	162	-51	173	-55	-172	-164	36	52	-177	53

Table 4.28. Computational results of mannitol conformers. (cont.)

Conformer	Rel. E (kcal/mol)	ϕ (degrees)													
		C1–C2–C3–C4	C2–C3–C4–C5	C3–C4–C5–C6	O1–C1–C2–O2	O2–C2–C3–O3	O3–C3–C4–O4	O4–C4–C5–O5	O5–C5–C6–O6	H1–O1–C1–C2	H2–O2–C2–C3	H3–O3–C3–C4	H4–O4–C4–C5	H5–O5–C5–C6	H6–O6–C6–C5
20	6.70	-63	174	60	-62	-59	62	58	51	158	-56	-79	-49	-39	-171
41	6.75	166	53	67	52	167	-60	63	-174	-172	-163	43	67	78	-47
45	6.05	65	174	-53	-64	60	64	-53	-177	80	-32	-85	32	73	-172
79	4.51	58	163	57	52	54	55	54	-84	-172	-165	-169	53	86	-90
08	5.43	53	65	79	-73	55	-49	82	-49	173	-42	-76	163	34	-63
46	5.47	59	63	169	-48	62	-55	169	53	-60	-106	163	167	-42	-173
60	4.63	-79	164	172	55	-81	49	171	167	-168	-171	-41	-175	-73	55
66	6.71	63	156	64	166	58	50	64	-67	73	-46	-54	37	71	178
93	6.73	179	-55	-173	57	171	-168	-174	55	-50	45	-50	-166	-45	-173
81	6.97	-155	-55	-63	60	-158	-163	-67	56	-51	82	155	81	-46	-168
09	2.35	174	72	153	52	174	-47	154	-73	-173	-162	37	-71	-171	62
22	5.25	-79	163	-98	54	-80	48	-98	-62	-170	-171	-47	-172	151	60
32	3.93	164	71	174	53	163	-48	172	173	-172	-165	40	-28	-176	177
44	6.26	57	64	167	-47	59	-54	167	164	-61	-107	166	167	-59	58
90	4.90	55	66	172	-73	55	-50	173	52	171	-44	-79	160	-39	84
63	5.58	-157	-55	-63	-178	-161	-162	-68	57	172	83	179	83	-48	-167

Table 4.28. Computational results of mannitol conformers. (cont.)

Conformer	Rel. E (kcal/mol)	ϕ (degrees)													
		C1–C2–C3–C4	C2–C3–C4–C5	C3–C4–C5–C6	O1–C1–C2–O2	O2–C2–C3–O3	O3–C3–C4–O4	O4–C4–C5–O5	O5–C5–C6–O6	H1–O1–C1–C2	H2–O2–C2–C3	H3–O3–C3–C4	H4–O4–C4–C5	H5–O5–C5–C6	H6–O6–C6–C5
05	4.95	-54	176	68	62	-54	68	66	-67	-50	-54	-95	39	69	-179
25	3.95	-161	-57	-68	54	-168	-161	-74	-55	-175	-162	-58	88	156	58
84	3.69	170	73	156	162	170	-45	156	-75	56	-170	36	-72	-171	63
29	5.50	166	67	55	164	167	-48	56	-73	56	178	35	51	83	172

Table 4.29. ϕ classes and $\overline{\Delta\delta}$ values of mannitol conformers.

Conformer	ϕ Class			$\overline{\Delta\delta}_{\mathrm{C}}$ (ppm)	$\overline{\Delta\delta}_{\mathrm{H}}$ (ppm)
	C–C–C–C	O–C–C–O	H–O–C–C		
71	G-TG-	G-G-G+G-G-	g-g-g-g+g+g-	1.388	0.016
39	G-TG-	G-G-G+G-T	g-g-g-g+g+t	2.609	0.165
17	G+TG+	G-G+G+G+G+	g-g-tg-g-t	3.610	0.129
70	G+TT	TG+G+TG+	tg-g-tg-g+	3.611	0.017
58	G-TG+	TG-G+G+G-	tg+g+tg+g+	3.828	0.258
53	G+TG-	TG+G+G-T	tg-g+ttt	3.879	0.313
43	G-TG-	G-G-G+G-G-	g+g-g-g+g+g-	4.490	0.082
98	G+TG+	G-G+G+G+T	tg-g+tg+t	4.539	0.109
18	TG+G+	G-TG-G+G-	tg-g+g-g+g-	4.540	0.211
54	G-TG+	G-G-G+G+G-	g+g+g+tg+g+	4.622	0.173
99	G-G+T	G-G-G-TG+	g+g+g+g-g+g-	4.742	0.039
36	TTG-	G+TG+G-G+	ttg+g+tg-	4.919	0.054
04	G-TG+	G+G-G+G+G+	ttg-tg+g-	5.054	0.095
68	G+TG-	G+G+G+G-G-	tttg+g+g+	5.493	0.198
23	G+TG-	G+G+G+G-G+	g-g-g+g+g-g+	5.536	0.169
94	TG+T	G+TG-TG-	ttg+g+tg+	5.604	0.005
20	G-TG+	G-G-G+G+G+	tg-g-g-g-t	5.680	0.273
41	TG+G+	G+TG-G+T	ttg+g+g+g-	5.697	0.134
45	G+TG-	G-G+G+G-T	g+g-g-g+g+t	5.746	0.270
79	G+TG+	G+G+G+G+G-	tttg+g+g-	5.883	0.140
08	G+G+G+	G-G+G-G+G-	tg-g-tg+g-	5.922	0.014
46	G+G+T	G-G+G-TG+	g-g-ttg-t	5.937	0.164
60	G-TT	G+G-G+TT	ttg-tg-g+	6.134	0.047
66	G+TG+	TG+G+G+G-	g+g-g-g+g+t	6.250	0.063
93	TG-T	G+TTTG+	g-g+g-tg-t	6.427	0.163
81	TG-G-	G+TTG-G+	g-g+tg+g-t	6.676	0.090
09	TG+T	G+TG-TG-	ttg+g-tg+	6.789	0.072
22	G-TG-	G+G-G+G-G-	ttg-ttg+	6.882	0.055
32	TG+T	G+TG-TT	ttg+g-tt	7.206	0.130
44	G+G+T	G-G+G-TT	g-g-ttg-g+	7.228	0.069

Table 4.29. ϕ classes and $\overline{\Delta\delta}$ values of mannitol conformers. (cont.)

Conformer	ϕ Class			$\overline{\Delta\delta_C}$ (ppm)	$\overline{\Delta\delta_H}$ (ppm)
	C–C–C–C	O–C–C–O	H–O–C–C		
90	G+G+T	G-G+G-TG+	tg-g-tg-g+	7.557	0.114
63	TG-G-	TTTG-G+	tg+tg+g-t	7.692	0.295
05	G-TG+	G+G-G+G+G-	g-g-g-g+g+t	7.759	0.090
25	TG-G-	G+TTG-G-	ttg-g+tg+	7.791	0.133
84	TG+T	TTG-TG-	g+tg+g-tg+	8.322	0.017
29	TG+G+	TTG-G+G-	g+tg+g+g+t	8.470	0.108

Table 4.30. Computational results of sorbitol conformers.

Conformer	Rel. E (kcal/mol)	ϕ (degrees)													
		C1–C2–C3–C4	C2–C3–C4–C5	C3–C4–C5–C6	O1–C1–C2–O2	O2–C2–C3–O3	O3–C3–C4–O4	O4–C4–C5–O5	O5–C5–C6–O6	H1–O1–C1–C2	H2–O2–C2–C3	H3–O3–C3–C4	H4–O4–C4–C5	H5–O5–C5–C6	H6–O6–C6–C5
46	1.84	-164	88	-56	-51	-45	-33	-54	-52	170	162	-90	153	172	53
43	3.59	-70	173	-176	-56	52	56	-180	-51	172	174	-163	81	-94	50
54	5.49	59	149	55	-59	169	39	58	-45	172	174	-45	-59	17	-67
83	4.10	60	155	58	-59	171	44	55	169	170	175	-40	-39	-156	76
90	3.25	-76	159	55	-58	45	45	53	55	171	174	-158	91	85	-47
16	1.07	175	164	177	-55	-71	48	180	-54	166	167	-40	-178	39	175
17	2.43	-77	161	60	-58	44	48	57	165	171	174	-156	89	81	76
41	1.81	175	166	-179	-55	-71	49	-179	-53	166	168	-41	-176	-89	49
07	3.90	-168	68	52	-53	-50	-51	54	162	167	162	-84	169	85	-85
06	2.45	-165	74	79	-54	-48	-43	82	-49	167	165	-86	162	36	-62
24	2.96	-65	-171	-52	-56	52	75	-53	180	172	175	-164	39	71	-170
21	4.20	-165	-174	-36	-59	-51	77	-40	62	52	-63	-83	27	-53	-164
22	2.92	-65	-171	-158	-56	54	75	-164	63	173	174	-165	65	-163	-53
02	0.84	174	164	176	-55	-72	48	176	56	165	167	-38	-178	-46	-171
14	0.34	-171	-60	-58	-51	-65	-162	-52	-72	165	162	-60	30	69	48
26	3.47	60	159	-78	-59	174	45	-80	52	170	173	66	84	-41	81

Table 4.30. Computational results of sorbitol conformers. (cont.)

Conformer	Rel. E (kcal/mol)	ϕ (degrees)													
		C1–C2–C3–C4	C2–C3–C4–C5	C3–C4–C5–C6	O1–C1–C2–O2	O2–C2–C3–O3	O3–C3–C4–O4	O4–C4–C5–O5	O5–C5–C6–O6	H1–O1–C1–C2	H2–O2–C2–C3	H3–O3–C3–C4	H4–O4–C4–C5	H5–O5–C5–C6	H6–O6–C6–C5
39	3.53	-166	-63	-57	-50	-55	-168	-53	62	168	160	-86	30	65	-48
74	3.82	174	157	71	-56	-71	43	71	163	166	168	-42	-165	-51	69
13	3.35	-67	-177	-64	-57	52	69	-62	-59	171	175	-166	50	88	63
10	1.47	175	175	-54	-56	-75	58	-57	63	163	167	32	165	-174	-53
59	3.79	-160	-60	-62	-58	-45	-173	-61	66	51	-78	-102	-166	-166	-57
23	4.11	-75	161	91	-58	46	48	90	-48	172	174	-161	97	30	-61
73	5.24	-160	-61	-54	-52	-53	-161	-55	-64	164	162	-67	42	-69	36
28	4.25	-64	-170	-53	-57	51	77	-52	59	43	67	-157	35	73	-47
38	0.00	-164	-162	-161	-59	-48	84	-164	-177	51	-66	-88	-51	-164	175
30	2.56	-166	175	-77	-57	-52	57	-80	55	50	46	40	165	-47	-168
82	5.24	-158	-59	-56	-53	-51	-165	-55	-68	162	165	-66	-168	177	41
36	0.88	175	165	173	-55	-72	50	172	167	166	167	-40	-178	-70	56
69	2.82	51	70	175	-58	164	-49	175	176	173	177	42	-39	-177	-79
15	1.99	-165	-177	-63	-59	-47	68	-58	-64	52	-62	-94	34	75	146
66	1.22	176	161	83	-55	-72	50	84	-50	167	168	-44	-173	34	-62
79	1.18	176	161	83	-55	-72	50	84	-50	167	168	-44	-173	34	-62

Table 4.31. ϕ classes and $\overline{\Delta\delta}$ values of sorbitol conformers.

Conformer	ϕ Class			$\overline{\Delta\delta}_{\mathrm{C}}$ (ppm)	$\overline{\Delta\delta}_{\mathrm{H}}$ (ppm)
	C–C–C–C	O–C–C–O	H–O–C–C		
46	TG+G-	G-G-G-G-G-	ttg-ttg+	1.989	0.236
43	G-TT	G-G+G+TG-	tttg+g-g+	2.400	0.242
54	G+TG+	G-TG+G+G-	ttg-g-g+g-	2.776	0.373
83	G+TG+	G-TG+G+T	ttg-g-tg+	2.910	0.212
90	G-TG+	G-G+G+G+G+	tttg+g+g-	3.067	0.263
16	TTT	G-G-G+TG-	ttg-tg+t	3.093	0.292
17	G-TG+	G-G+G+G+T	tttg+g+g+	3.154	0.262
41	TTT	G-G-G+TG-	ttg-tg-g+	3.221	0.263
07	TG+G+	G-G-G-G+T	ttg-tg+g-	3.228	0.258
06	TG+G+	G-G-G-G+G-	ttg-tg+g-	3.805	0.361
24	G-TG-	G-G+G+G-T	tttg+g+t	4.009	0.272
21	TTG-	G-G-G+G-G+	g+g-g-g+g-t	4.327	0.387
22	G-TT	G-G+G+TG+	tttg+tg-	4.347	0.263
02	TTT	G-G-G+TG+	ttg-tg-t	4.610	0.271
14	TG-G-	G-G-TG-G-	ttg-g+g+g+	4.694	0.302
26	G+TG-	G-TG+G-G+	ttg+g+g-g+	4.864	0.236
39	TG-G-	G-G-TG-G+	ttg-g+g+g-	4.946	0.227
74	TTG+	G-G-G+G+T	ttg-tg-g+	5.028	0.406
13	G-TG-	G-G+G+G-G-	tttg+g+g+	5.089	0.371
10	TTG-	G-G-G+G-G+	ttg+ttg-	5.154	0.237
59	TG-G-	G-G-TG-G+	g+g-g-ttg-	5.338	0.363
23	G-TG+	G-G+G+G+G-	tttg+g+g-	5.345	0.282
73	TG-G-	G-G-TG-G-	ttg-g+g-g+	5.507	0.240
28	G-TG-	G-G+G+G-G+	g+g+tg+g+g-	5.573	0.330
38	TTT	G-G-G+TT	g+g-g-g-tt	5.699	0.298
30	TTG-	G-G-G+G-G+	g+g+g+tg-t	5.707	0.265
82	TG-G-	G-G-TG-G-	ttg-ttg+	5.759	0.420
36	TTT	G-G-G+TT	ttg-tg-g+	5.797	0.246
69	G+G+T	G-TG-TT	ttg+g-tg-	5.936	0.278
15	TTG-	G-G-G+G-G-	g+g-g-g+g+t	6.055	0.257

Table 4.31. ϕ classes and $\overline{\Delta\delta}$ values of sorbitol conformers. (cont.)

Conformer	ϕ Class			$\overline{\Delta\delta_C}$ (ppm)	$\overline{\Delta\delta_H}$ (ppm)
	C–C–C–C	O–C–C–O	H–O–C–C		
66	TTG+	G-G-G+G+G-	ttg-tg+g-	6.730	0.423
79	TTG+	G-G-G+G+G-	ttg-tg+g-	6.736	0.423

Table 4.32. Computational results of tagatose conformers.

Conformer	Rel. E (kcal/mol)	ϕ (degrees)												
		C1–C2–C3–C4	C2–C3–C4–C5	C3–C4–C5–C6	C4–C5–C6–O6	O1–C1–C2–O2	O2–C2–C3–O3	O3–C3–C4–O4	O4–C4–C5–O5	H1–O1–C1–C2	H2–O2–C2–C3	H3–O3–C3–C4	H4–O4–C4–C5	H5–O5–C5–C6
19	3.97	170	-52	55	-58	-47	171	-53	-65	177	-95	46	51	-77
06	3.05	167	-50	55	-59	-53	167	-51	-65	-88	-92	42	50	-76
17	3.98	175	-54	53	-55	-47	175	-54	-64	174	-96	-76	-84	169
15	3.47	169	-50	54	-56	-52	168	-51	-63	-88	-93	42	42	54
21	4.17	168	-50	54	-57	-52	167	-47	-67	-89	-95	38	151	178
20	3.49	170	-53	57	-57	-54	168	-55	-64	50	170	51	52	-82
18	4.41	167	-50	55	-58	-61	170	-51	-62	165	-80	152	-81	168
27	3.92	170	-52	55	-56	-54	169	-51	-66	52	168	45	154	178
26	3.75	174	-54	53	-54	-56	172	-54	-63	52	172	-78	-84	169
38	1.33	169	-51	55	-58	53	171	-53	-62	66	-162	147	-78	167
01	0.00	168	-51	56	-59	52	168	-53	-65	69	-160	46	50	-77
37	2.83	169	-51	55	-59	42	168	-53	-65	-171	-160	46	49	-77
04	3.53	76	49	-53	58	50	75	55	-168	67	-162	171	-176	36
31	4.18	171	-53	55	-55	-55	170	-55	-62	52	172	51	42	56
24	2.94	170	-51	53	-56	174	167	-51	-64	-62	44	-150	-82	172
07	5.04	73	51	-50	53	50	73	55	-165	66	-162	173	-175	-43
16	5.37	73	50	-48	51	50	72	54	-165	66	-163	175	-172	-171
23	0.65	170	-52	55	-57	52	169	-50	-67	69	-161	43	151	178
11	1.56	162	-47	56	-60	-68	161	-49	-61	61	169	160	-84	167

Table 4.32. Computational results of tagatose conformers. (cont.)

Conformer	Rel. E (kcal/mol)	ϕ (degrees)												
		C1–C2–C3–C4	C2–C3–C4–C5	C3–C4–C5–C6	C4–C5–C6–O6	O1–C1–C2–O2	O2–C2–C3–O3	O3–C3–C4–O4	O4–C4–C5–O5	H1–O1–C1–C2	H2–O2–C2–C3	H3–O3–C3–C4	H4–O4–C4–C5	H5–O5–C5–C6
41	3.73	169	-51	54	-57	42	168	-49	-67	-177	-161	42	149	178
12	0.29	170	-51	54	-56	52	169	-53	-63	69	-160	46	42	55
02	2.84	174	-53	51	-55	42	173	-54	-64	-164	-160	-76	-83	170
40	3.17	170	-51	53	-56	43	169	-53	-63	-176	-160	46	42	54
33	5.67	75	49	-51	57	47	73	55	-166	-163	-166	172	-177	36
03	0.42	170	-52	55	-56	178	171	-52	-63	-59	179	-153	-81	169
09	3.03	169	-50	56	-59	174	165	-52	-65	50	-179	45	51	-77
08	3.88	173	-53	56	-56	-174	171	-52	-62	177	171	-149	-80	168
36	6.89	176	-55	52	-52	40	173	-56	-61	-164	-158	-66	45	55
35	7.73	72	50	-46	50	48	70	55	-164	-165	-168	176	-173	-172
25	3.92	170	-50	54	-57	174	166	-48	-67	48	-180	40	150	179
22	3.66	170	-51	54	-56	173	167	-52	-62	50	-177	45	42	54
32	4.63	175	-53	53	-55	180	171	-53	-63	67	-179	-75	-83	168
28	7.09	74	50	-48	53	58	70	55	-163	-48	83	177	-174	-52

Table 4.33. ϕ classes and $\overline{\Delta\delta}$ values of tagatose conformers.

Conformer	ϕ Class			$\overline{\Delta\delta}_C$ (ppm)	$\overline{\Delta\delta}_H$ (ppm)
	C–C–C–C	O–C–C–O	H–O–C–C		
19	TG-G+G-	G-TG-G-	tg-g+g+g-	2.935	0.341
06	TG-G+G-	G-TG-G-	g-g-g+g+g-	3.240	0.287
17	TG-G+G-	G-TG-G-	tg-g-g-t	3.304	0.227
15	TG-G+G-	G-TG-G-	g-g-g+g+g+	3.523	0.171
21	TG-G+G-	G-TG-G-	g-g-g+tt	3.525	0.288
20	TG-G+G-	G-TG-G-	g+tg+g+g-	3.552	0.315
18	TG-G+G-	G-TG-G-	tg-tg-t	3.651	0.137

Table 4.33. ϕ classes and $\overline{\Delta\delta}$ values of tagatose conformers. (cont.)

Conformer	ϕ Class			$\overline{\Delta\delta}_C$ (ppm)	$\overline{\Delta\delta}_H$ (ppm)
	C–C–C–C	O–C–C–O	H–O–C–C		
27	TG-G+G-	G-TG-G-	g+tg+tt	3.742	0.268
26	TG-G+G-	G-TG-G-	g+tg-g-t	3.770	0.187
38	TG-G+G-	G+TG-G-	g+ttg-t	3.898	0.212
01	TG-G+G-	G+TG-G-	g+tg+g+g-	3.959	0.306
37	TG-G+G-	G+TG-G-	ttg+g+g-	4.013	0.264
04	G+G+G-G+	G+G+G+T	g+tttg+	4.014	0.297
31	TG-G+G-	G-TG-G-	g+tg+g+g+	4.071	0.275
24	TG-G+G-	TTG-G-	g-g+tg-t	4.151	0.285
07	G+G+G-G+	G+G+G+T	g+tttg-	4.174	0.379
16	G+G+G-G+	G+G+G+T	g+tttt	4.194	0.313
23	TG-G+G-	G+TG-G-	g+tg+tt	4.213	0.287
11	TG-G+G-	G-TG-G-	g+ttg-t	4.277	0.155
41	TG-G+G-	G+TG-G-	ttg+tt	4.283	0.225
12	TG-G+G-	G+TG-G-	g+tg+g+g+	4.296	0.199
02	TG-G+G-	G+TG-G-	ttg-g-t	4.321	0.224
40	TG-G+G-	G+TG-G-	ttg+g+g+	4.354	0.151
33	G+G+G-G+	G+G+G+T	ttttg+	4.519	0.291
03	TG-G+G-	TTG-G-	g-ttg-t	4.526	0.261
09	TG-G+G-	TTG-G-	g+tg+g+g-	4.646	0.330
08	TG-G+G-	TTG-G-	tttg-t	4.674	0.258
36	TG-G+G-	G+TG-G-	ttg-g+g+	4.687	0.157
35	G+G+G-G+	G+G+G+T	ttttt	4.761	0.299
25	TG-G+G-	TTG-G-	g+tg+tt	4.885	0.283
22	TG-G+G-	TTG-G-	g+tg+g+g+	5.027	0.282
32	TG-G+G-	TTG-G-	g+tg-g-t	5.036	0.255
28	G+G+G-G+	G+G+G+T	g-g+ttg-	5.838	0.315

Table 4.34. Computational results of fructose conformers.

Conformer	Rel. E (kcal/mol)	ϕ (degrees)												
		C1–C2–C3–C4	C2–C3–C4–C5	C3–C4–C5–C6	C4–C5–C6–O6	O1–C1–C2–O2	O2–C2–C3–O3	O3–C3–C4–O4	O4–C4–C5–O5	H1–O1–C1–C2	H2–O2–C2–C3	H3–O3–C3–C4	H4–O4–C4–C5	H5–O5–C5–C6
25	4.47	-174	57	-52	51	180	-57	-60	-52	53	175	151	169	168
26	3.59	-170	53	-52	53	180	-51	-67	-53	58	37	151	173	169
12	2.78	-171	53	-52	53	-41	-55	-62	-53	164	157	-76	167	168
33	3.96	-175	57	-52	51	-53	-58	-60	-52	-64	161	153	171	169
15	2.21	-168	53	-53	53	-176	-53	-63	-54	50	171	-78	165	167
01	0.00	-171	53	-52	52	-51	-56	-63	-53	-68	159	-77	167	168
27	5.08	-167	48	-53	59	177	-50	-68	-53	178	35	49	41	36
31	4.18	-176	56	-50	49	-52	-63	-62	-47	-66	158	53	-90	163
19	3.93	-168	52	-52	54	-175	-52	-65	-53	56	37	49	44	-69
30	2.93	-174	54	-51	54	-50	-62	-59	-50	-67	157	43	38	37
23	3.80	-176	56	-50	51	-51	-63	-58	-50	-67	158	43	41	-67
07	4.72	-169	55	-57	58	-51	-53	-59	-59	-68	158	-78	167	-65
13	4.10	-168	52	-56	60	-49	-53	-61	-56	-70	157	-77	170	40
11	4.00	-173	55	-52	50	58	-55	-61	-51	-59	-169	-174	167	166
06	3.32	-170	48	-51	57	-49	-57	-62	-53	-70	156	-66	44	36
35	4.20	-171	52	-52	54	-50	-58	-60	-55	-69	157	-67	50	-70
34	2.66	-171	54	-52	52	45	-57	-62	-53	60	145	-71	165	169
14	4.29	-179	57	-50	49	45	-64	-62	-48	62	100	53	-90	164
32	3.63	-179	57	-50	50	46	-64	-58	-51	61	97	43	41	-65
02	2.89	-177	54	-51	54	46	-63	-60	-50	62	98	44	38	35

Table 4.35. ϕ classes and $\overline{\Delta\delta}$ values of fructose conformers.

Conformer	ϕ Class		$\overline{\Delta\delta}_{\mathrm{C}}$ (ppm)	$\overline{\Delta\delta}_{\mathrm{H}}$ (ppm)
	O1–C1–C2–O2	H–O–C–C		
25	T	g+tttt	2.912	0.289
26	T	g+g+ttt	3.090	0.253
12	G-	ttg-tt	3.156	0.225
33	G-	g-tttt	3.190	0.176
15	T	g+tg-tt	3.304	0.237
01	G-	g-tg-tt	3.499	0.156
27	T	tg+g+g+g+	3.514	0.345
31	G-	g-tg+g-t	3.679	0.215
19	T	g+g+g+g+g-	3.702	0.314
30	G-	g-tg+g+g+	3.951	0.348
23	G-	g-tg+g+g-	3.986	0.246
07	G-	g-tg-tg-	4.180	0.224
13	G-	g-tg-tg+	4.191	0.286
11	G+	g-tttt	4.516	0.211
06	G-	g-tg-g+g+	4.578	0.428
35	G-	g-tg-g+g-	4.726	0.303
34	G+	g+tg-tt	4.934	0.190
14	G+	g+g+g+g-t	5.227	0.289
32	G+	g+g+g+g+g-	5.345	0.300
02	G+	g+g+g+g+g+	5.439	0.328

Table 4.36. Computational results of sucrose conformers.

Conformer	Rel. E (kcal/mol)	ϕ (degrees)														
		C1–C2–C3–C4	C2–C3–C4–C5	C3–C4–C5–C6	C3–C4–C5–O5	C4–C5–O5–C1	C5–O5–C1–O2′	H1a–C1–O2′–C2′	C1–O2′–C2′–C1′	C1′–C2′–C3′–C4′	C2′–C3′–C4′–C5′	C3′–C4′–C5′–C6′	C3′–C4′–C5′–O5′	C4′–C5′–O5′–C2′	O2–C2–C3–O3	O3–C3–C4–O4
31	5.36	-57	57	-176	-56	60	61	-8	84	-151	38	-151	-31	12	59	-64
16	4.23	-54	53	-176	-55	62	58	-16	94	-151	39	-155	-34	17	62	-63
02	4.01	-55	56	-178	-58	62	59	-21	105	-151	39	-155	-33	15	60	-63
12	2.24	-53	56	-179	-58	63	61	-17	94	-149	36	-154	-33	18	65	-63
10	3.83	-55	57	-179	-58	59	66	-2	80	-149	33	-147	-25	6	62	-61
24	1.38	-56	54	-170	-53	58	63	-10	83	-150	34	-151	-30	13	60	-65
13	0.00	-56	55	-170	-54	58	62	-5	70	-153	37	-150	-28	7	60	-65
17	4.88	-54	53	-173	-54	61	60	-2	72	-151	39	-157	-33	14	61	-63
39	2.57	-53	55	-178	-57	62	62	-9	79	-148	35	-151	-30	13	65	-64
09	5.80	-53	55	-177	-58	64	59	-23	-42	-150	32	-140	-20	-1	64	-66
45	5.20	-54	55	-174	-56	60	61	-13	70	-100	-28	-98	28	-17	62	-65
46	0.06	-53	54	-177	-56	62	61	-5	76	-153	38	-152	-30	9	63	-62
14	4.82	-55	54	-170	-53	56	66	-6	63	-150	36	-148	-28	8	61	-65
79	3.46	-52	55	-177	-58	62	62	-37	-76	-160	38	-141	-20	-7	60	-63
55	6.37	-55	52	-170	-51	59	59	-5	68	-154	40	-154	-32	10	61	-64
08	4.89	-56	54	-171	-54	59	62	-3	72	-157	39	-149	-28	4	60	-65

Table 4.36. Computational results of sucrose conformers. (cont.)

Conformer	Rel. E (kcal/mol)	ϕ (degrees)														
		C1–C2–C3–C4	C2–C3–C4–C5	C3–C4–C5–C6	C3–C4–C5–O5	C4–C5–O5–C1	C5–O5–C1–O2′	H1a–C1–O2′–C2′	C1–O2′–C2′–C1′	C1′–C2′–C3′–C4′	C2′–C3′–C4′–C5′	C3′–C4′–C5′–C6′	C3′–C4′–C5′–O5′	C4′–C5′–O5′–C2′	O2–C2–C3–O3	O3–C3–C4–O4
60	4.80	-54	51	-172	-52	61	56	-11	74	-97	-29	-95	28	-16	63	-65
92	6.42	-49	54	-180	-60	66	61	-48	33	-151	35	-148	-26	6	63	-62
91	7.31	-54	53	-173	-54	60	60	-3	73	-155	40	-153	-31	9	62	-63
04	5.32	-54	56	-176	-57	60	65	0	81	-153	35	-144	-24	2	62	-62
37	4.08	-54	56	-176	-57	59	63	-3	75	-155	36	-145	-24	3	59	-62
51	5.54	56	-49	-86	44	-49	178	-46	44	-154	34	-140	-19	-4	168	-160

Table 4.36. Computational results of sucrose conformers. (cont.)

Conformer	Rrel. E (kcal/mol)	ϕ (degrees)														
		O4–C4–C5–O5	O5–C5–C6–O6	O1′–C1′–C2′–O2′	O2′–C2′–C3′–O3′	O3′–C3′–C4′–O4′	O4′–C4′–C5′–O5′	O5′–C5′–C6′–O6′	H2–O2–C2–C3	H3–O3–C3–C4	H4–O4–C4–C5	H6–O6–C6–C5	H1′–O1′–C1′–C2′	H3′–O3′–C3′–C4′	H4′–O4′–C4′–C5′	H6′–O6′–C6′–C5′
31	5.36	-175	-67	-58	-38	-78	-149	-70	-44	60	-88	69	78	66	-89	56
16	4.23	-178	79	-56	-36	-77	-152	-66	-49	51	54	-71	72	67	-98	50
02	4.01	-179	71	-54	-35	-78	-152	-72	111	-175	167	-74	-72	65	-105	50
12	2.24	-179	78	-56	-34	-81	-154	-63	-93	151	173	-72	71	-81	-172	50
10	3.83	180	-74	-65	-37	-84	-146	-72	164	-175	168	-81	-67	-80	-171	64
24	1.38	-171	-177	-58	-36	-82	-151	-66	-47	56	-50	-175	80	-82	-177	57
13	0.00	-172	-175	57	-37	-80	-150	-64	-48	57	-50	-172	-77	-172	-176	57
17	4.88	-178	69	58	-34	-77	-156	-76	-53	50	52	-53	-79	-173	177	-83
39	2.57	-178	83	51	-35	-80	-152	-61	-135	172	171	-67	-65	-84	-176	51
09	5.80	-179	69	-62	-46	-83	-142	-63	-57	101	-167	-42	-51	-56	-175	47
45	5.20	-174	-64	54	22	-153	-91	-62	-49	57	-85	63	-69	-149	-179	-36
46	0.06	-179	89	55	-37	-80	-151	-61	-53	50	50	-65	-77	-172	-175	52
14	4.82	-171	-175	-81	-40	-80	-149	-62	-50	55	-51	-175	-57	-82	-177	56
79	3.46	-180	63	79	-55	-78	-141	-52	71	-170	168	-178	-97	-179	-177	48
55	6.37	-175	63	59	-37	-77	-155	167	-52	52	55	-61	-78	-173	177	49
08	4.89	-172	-179	57	-40	-77	-151	173	-50	57	-48	179	-78	-167	178	41

Table 4.36. Computational results of sucrose conformers. (cont.)

Conformer	Rrel. E (kcal/mol)	ϕ (degrees)														
		O4–C4–C5–O5	O5–C5–C6–O6	O1′–C1′–C2′–O2′	O2′–C2′–C3′–O3′	O3′–C3′–C4′–O4′	O4′–C4′–C5′–O5′	O5′–C5′–C6′–O6′	H2–O2–C2–C3	H3–O3–C3–C4	H4–O4–C4–C5	H6–O6–C6–C5	H1′–O1′–C1′–C2′	H3′–O3′–C3′–C4′	H4′–O4′–C4′–C5′	H6′–O6′–C6′–C5′
60	4.80	-176	72	53	18	-150	-91	-70	-52	55	58	175	-69	-50	177	120
92	6.42	179	67	52	-43	-81	-148	61	-47	-63	163	-50	47	-80	-177	-78
91	7.31	-179	169	57	-38	-77	-154	169	-54	52	57	62	-79	-170	178	46
04	5.32	-179	166	-67	-41	-82	-146	65	164	-176	172	52	-67	-78	-176	-66
37	4.08	-179	165	49	-43	-81	-146	64	81	-167	174	52	53	-71	-175	-64
51	5.54	-81	-64	-81	-45	-82	-141	-63	158	-41	82	88	-47	-75	-173	64

Table 4.37. ϕ classes and $\overline{\Delta\delta}$ values of sucrose conformers.

Conformer	ϕ Class				$\overline{\Delta\delta}_C$ (ppm)	$\overline{\Delta\delta}_H$ (ppm)
	Φ,Ψ	C–C–C–C	O–C–C–O	H–O–C–C		
31	ECLG+	G-G+TG-G+TG+TECL	G+G-G-G-G-G-G-	g-g+g-g+g+g+g-g+	3.904	0.371
16	G-G+	G-G+TG-G+TG+TG+	G+G-G+G-G-G-G-	g-g+g+g-g+g+g-g+	4.817	0.323
02	G-G+	G-G+TG-G+TG+TG+	G+G-G+G-G-G-G-	g+ttg-g-g+g-g+	4.869	0.287
12	G-G+	G-G+TG-G+TG+TG+	G+G-G+G-G-G-G-	g-ttg-g+g-tg+	5.066	0.259
10	ECLG+	G-G+TG-G+TG+TECL	G+G-G-G-G-G-G-	tttg-g-g-tg+	5.086	0.277
24	ECLG+	G-G+TG-G+TG+TECL	G+G-TG-G-G-G-	g-g+g-tg+g-tg+	5.155	0.323
13	ECLG+	G-G+TG-G+TG+TECL	G+G-TG+G-G-G-	g-g+g-tg-ttg+	5.185	0.265
17	ECLG+	G-G+TG-G+TG+TECL	G+G-G+G+G-G-G-	g-g+g+g-g-ttg-	5.243	0.163
39	ECLG+	G-G+TG-G+TG+TECL	G+G-G+G+G-G-G-	g-ttg-g-g-tg+	5.344	0.151
09	G-G-	G-G+TG-G+TG+TECL	G+G-G+G-G-G-G-	g-g+tg-g-g-tg+	5.355	0.219
45	ECLG+	G-G+TG-G+G-G-G-G-	G+G-G-G+G+TG-	g-g+g-g+g-ttg-	5.407	0.192
46	ECLG+	G-G+TG-G+TG+TECL	G+G-G+G+G-G-G-	g-g+g+g-g-ttg+	5.480	0.185
14	ECLG+	G-G+TG-G+TG+TECL	G+G-TG-G-G-G-	g-g+g-tg-g-tg+	5.715	0.357
79	G-G-	G-G+TG-G+TG+TECL	G+G-G+G+G-G-G-	g+tttg-ttg+	5.731	0.332
55	ECLG+	G-G+TG-G+TG+TECL	G+G-G+G+G-G-T	g-g+g+g-g-ttg+	6.098	0.165
08	ECLG+	G-G+TG-G+TG+TECL	G+G-TG+G-G-T	g-g+g-tg-ttg+	6.243	0.180
60	ECLG+	G-G+TG-G+G-G-G-G-	G+G-G+G+G+TG-	g-g+g+tg-g-tg+	6.335	0.204
92	G-G+	G-G+TG-G+TG+TECL	G+G-G+G+G-G-G+	g-g-tg-g+g-tg-	6.604	0.268

Table 4.37. ϕ classes and $\overline{\Delta\delta}$ values of sucrose conformers. (cont.)

Conformer	ϕ Class				$\overline{\Delta\delta}_{\mathrm{C}}$ (ppm)	$\overline{\Delta\delta}_{\mathrm{H}}$ (ppm)
	Φ,Ψ	C–C–C–C	O–C–C–O	H–O–C–C		
91	ECLG+	G-G+TG-G+TG+TECL	G+G-TG+G-G-T	g-g+g+g+g-ttg+	6.631	0.126
04	ECLG+	G-G+TG-G+TG+TECL	G+G-TG-G-G-G+	tttg+g-g-tg-	6.683	0.215
37	ECLG+	G-G+TG-G+TG+TECL	G+G-TG+G-G-G+	g+ttg+g+g-tg-	6.906	0.170
51	G-G+	G+G-G-G+G-TG+TECL	TTG-G-G-G-G-	tg-g+g+g-g-tg+	6.949	0.288

5. CONCLUSION

The examination of hydrogen bonding properties of hydroxy protons is studied experimentally and computationally for the selected sweeteners including glycol, glycerol, erythritol, xylitol, mannitol, sorbitol, tagatose, fructose and sucrose.

The experimental results reveal that terminal hydroxy protons are in a fast chemical exchange with water protons. The internal hydroxy protons tend to get involved in intramolecular hydrogen bondings. The possibility of getting involved in hydrogen bonding interactions is higher for the innermost hydroxy protons. Hydrogen bonding tendencies in cyclic molecules however, are more dependent on steric factors and consequently accessibility of water molecules.

Computational studies on selected molecules indicate that most of the lower energy conformers (Conformational classes based on heavy atoms' dihedral angles may be found in tables) coexist in the aqueous solutions. There are distinct hydrogen bonding attributes in agreement with the experimental results. Computed chemical shifts of cyclic molecules with extended hydrogen bonding arrays in clockwise or counterclockwise direction are closer to experimental values.

The diastereotopicity of all the molecules observed by coupling constants, except glycol, along with the conformational analysis results depicting hydrogen bond and exchange tendencies, display and stress the importance of molecular geometry of sugar compounds in the sweet-taste chemoreception.

6. FUTURE WORK

This thesis is a part of a study that originally comprises of 11 natural and 8 synthetic sweeteners that have been planned to studied by the funds of BAP (Grant No: 5183) and TÜBITAK (Grant No: 109T606). Eight of the natural ones (and additionally glycol) are represented in this dissertation. The computational work is in progress for the two of natural sweeteners; lactitol and maltitol (Figure 6.1). The experimental measurements and calculations are continuing for the artificial selected sweeteners (Figure 6.2).

For further investigation on hydroxy protons of sweeteners, NMR experiments of their inclusion complexes with α-, β- and γ-cyclodextrins were performed and being evaluated. The comparison of hydrogen bonding properties in aqueous solutions and cyclodextrin environments is expected to provide further geometrical information about sweeteners. Processing and data mining on the supramolecular complexes are ongoing.

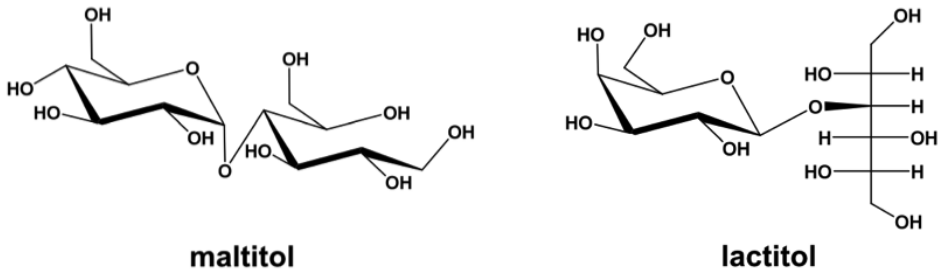

Figure 6.1. Natural sweeteners to be studied.

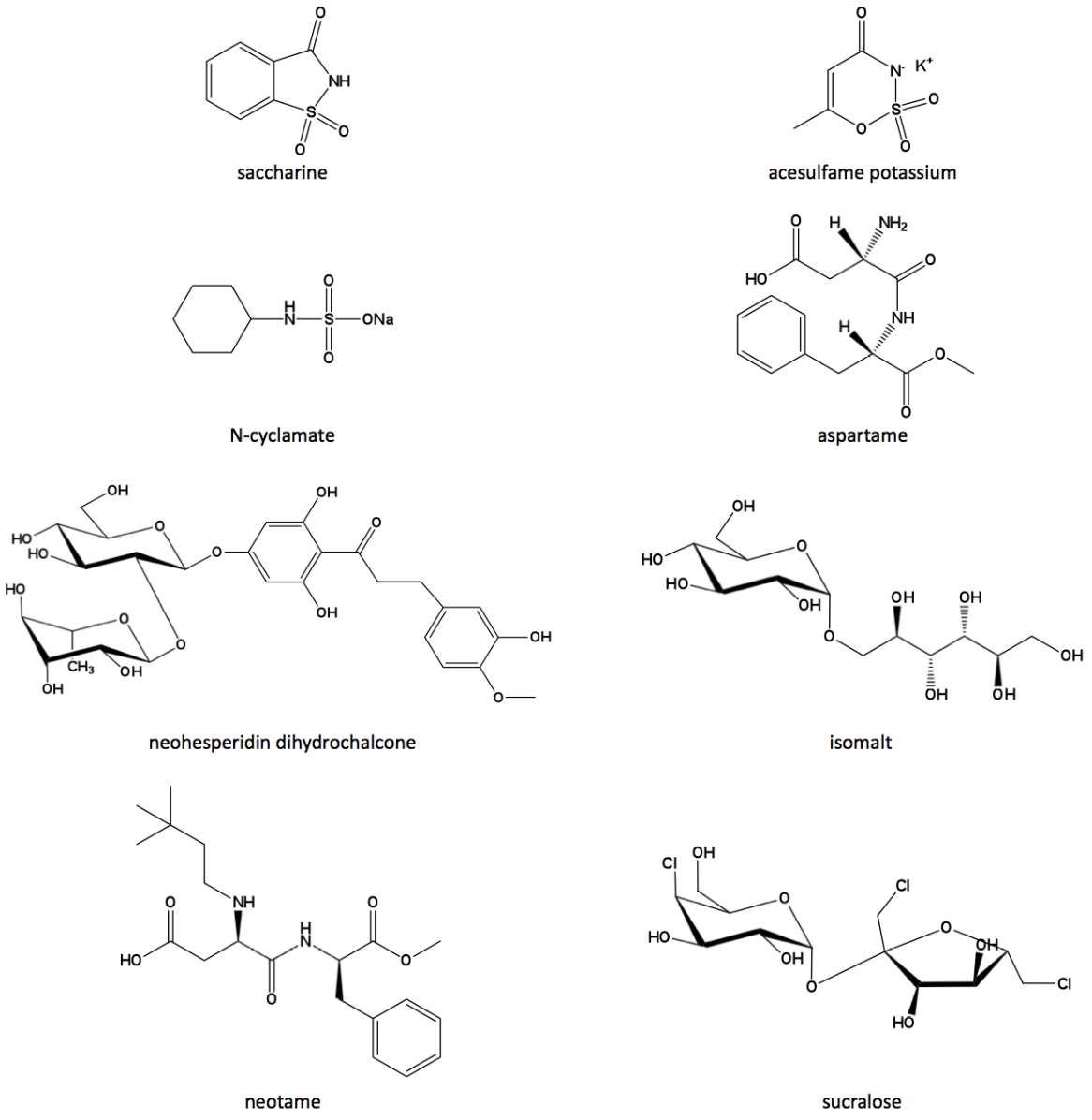

Figure 6.2. The artificial sweeteners planned to be studied.

APPENDIX A: NMR SPECTRA OF SELECTED SWEETENERS

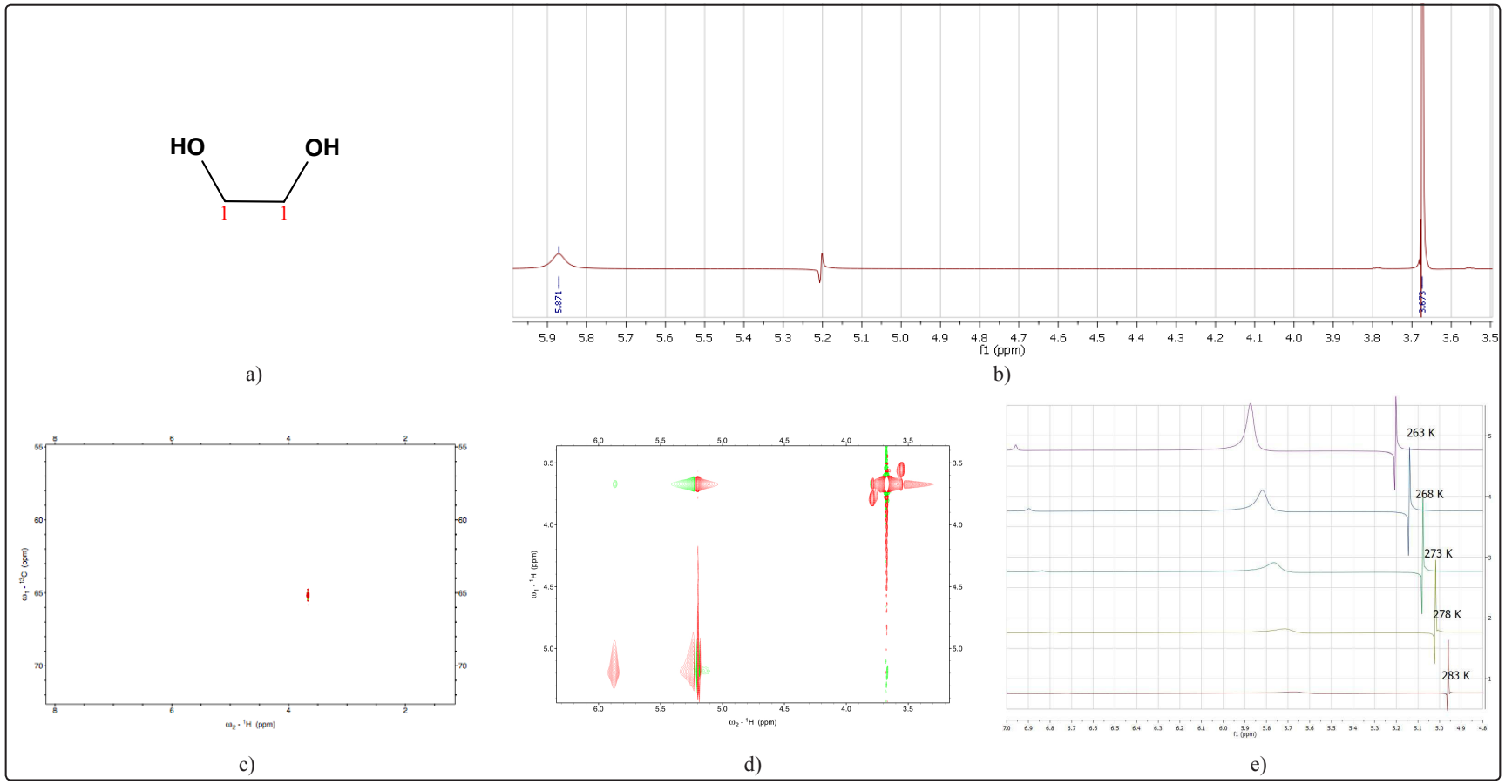

Figure A.1. Glycol (a) Structure (b) 1H spectrum (c) HSQC spectrum (d) NOESY spectrum (e) Temperature dependence.

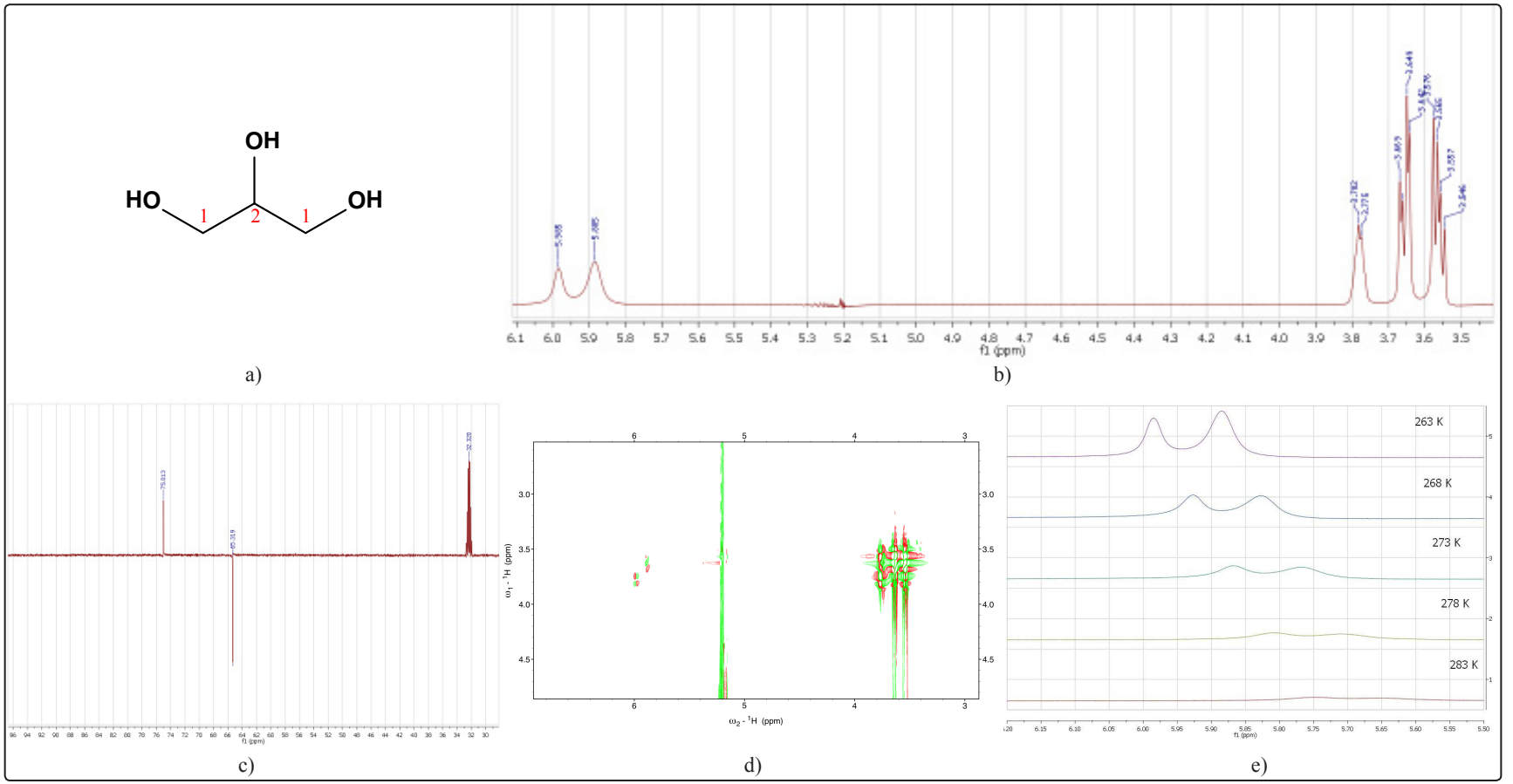

Figure A.2. Glycerol (a) Structure (b) 1H spectrum (c) APT spectrum (d) DQF-COSY spectrum (e) Temperature dependence.

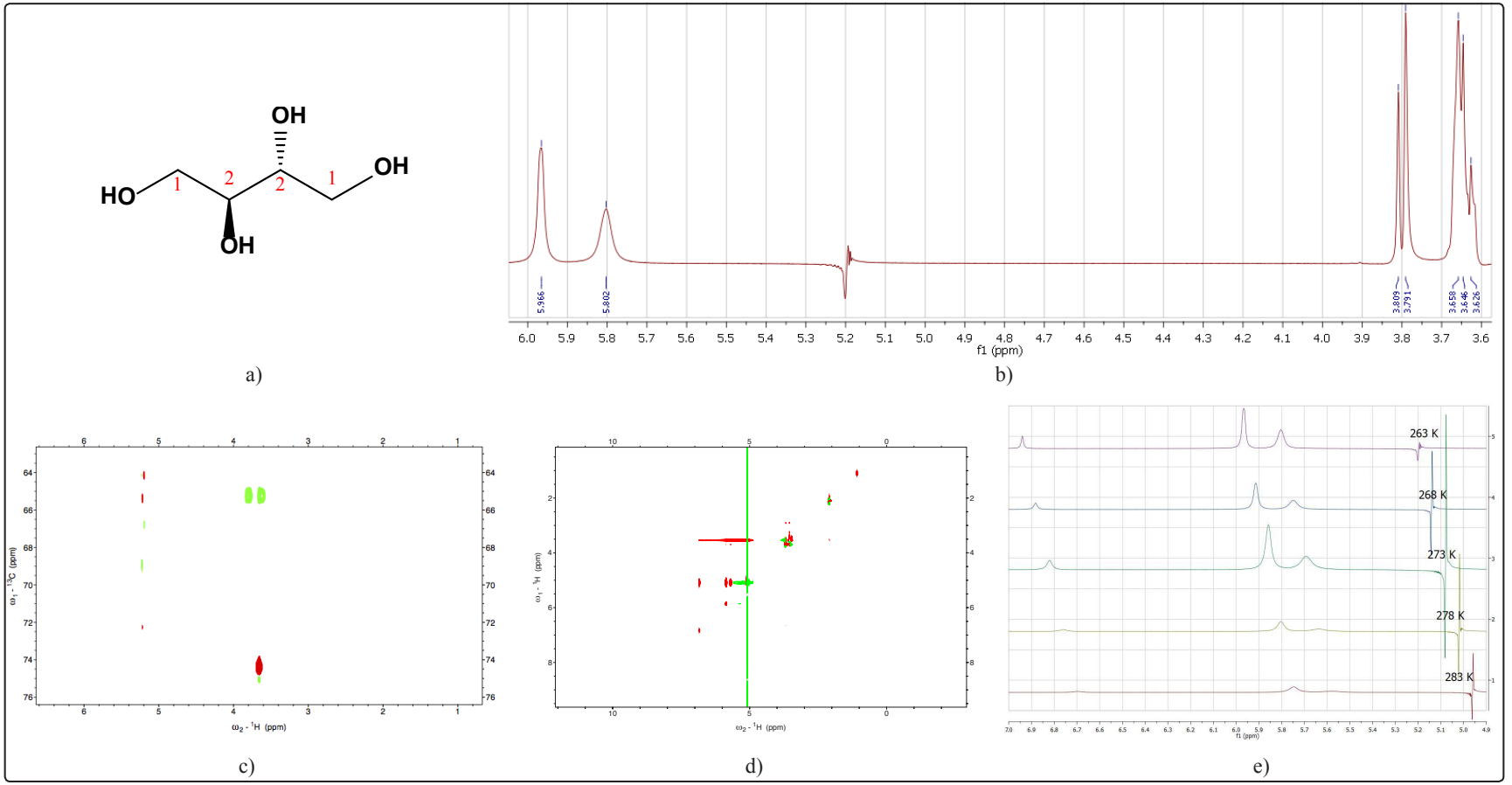

Figure A.3. Erythritol (a) Structure (b) 1H spectrum (c) HSQC spectrum (d) TOCSY spectrum (e) Temperature dependence.

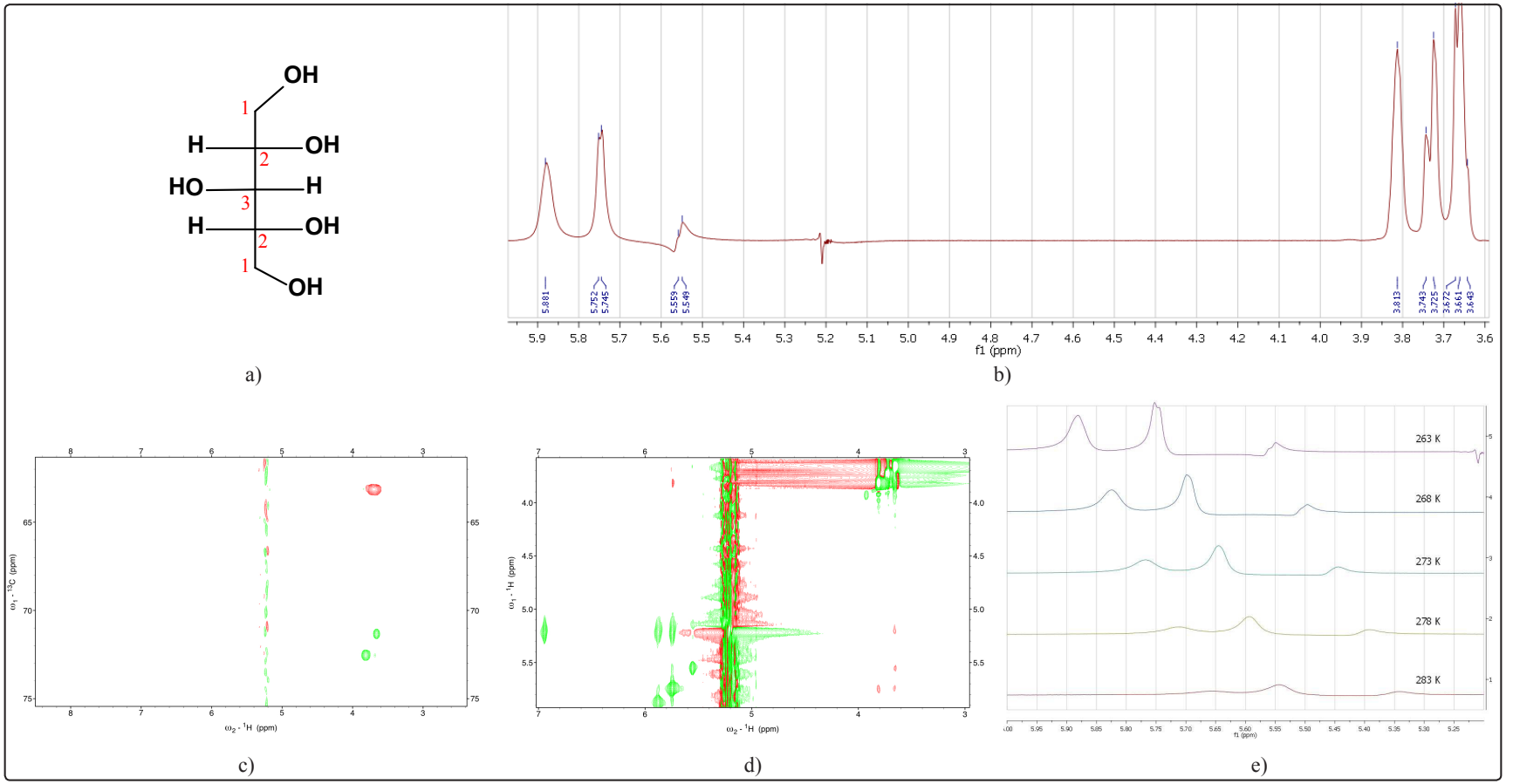

Figure A.4. Xylitol (a) Structure (b) 1H spectrum (c) HSQC spectrum (d) NOESY spectrum (e) Temperature dependence.

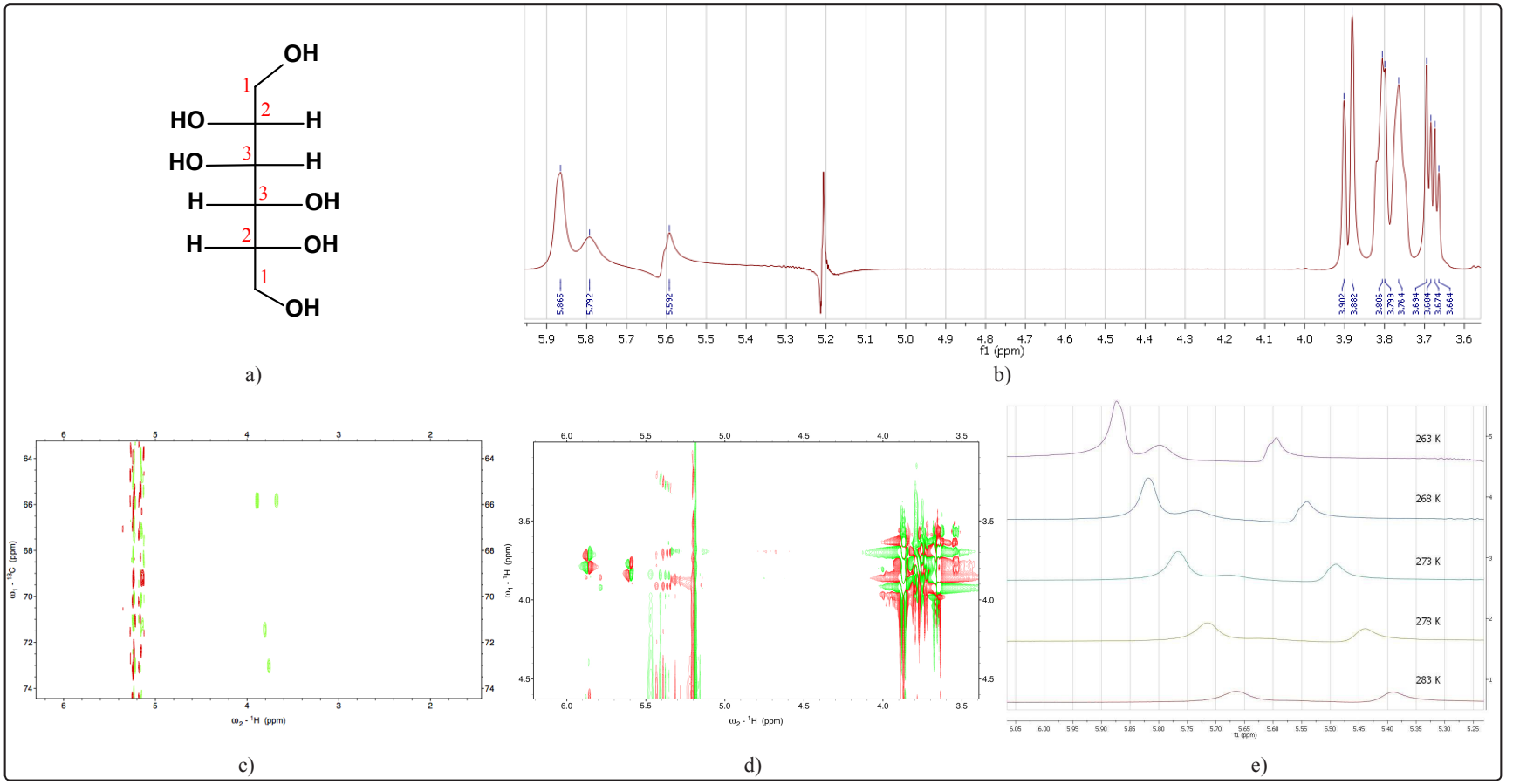

Figure A.5. Mannitol (a) Structure (b) 1H spectrum (c) HSQC spectrum (d) DQF-COSY spectrum (e) Temperature dependence.

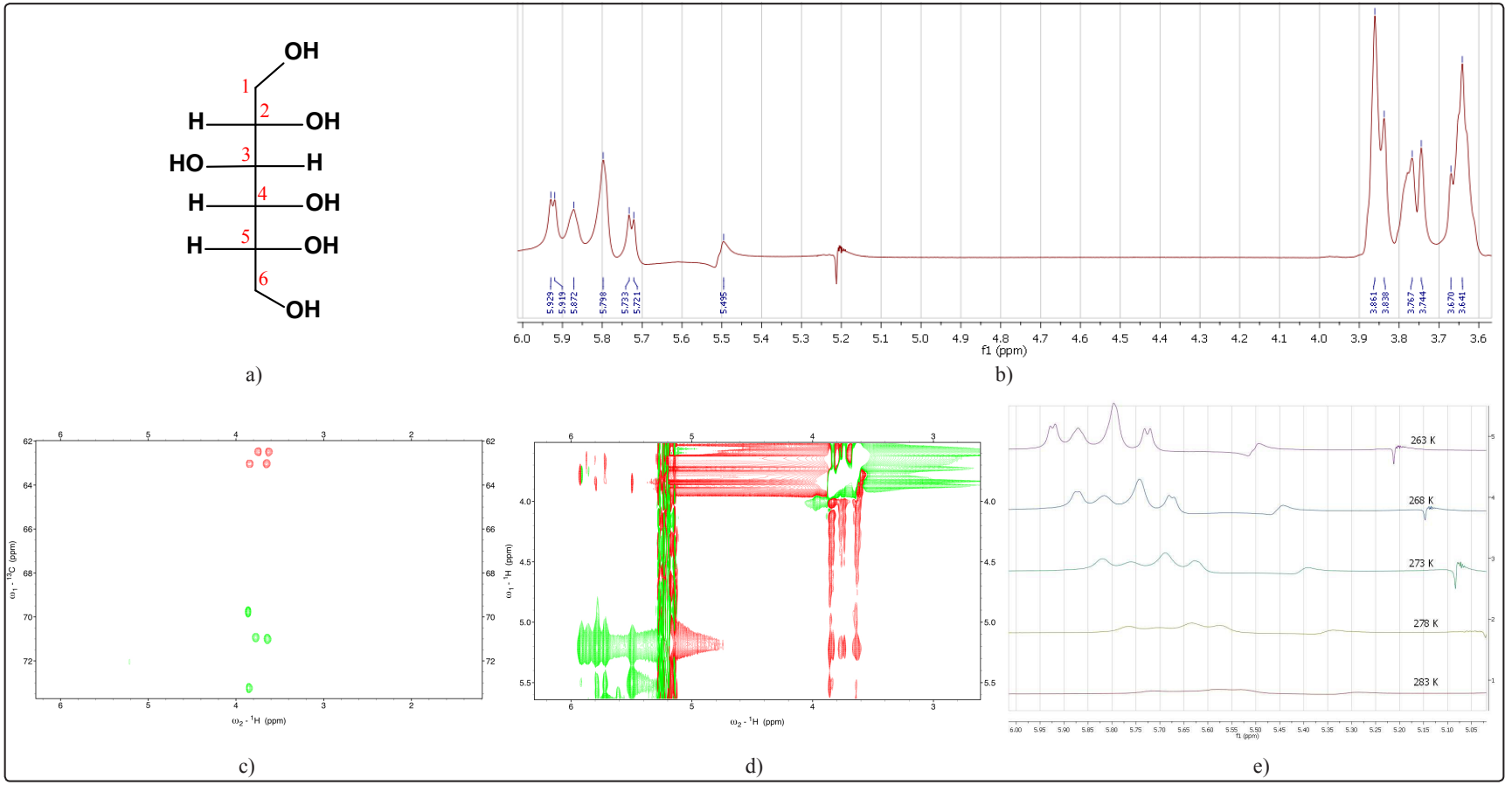

Figure A.6. Sorbitol (a) Structure (b) 1H spectrum (c) HSQC spectrum (d) NOESY spectrum (e) Temperature dependence.

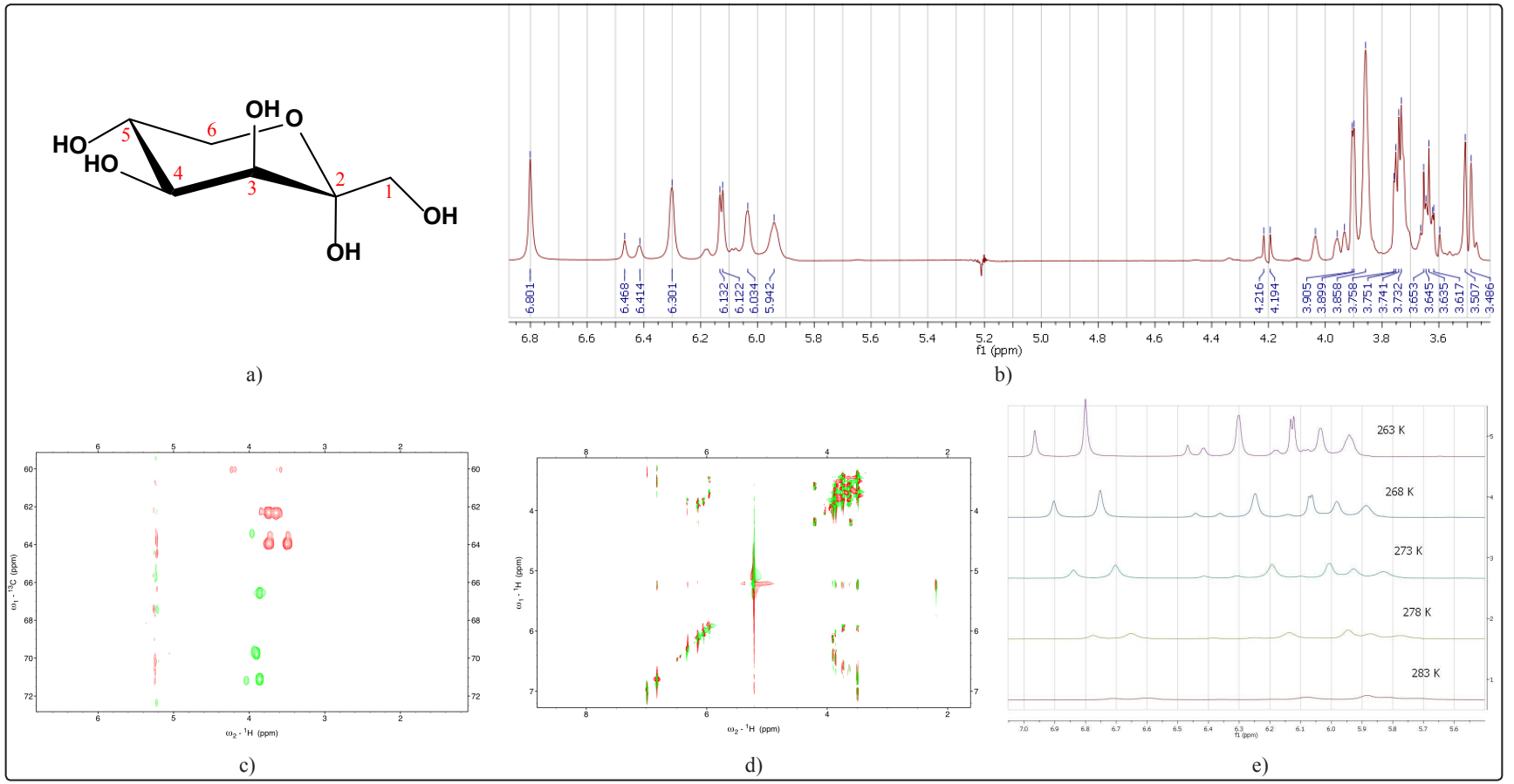

Figure A.7. Tagatose (a) Structure (b) 1H spectrum (c) HSQC spectrum (d) DQF-COSY spectrum (e) Temperature dependence.

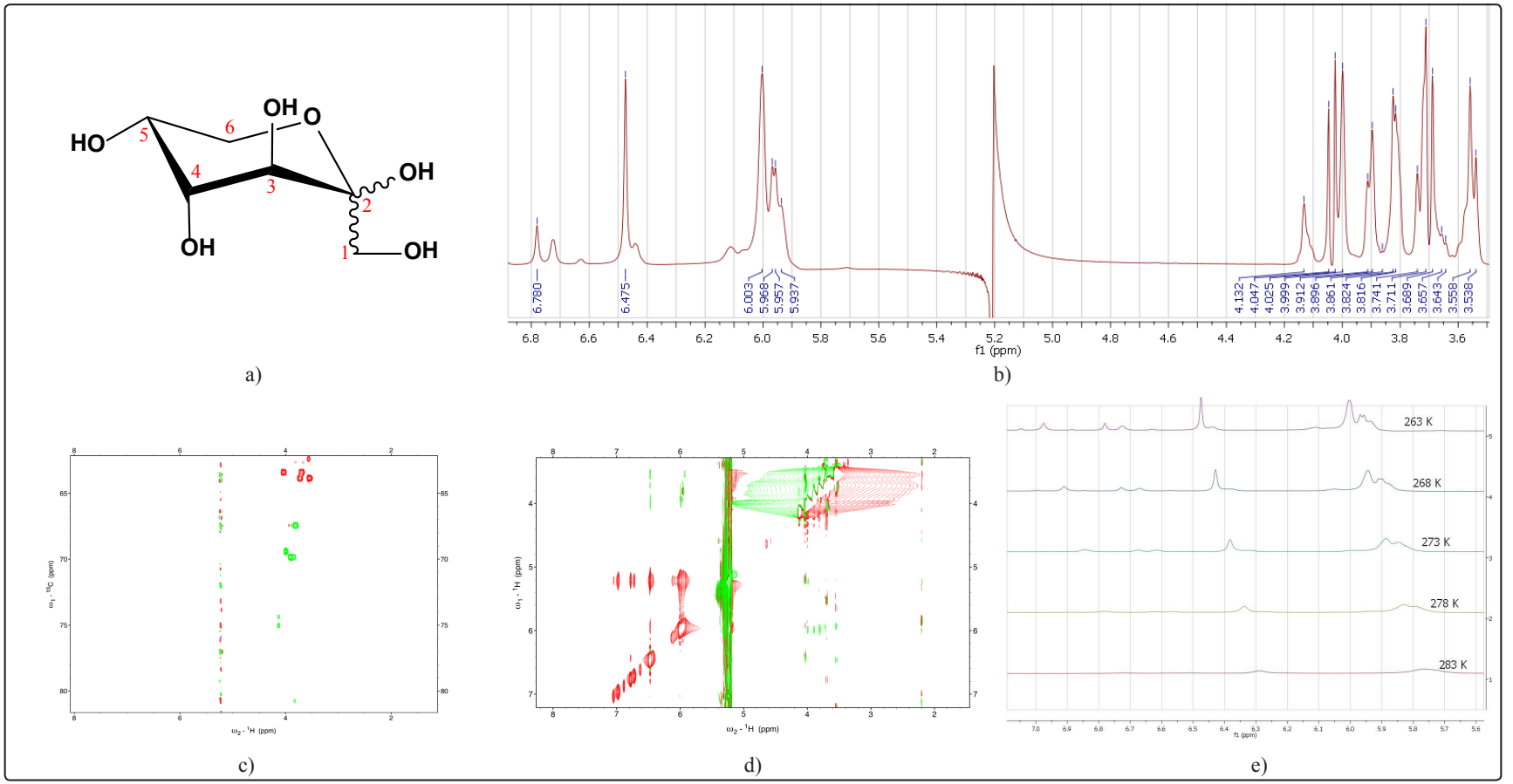

Figure A.8. Fructose (a) Structure (b) 1H spectrum (c) HSQC spectrum (d) NOESY spectrum (e) Temperature dependence.

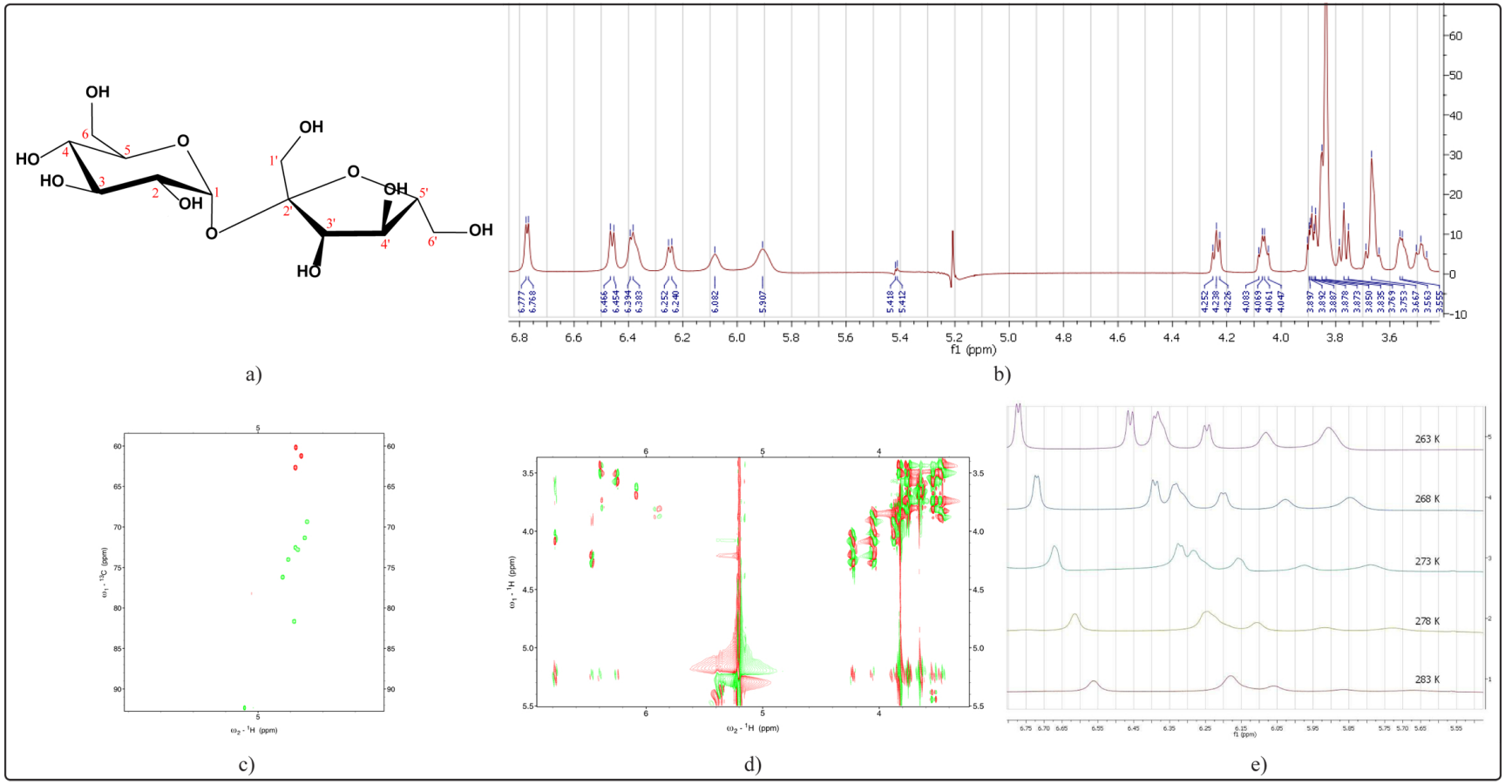

Figure A.9. Sucrose (a) Structure (b) 1H spectrum (c) HSQC spectrum (d) DQF-COSY spectrum (e) Temperature dependence.

REFERENCES

1. Lindemann, B., "Receptors and Transduction in Taste", *Nature*, Vol. 413, pp. 219–225, 2001.

2. Margolskee, R. F., "Molecular Mechanism of Bitter and Sweet Taste Transduction", *Journal of Biological Chemistry*, Vol. 227, No. 1, pp. 1–4, 2002.

3. Meyers, B. and M. S. Brewer, "Sweet Taste in Man: A Review", *Journal of Food Science*, Vol. 73, No. 6, pp. R81–R90, 2008.

4. Behrens, M., W. Meyerhof, C. Hellfritsch and T. Hofmann, "Sweet and Umami Taste: Natural Products, Their Chemosensory Targets, and Beyond", *Angewandte Chemie International Edition*, Vol. 50, pp. 2220 – 2242, 2011.

5. Li, X., M. Inoue, D. R. Reed, T. Hunque, R. B. Puchalski, M. G. Tordoff, Y. Ninomiiya, G. K. Beauchamp and A. A. Bachmanov, "High- Resolution Genetic Mapping of the Saccharin Preference Locus (Sac) and the Putative Sweet Taste Receptor (T1R1) Gene (Gpr70) to Mouse Distal Chromosome 4", *Mammalian Genome*, Vol. 12, No. 1, pp. 13–16, 2001.

6. Max, M., Y. G. Shanker, L. Huang, M. Rong, Z. Liu, F. Campagne, H. Weinstein, S. Damak and R. F. Margolskee, "Tas1r3, Encoding a New Candidate Taste Receptor, is Allelic to the Sweet Responsiveness Locus Sac", *Nature Genetics*, Vol. 28, pp. 58–63, 2001.

7. Nelson, G., M. A. Hoon, J. Chandrashekar, Y. Zhang, N. J. Ryba and C. S. Zuker, "Mammalian Sweet Taste Receptors", *Cell*, Vol. 106, pp. 381–390, 2001.

8. Temussi, P., "The History of Sweet Taste: Not Exactly a Piece of Cake", *Journal of Molecular Recognition*, Vol. 19, pp. 188–199, 2006.

9. Ager, D. J., D. P. Pantaleone, S. A. Henderson, A. R. Katritzky, I. Prakash and D. E. Walters, "Commercial, Synthetic Nonnutritive Sweeteners", *Angewandte Chemie International Edition*, Vol. 37, pp. 1802–1817, 1998.

10. Morini, G., A. Bassoli and G. Borgonovo., "Molecular Modelling and Models in the Study of Sweet and Umami Taste Receptors. A Review.", *Flavour and Fragrance Journal*, Vol. 26, pp. 254–259, 2011.

11. Cohn, G., *Die Organischen Geschmacksstoffe*, Franz Siemenroth, Berlin, 1914.

12. Shallenberger, R. S. and T. E. Acree, "Molecular Theory of Sweet Taste", *Nature*, Vol. 216, pp. 480–482, 1967.

13. Kier, L. B., "Molecular Theory of Sweet Taste", *Journal of Pharmaceutical Sciences*, Vol. 61, pp. 1394–1396, 1972.

14. Temussi, P. A., F. Lelj and T. Tancredi, "Three-dimensional Mapping of the Sweet Taste Receptor", *Journal of Medicinal Chemistry*, Vol. 21, pp. 1154–1158, 1978.

15. Temussi, P. A., F. Lelj and T. Tancredi, "Structure Activity Relationship of Sweet Molecules", *American Chemical Society Symposium Series*, Vol. 450, pp. 143–161, 1991.

16. Goodman, M., J. Coddington and D. F. Mierke, "A Model for the Sweet Taste of Stereoisomeric Retro-Inverso and Dipeptide Amides", *Journal of the American Chemical Society*, Vol. 109, pp. 4712–4714, 1987.

17. Nofre, C. and J. Tinti, "Sweetness Perception in Man: The Multipoint Attachment Theory", *Food Chemistry*, Vol. 56, No. 3(issue), pp. 263–274, 1996.

18. Goodman, M., J. R. D. Valle, Y. Amino and E. Benedetti, "Molecular basis of sweet taste in dipeptide taste ligands", *Pure and Applied Chemistry*, Vol. 74, No. 7, pp. 1109–1116, 2002.

19. Morris, J. A., "Sweetening Agents from Natural Sources", *Lloydia*, Vol. 39, pp. 25–38, 1976.

20. Esposito, V., R. Galluci, D. Picone, G. Saviano, T. Tancredi and P. A. Temussi, "The importance of electrostatic potential in the interaction of sweet proteins with the sweet taste receptor", *Journal of Molecular Biology*, Vol. 360, pp. 448–456, 2006.

21. Li, X., L. Staszewski, H. Xu, K. Durick, M. Zoller and E. Adler, "Human receptors for sweet and umami taste", *Proceedings of the National Academy of Sciences of the United States of America*, Vol. 99, No. 7, pp. 4692–4696, 2002.

22. G., M., A. Bassoli and P. A. Temussi, "From small sweeteners to sweet proteins: anatomy of the binding sites of the human T1R2-T1R3 Receptor", *Journal of Medicinal Chemistry*, Vol. 48, pp. 5520–5529, 2005.

23. DuBois, G. E., "Validity of Early Indirect Models of Taste Active Sites and Advances in New Taste Technologies Enabled by Improved Models", *Flavour and Fragrance Journal*, Vol. 26, pp. 239–253, 2011.

24. Morini, G. and A. Bassoli, "Modelling of Taste Receptor-Ligands Interactions", *Agro Food Industry Hi-Tech*, Vol. 18, pp. 14–16, 2007.

25. Morini, G., A. Bassoli and P. A. Temussi, "In Sweetness and Sweeteners: Biology, Chemistry and Psychophysics", D. K. Weerasinghe and G. E. DuBois (Editors), *ACS Symposium Series 979*, pp. 147–161, American Chemical Society, Washington, DC, 2008.

26. Wiggins, P. M., "Role of Water in Some Biological Processes", *Microbiological Reviews*, Vol. 54, No. 4, pp. 432–449, 1990.

27. Simons, J. P., R. A. Jockusch, P. Carcabal, I. Hunig, R. T. Kroemer, N. A. Macleod and L. C. Snoek, "Sugars in the Gas Phase. Spectroscopy, Conformation, Hydra-

tion, Co-operativity and Selectivity", *International Reviews in Physical Chemistry*, Vol. 24, pp. 489–531, 2005.

28. Lemieux, R. U., "How Water Provides the Impetus for Molecular Recognition in Aqueous Solution", *Accounts of Chemical Research*, Vol. 29, pp. 373–380, 1996.

29. Chervernak, M. C. and E. J. Toone, "A Direct Measure of the Contribution of Solvent Reorganization to the Enthalpy of Ligand Binding", *Journal of the American Chemical Society*, Vol. 116, pp. 10533–10539, 1994.

30. Birch, G. G., "Role of Water in Sweet Taste Chemoreception", *Pure and Applied Chemistry*, Vol. 74, No. 7, pp. 1103–1108, 2002.

31. Aroulmoji, V., M. Mathlouthi, L. Feruglio, E. Murano and M. Grassi, "Hydration Properties and Proton Exchange in Aqueous Sugar Solutions Studied by Time Domain Nuclear Magnetic Resonance", *Food Chemistry*, Vol. 132, pp. 1644–1650, 2012.

32. Duus, J. Ø., C. H. Gotfredsen and K. Bock, "Carbohydrate Structural Determination by NMR Spectroscopy: Modern Methods and Limitations", *Chemical Reviews*, Vol. 100, pp. 4589–4614, 2000.

33. Harvey, J. M., M. C. R. Symons and R. J. Naftalin, "Proton Magnetic Resonance Study of the Hydration of Glucose", *Nature*, Vol. 261, pp. 435–436, 1976.

34. Poppe, L. and H. van Halbeek, "Nuclear Magnetic Resonance of Hydroxyl and Amido, protons of oligosaccharides in aqueous solution: evidence for a strong intramolecular hydrogen bond in sialic acid residues", *Journal of the American Chemical Society*, Vol. 113, pp. 363–365, 1991.

35. van Halbeek, H. and L. Poppe, "Conformation and Dynamics of Glycoprotein Oligosaccharides as Studied by 1H NMR Spectroscopy", *Magnetic Resonance in Chemistry*, Vol. 30, pp. S74–S86, 1992.

36. Poppe, L., R. Stuike-Prill, B. Meyer and H. van Halbeek, "The Solution Conformation of sialyl-$\alpha(2\rightarrow6)$-lactose Studied by Modern NMR Techniques and Monte Carlo Simulations", *Journal of Biomolecular NMR*, Vol. 2, pp. 109–136, 1992.

37. Brisson, J. R., S. Uhrinova, R. J. Woods, M. van der Zwan, H. C. Jarrell, L. C. Paoletti, D. L. Kasper and H. J. Jennings, "NMR and Molecular Dynamics Studies of the Conformational Epitope of the Type III Group B Streptococcus Capsular Polysaccharide and Derivatives", *Biochemistry*, Vol. 36, No. 11, pp. 3278–3292, 1997.

38. Harris, R., T. J. Rutherford, M. J. Milton and S. W. Homans, "Three-dimensional Heteronuclear NMR Techniques for Assignment and Conformational Analysis Using Exchangeable Protons in Uniformly C-13-enriched Oligosaccharides", *Journal of Biomolecular NMR*, Vol. 9, No. 1, pp. 47–54, 1997.

39. Sandstrom, C., H. Baumann and L. Kenne, "The Use of Chemical Shifts of Hydroxy Protons of Oligosaccharides as Conformational Probes for NMR Studies in Aqueous Solution. Evidence for Persistent Hydrogen Bond Interaction in Branched Trisaccharides", *Journal of the Chemical Society, Perkins Transactions*, Vol. 2, No. 11, pp. 2385–2393, 1998.

40. Sandstrom, C., H. Baumann and L. Kenne, "NMR Spectroscopy of Hydroxy Protons of 3,4-disubstituted Methyl alpha-D-galactopyranosides in Aqueous Solution", *Journal of the Chemical Society, Perkins Transactions*, Vol. 2, No. 4, pp. 809–815, 1998.

41. Bekiroglu, S., C. Sandstrom, T. Norberg and L. Kenne, "Hydroxy Protons in Conformational Study of a Lewis b Tetrasaccharide Derivative in Aqueous Solution by NMR Spectroscopy", *Carbohydrate Research*, Vol. 328, pp. 409–418, 2000.

42. Zhang, T. and X. A. Mao, "Rate Constants for Chemical Exchange Between Water and Hydroxyl Protons in Natural Compounds Evaluated with NMR Two-dimensional Exchange Spectroscopy and Geometric Average Method", *Applied*

Magnetic Resonance, Vol. 20, pp. 189–202, 2001.

43. Bekiroglu, S., L. Kenne and C. Sandstrom, "H-1 NMR Studies of Maltose, Maltoheptaose, Alpha-, Beta-, and Gamma-cyclodextrins, and Complexes in Aqueous Solutions with Hydroxy Protons as Structural Probes", *Journal of Organic Chemistry*, Vol. 68, No. 5, pp. 1671–1678, 2003.

44. Bekiroglu, S., L. Kenne and C. Sandstrom, "NMR Study on the Hydroxy Protons of the Lewis X and Lewis Y Oligosaccharides", *Carbohydrate Research*, Vol. 339, No. 14, pp. 2465–2468, 2004.

45. Lin, J. and P. A. Frey, "Strong Hydrogen Bonds in Aqueous and Aqueous−Acetone Solutions of Dicarboxylic Acids: Activation Energies for Exchange and Deuterium Fractionation Factors", *Journal of the American Chemical Society*, Vol. 122, No. 45, pp. 11258–11259, 2000.

46. Fraser, R. R., M. Kaufman, P. Morand and G. Govil, "Stereochemical Dependence of Vicinal H-C-O-H Coupling Constants", *Canadian Journal of Chemistry*, Vol. 47, No. 3, pp. 403–409, 1969.

47. Konrat, R., M. Tollinger, G. Kontaxis and B. Kräutler, "NMR Techniques to Study Hydrogen Bonding in Aqueous Solution", *Monatshefte für Chemie*, Vol. 130, pp. 961–982, 1999.

48. Jeener, J., P. B. B. H. Meier and R. R. Ernst, "Investigation of Exchange Processes by Two-Dimensional NMR Spectroscopy", *Journal of Chemical Physics*, Vol. 71, No. 11, pp. 4546–4553, 1979.

49. Kumar, A., G. Wagner, R. R. Ernst and K. Wüthrich, "Buildup Rates of the Nuclear Overhauser Effect Measured by Two-Dimensional Proton Magnetic Resonance Spectroscopy: Implications for Studies of Protein Conformation", *Journal of the American Chemical Society*, Vol. 103, pp. 3654–3658, 1981.

50. Gronenborn, A. M. and G. M. Clore, "Investigation of the Solution Structures of Short Nucleic Acid Fragments by Means of Nuclear Overhauser Enhancement Measurements", *Progress in Nuclear Magnetic Resonance Spectroscopy*, Vol. 17, pp. 1–32, 1985.

51. Poppe, L. and H. van Halbeek, "NMR Spectroscopy of Hydroxyl Protons in Supercooled Carbohydrates", *Nature Structural and Molecular Biology*, Vol. 1, pp. 215–216, 1994.

52. Sheng, S. and H. van Halbeek, "Evidence for a Transient Interresidue Hydrogen Bond in Sucrose in Aqueous Solution Obtained by Rotating-frame Exchange NMR Spectroscopy Under Supercooled Conditions", *Biochemical and Biophysical Research Communications*, Vol. 215, pp. 504–510, 1995.

53. Bekiroglu, S., *Hydroxy Protons in Structural Analysis of Carbohydrates by NMR Spectroscopy and Computational Methods*, Ph.D. Thesis, Swedish University of Agricultural Sciences, 2003.

54. Bekiroglu, S., A. Sandstrom, L. Kenne and C. Sandstrom, "Ab Initio and NMR Studies on the Effect of Hydration on the Chemical Shift of Hydroxy Protons in Carbohydrates Using Disaccharides and Water/Methanol/Ethers as Model Systems", *Organic and Biomolecular Chemistry*, Vol. 2, No. 2, pp. 200–205, 2004.

55. Wach, W., *Fructose*, chap. Ullmann's Encyclopedia of Industrial Chemistry, Wiley-VCH Verlag GmbH & Co. KGaA, 2000.

56. Wolff, G. and E. Breitmaier, "C-13 NMR Spectroscopic Analysis of Keto Form in Aqueous-Solutions of D-Fructose, L-Sorbose and D-Tagatose", *CHEMIKER-ZEITUNG*, Vol. 103, No. 6, pp. 232–233, 1979.

57. Young, D. C., *Computational Chemistry: A Practical Guide for Applying Techniques to Real-World Problems.*, John Wiley & Sons, Inc., New York, 2001.

58. Mazzanti, A. and D. Casarini, "Recent Trends in Conformational Analysis", *WIREs Computational Molecular Science*, 2011.

59. Halgren, T. A., "Merck Molecular Force Field. I. Basis, Form, Scope, Parameterization, and Performance of MMFF94", *Journal of Computational Chemistry*, Vol. 17, pp. 490–552, 1996.

60. Poltev, V., *Handbook of Computational Chemistry*, chap. Molecular Mechanics: Method and Applications, pp. 259–291, Springer Netherlands, doi: 10.1007/978-94-007-0711-5_9, 2012.

61. Hohenberg, P. and W. Kohn, "Inhomogeneous Electron Gas", *Physical Review*, Vol. 136, pp. B864–B871, 1964.

62. Kohn, W. and L. J. Sham, "Self-Consistent Equations Including Exchange and Correlation Effects", *Physical Review*, Vol. 140, pp. A1133–A1138, 1965.

63. Becke, A. D., "Density Functional Thermochemistry. III. The Role of Exact Exchange", *Journal of Chemical Physics*, Vol. 98, pp. 5648–5652, 1993.

64. Csonka, G. I., A. D. French, G. P. Johnson and C. A. Stortz, "Evaluation of Density Functionals and Basis Sets for Carbohydrates", *Journal of Chemical Theory and Computation*, Vol. 5, pp. 679–692, 2009.

65. Csonka, G. I. and J. G. Angyan, "The Origin of the Problems with the PM3 Core Repulsion Function", *Journal of Molecular Structure (THEOCHEM)*, Vol. 393, pp. 31–38, 1997.

66. Teppen, B. J., M. Cao, R. F. Frey, C. van Alsenoy, D. M. Miller and L. Schafer, "An Investigation into Intramolecular Hydrogen Bonding: Impact of Basis Set and Electron Correlation on the ab Initio Conformational Analysis of 1,2-ethanediol and 1,2,3-propanetriol", *Journal of Molecular Structure (THEOCHEM)*, Vol. 314, pp. 169–190, 1994.

67. Chelli, R., F. L. Gervasio, C. Gellini, P. Procacci, G. Cardini and V. Schettino, "Density Functional Calculation of Structural and Vibrational Properties of Glycerol", *Journal of Physical Chemistry A*, Vol. 104, pp. 5351–5357, 2000.

68. Chelli, R., F. L. Gervasio, C. Gellini, P. Procacci, G. Cardini and V. Schettino, "Conformational Distribution of Gas-phase Glycerol", *Journal of Physical Chemistry A*, Vol. 104, pp. 11220–11222, 2000.

69. Callam, C. S., S. J. Singer, T. L. Lowary and C. M. Hadad, "Computational Analysis of the Potential Energy Surfaces of Glycerol in the Gas and Aqueous Phases: Effects of Level of Theory, Basis Set, and Solvation on Strongly Intramolecularly Hydrogen-Bonded Systems", *Journal of the American Chemical Society*, Vol. 123, pp. 11743–11754, 2001.

70. Jesus, A. J. L., L. I. N. Tomé, M. T. S. Rosado, M. L. P. Leitão and J. S. Redinha, "Conformational Study of Erythritol and Threitol in the Gas State by Density Functional Theory Calculations", *Carbohydrate Research*, Vol. 340, pp. 283–291, 2005.

71. Csonka, G. I., "Proper Basis Set for Quantum Mechanical Studies of Potential Energy Surfaces of Carbohydrates", *Journal of Molecular Structure (THEOCHEM)*, Vol. 584, pp. 1–4, 2002.

72. Jain, R., T. Bally and P. R. Rablen, "Calculating Accurate Proton Chemical Shifts of Organic Molecules with Density Functional Methods and Modest Basis Sets", *Journal of Organic Chemistry*, Vol. 74, No. 11, pp. 4017–4023, 2009.

73. Rablen, P. R., S. A. Pearlman and J. Finkbiner, "A Comparison of Density Functional Methods for the Estimation of Proton Chemical Shifts with Chemical Accuracy", *Journal of Physical Chemistry A*, Vol. 103, pp. 7357–7363, 1999.

74. Cheeseman, J. R., G. W. Trucks, T. A. Keith and M. J. Frisch, "A Comparison of Models for Calculating Nuclear Magnetic Resonance Shielding Tensors", *Journal*

of Chemical Physics, Vol. 104, pp. 5497–5509, 1996.

75. Lodewyk, M. W., M. R. Siebert and D. J. Tantillo, "Computational Prediction of H-1 and C-13 Chemical Shifts: A Useful Tool for Natural Product, Mechanistic, and Synthetic Organic Chemistry", *Chemical Reviews*, Vol. 112, No. 3, pp. 1839–1862, 2012.

76. Wavefunction, Inc., Irvine, CA, *Spartan'04*.

77. Imberty, A. and S. Pérez, "Structure, Conformation, and Dynamics of Bioactive Oligosaccharides: Theoretical Approaches and Experimental Validations", *Chemical Reviews*, Vol. 100, No. 12, pp. 4567–4588, 2000.

78. Peters, T., R. S.-P. B. Meyer, R. Somorjai and J. R. Brisson, "A Monte Carlo Method for Conformational Analysis of Saccharides", *Carbohydrate Research*, Vol. 238, pp. 49–73, 1993.

79. Frisch, M. J., G. W. Trucks, H. B. Schlegel, G. E. Scuseria, M. A. Robb, J. R. Cheeseman, G. Scalmani, V. Barone, B. Mennucci, G. A. Petersson, H. Nakatsuji, M. Caricato, X. Li, H. P. Hratchian, A. F. Izmaylov, J. Bloino, G. Zheng, J. L. Sonnenberg, M. Hada, M. Ehara, K. Toyota, R. Fukuda, J. Hasegawa, M. Ishida, T. Nakajima, Y. Honda, O. Kitao, H. Nakai, T. Vreven, J. A. Montgomery, , J. E. Peralta, F. Ogliaro, M. Bearpark, J. J. Heyd, E. Brothers, K. N. Kudin, V. N. Staroverov, T. Keith, R. Kobayashi, J. Normand, K. Raghavachari, A. Rendell, J. C. Burant, S. S. Iyengar, J. Tomasi, M. Cossi, N. Rega, J. M. Millam, M. Klene, J. E. Knox, J. B. Cross, V. Bakken, C. Adamo, J. Jaramillo, R. Gomperts, R. E. Stratmann, O. Yazyev, A. J. Austin, R. Cammi, C. Pomelli, J. W. Ochterski, R. L. Martin, K. Morokuma, V. G. Zakrzewski, G. A. Voth, P. Salvador, J. J. Dannenberg, S. Dapprich, A. D. Daniels, O. Farkas, J. B. Foresman, J. V. Ortiz, J. Cioslowski, and D. J. Fox, Gaussian 09, Revision B.01; Gaussian, Inc.: Wallingford CT, 2010.